UNIVERSITA' DEGLI STUDI DEL PIEMONTE ORIENTALE
"AMEDEO AVOGADRO"
DIPARTIMENTO DI SCIENZE ED INNOVAZIONE TECNOLOGICA

TESI DI DOTTORATO DI RICERCA IN SCIENZE CHIMICHE (XXVI CICLO)

DEVELOPMENT AND APPLICATION OF ANALYTICAL AND STATISTICAL TECHNIQUES FOR THE NON-INVASIVE MONITORING AND ANALYSIS OF CULTURAL HERITAGE

RELATORE: prof. Emilio Marengo
COORDINATORE: prof. Domenico Osella
CORRELATORE: prof. Greg Bearman

CANDIDATO: dott. Marcello Manfredi

ANNI ACCADEMICI: 2010-2013

INDEX

SCIENTIFIC CURRICULUM

Name: Marcello Manfredi

Address: via Stazione 37, Valle Lomellina (PV) 27020

Tel. 3334722270

Email: isverycool@hotmail.it

Birth date: 25/03/1986

Educational qualifications:

October 2010 – Master of Science in Chemistry, vote: 110/110 cum lode, Università degli Studi del Piemonte Orientale "Amedeo Avogadro", thesis: "Development of a technique based on LED multispectral imaging for monitoring the conservation of cultural heritage surfaces", relator prof. Emilio Marengo.

December 2009 – Master of first level in Sciences and Advanced Chemistry Technologies, Università delgli Studi del Piemonte Orientale "Amedeo Avogadro".

December 2008 – Bachelor Degree in Chemistry, vote: 108/110, Università degli Studi del Piemonte Orientale "Amedeo Avogadro", thesis: "Characterization of geographic provenance of wood samples by ICP-MS and advanced multivariate statistics methods", relator prof. Emilio Marengo.

Awards

Rotary Alessandria Award – Corrado Tartuferi, for the best thesis of Master of Science in Chemistry of the Sciences Faculty of Università degli Studi del Piemonte Orientale for the year 2010.

Grant Award from the Division of Analytical Chemistry of the European Association of Chemical and Molecolar Sciences offered by IUPAC for the participation at the XVI European Conference on Analytical Chemistry (Euroanalysis 2011).

Best poster Award from the National Society of Near Infrared Spectroscopy, National Conference NIR Spectroscopy, Padova, 2012.

Start Cup Piemonte e Valle d'Aosta, Business plan competition, Third classified with the project: ISALIT, Imaging techniques for monitoring the conservation of cultural heritage.

Best Spin-off 2013 of Università del Piemonte Orientale with the company ISALIT.

Relevant post-degree courses

- National School on Chemistry of Cultural Heritage and Environmental, Feltre; Belluno, 4-8/07/2011.
- National School on Analytical and Bio-analytical Methodologies in Mass Spectrometry, Parma, 14-18/05/2012.
- National School of Analytical Chemistry for PhD Students, Roma, 1-5/10/2012.
- Workshop on: SUMUS, Sistema per imaging multispectral 3D, CNR Firenze, 30/05/2011.
- Annual Chemometric Workshop, Albano Laziale, 26-28/05/2011.
- Course on Statistics using R, Alessandria, 14-15/03/2012.

Research Experiences:

November 2011-March 2012: Preservation Research and Testing Division, Library of Congress of United States of America, Washington D.C., USA –

Development of LED multispectral imaging technique for monitoring the conservation of objects, artificial ageing of parchment and DART-MS studies.

March-May 2013: New Mexico Highland University and Georgia O'Keeffe Museum, Santa Fe, New Mexico, USA - Development of RTI (imaging 3D) for morphological and physical change detections. (External tutors: Dale Kronkright and Greg Bearman).

Publications:

1. **"Technique Based on LED Multispectral Imaging and Multivariate Analysis for Monitoring the Conservation State of the Dead Sea Scrolls"**, *Anal. Chem., 2011, 83 (17), pp 6609–6618: Emilio Marengo, Marcello Manfredi, Orfeo Zerbinati, Elisa Robotti, Eleonora Mazzucco, Fabio Gosetti, Greg Bearman, Fenella France, and Pnina Shor***.**
2. **"Development of a technique based on multi-spectral imaging for monitoring the conservation of cultural heritage objects"**, *Anal. Chim. Acta (2011), Emilio Marengo, Marcello Manfredi, Orfeo Zerbinati, Elisa Robotti, Eleonora Mazzucco, Fabio Gosetti, Greg Bearman, Fenella France, Pnina Shor.*
3. **"DART-MS for the non-destructive investigation of conservation treatments of the Dead Sea Scrolls"**, *Marcello Manfredi, Greg Bearman, Fenella France and Pnina Shor, Emilio Marengo; Analytical and Bioanalytical Chemistry, under revision.*
4. **"Conservation of frescoes: a new non-invasive tool"**, *Marcello Manfredi, Emilio Marengo, Elisa Robotti, Marco Bobba, Greg Bearman, Bill Christens-Barry, proceedings del congresso "Diagnosis for the*

conservation and valorization of cultural heritage" , 13-14 dicembre, Napoli, Printed - ISBN 978-88-908168-0-2.

5. **"The Leon Levy Dead Sea Scrolls Digital Library: the digitization project of the Dead Sea Scrolls"**, *Pnina Shor, Greg Bearman, Marcello Manfredi, Emilio Marengo, Journal of Eastern Mediterranean Archaeology and Heritage Studies and Society, in press.*
6. **"Measuring Changes in Cultural Heritage Objects with Reflectance Transformation Imaging"**, Manfredi M., Williamson G., Kronkright D., Marengo E., Jacobs M., Bearman G., Proceeding of Digital Heritage 2013 Conference IEEE, 2013.
7. **"Quantitative multispectral imaging for the detection of parchment ageing: a comparison with ATR-FTIR, GC-MS and TGA analyses"**, *Marcello Manfredi, Greg Bearman, Fenella France and Pnina Shor, Emilio Marengo, under revision.*
8. **"Portable Diffuse Reflectance Infrared Fourier Transform (DRIFT) technique for the non-invasive identification of canvas ground: IR spectra reference collection",** *Marcello Manfredi, Elettra Barberis, Emilio Marengo, under revision.*
9. **"A new method for the non-invasive detection of morphological and physical damages in paintings using imaging 3D",** *Marcello Manfredi, Greg Bearman, Greg Williamson, Dale Kronkright, Eric Doehne, Megan Jacobs and Emilio Marengo, Sensors for Cultural Heritage Diagnostic, Sensors,* ISSN 1424-8220, in press.
10. **"Portable non-invasive imaging method for monitoring the conservation of frescoes",** *Marcello Manfredi, Greg Bearman, Bill Christens-Barry, Emilio Marengo, under revision.*
11. **Handbook of Food Analysis 3rd edition - chapter 30 organic bases** CRCPress (Boca Raton, Florida, USA).

12. "**A traceability study on the Moscato wine chain**", Aceto M., Robotti E., Oddone M., Baldizzone M., Bonifacino G., Bezzo G., Di Stefano R., Gosetti F., Mazzucco E., Manfredi M., Marengo E., Food Chemistry 138 (2013) 1914–1922.

Conference presentations:

1. **LED multispectral Imaging for the monitoring of conservation state of cultural heritage,** *oral presentation Workshop Italiano di Chemiometria, Albano Laziale, 26-28/05/2011*.
2. **A new technique based on LED multispectral Imaging and multivariate analysis for monitoring the conservation state of the Dead Sea Scrolls,** *oral presentation***,** *Congresso Europeo di Chimica Analitica, Euroanalysis XVI, Belgrade, 11-15/09/2011*.
3. **Monitoring the conservation of cultural heritage with imaging spectroscopy: how to distinguish physical-chemical changes from shape changes,** *poster Congresso Nazionale della divisione di Chimica Analitica 16-20/9/2012Isola d'Elba.*
4. **Direct Analysis in Real Time Mass Spectrometry for the non-invasive identification of conservation treatments of the Dead Sea Scrolls,** *oral presentation al Congresso Nazionale della divisione di Chimica Analitica 16-20/9/2012, Isola d'Elba*.
5. **A VIS-NIR Led imaging and chemometric approach for monitoring the conservation state of Dead Sea Scrolls,** *poster al Congresso Nazionale di Spettroscopia NIR 27-28/9/2012, Padova*.
6. **Using a Conservation Damage Detection Tool Through Spectral Imaging,** *oral presentation Parchment Research Update at the Library of Congress, 16/2/2012, Washington, D.C.*

7. **Sistema innovativo per il monitoraggio degli affreschi di Santa Maria di Castello: conservazione programmata e diffusione,** *oral presentation Convegno sugli affreschi di Santa Maria di Castello, 22/6/2012, Valle Lomellina (PV).*
8. **Conservation of frescoes: a new non-invasive tool**, *oral presentation* "Diagnosis for the conservation and valorization of cultural heritage", 13-14 dicembre, Napoli.
9. **Optimization of the extraction of the volatile fraction from honey samples by SPME-GC-MS, experimental design and multivariate target functions based on principal component analysis,** *oral presentation Congresso Nazionale della divisione di Chimica Analitica 16-19/9/2013, Sestri Levante.*
10. **Non-destructive identification of conservation treatments of the dead sea scrolls by using DART-MS,** *poster Congresso Nazionale della divisione di Chimica Analitica 16-19/9/2013, Sestri Levante.*
11. **Measuring changes in cultural heritage objects with Reflectance Transformation Imaging,** *oral presentation Digital Heritage Conference 2013, 28 ottobre – 1 Novembre 2013, Marsiglia.*
12. **From Documentation to Discovery: Preservation Photographic Imaging Leaps from the Illustrative to the Quantitative,** Dale Kronkright, John ffrench, Greg Bearman, Marcello Manfredi, Greg Williamson, Eric Doehne, John Delaney, *Museum Computer Network 2013, 20-23/11/2013, Montreal.*
13. **Authentication and traceability studies on truffles from Piedmont,** E. Mazzucco, M. Oddone, E. Robotti, F. Gosetti, M. Manfredi, M. Aceto, E. Marengo, IX Congresso Italiano di chimica degli alimenti, 3-7/6/2011, Ischia.

ABSTRACT

The aim of this doctoral thesis is the development and application of analytical and statistical techniques for the non-invasive monitoring and analysis of cultural heritage.

In particular, my research focused on the development and application of non-invasive imaging techniques for monitoring the conservation state of artwork and the development of non-invasive methods for the characterization of objects of art by using direct analysis in real time mass spectrometry (DART-MS) and diffuse reflectance infrared Fourier transform spectroscopy (DRIFT).

My research activities were carried out in collaboration with the Israel Antiquities Authority (Jerusalem), the Library of Congress of United States of America (Washington D.C.), the New Mexico Highland University (Las Vegas, NM, USA) and the Georgia O'Keeffe Museum (Santa Fe, NM, USA).

The monitoring of cultural heritage objects over time is critically important in order to alert the conservator when potentially damaging changes are occurring.

The purpose of this research is the development of a non-invasive technique based on LED Multi-Spectral Imaging coupled to statistics for monitoring the conservation of cultural heritage objects, specifically of the Dead Sea Scrolls (DSS).

The method described follows a new approach in the context of cultural heritage aimed at the automatic and fast detection of a developing deterioration process, and its localization and identification. This requires the direct measurement of the reflectance spectrum of the artifact through a non-invasive method, leaving the object unchanged for successive examinations, and the use of statistics.

We tested the method monitoring the degradation of parchment artificially aged using light, temperature and relative humidity.
The technique is now in use for monitoring the conservation of the Dead Sea Scrolls, which are manuscripts of inestimable archaeological cultural and religious value. A number of fragments have been selected for periodic imaging and analysis. These are representative of the state of the scrolls as identified by the conservators. Issues include delamination, gelatinization, organic residues and cockling.
The technique was also used for monitoring the conservation state of S. Maria di Castello frescoes in Valle Lomellina (PV) for which we developed a portable LED multispectral imager.

Usually, the evaluation and quantification of changes and defects of cultural heritage results mostly from an optical and subjective assessment, comparison of the previous and the subsequent state of conservation and by means of condition reports. We developed a reliable 3D imaging method for the non-invasive detection of morphological and physical changes in paintings and drawings. Using reflectance transformation imaging we were able to provide detailed information on the geometry and morphology of painting and drawing surface.

A part of my research focused on the development of a quick and direct method for the non-destructive identification of the various interventions of parchment by means of direct analysis in real time (DART) ionization and high resolution time-of-flight mass spectrometry and chemometrics. Due to the high sensitivity, simplicity and no sample preparation requirement, the proposed analytical methodology may help conservators in the challenging analysis of unknown conservation treatments in cultural heritage. In particular, this method could be very useful for the Dead Sea Scrolls conservation because in the first years after

their discovery they were unknowingly mishandled and subjected to interventions which eventually were found to be harmful.

A portable diffuse reflectance infrared Fourier transform (DRIFT) method for the non-invasive characterization of grounds in painting was developed: with this method there is no need to touch the sample and the analysis can be done directly on site. No sample needs to be removed to analyze the object and, in fact, a number of areas on the object can be analyzed quickly in a non-destructive manner. We prepared 16 canvas grounds: all of them were used by the most important artist from XIV to XX century such as Vasari, Mantegna, Veronese, Caravaggio, De Chirico and we performed the analysis using DRIFT, building a reference library of spectra. We also applied the method on a real canvas from Moncalvo.

The technique was also applied for the non-invasive characterization of parchment and the results were compared to the bench IR instrument spectra.

1. INTRODUCTION

Cultural heritage are all the artifacts that are in libraries, archives, churches and museums and that are of cultural or historical value.

The study of cultural heritage, archaeological, historical, artistic and archive, library or museum objects must be dealt with on an interdisciplinary level, making use of different experiences and skills necessary in achieving a common objective: preservation of the original object, both substrate and the media that contains the information on the object.

Today, in a context of globalization, cultural heritage is widely recognized as a vehicle of cultural identity and reflects the multitude of characteristics that make each country so unique in its diversity. The long term conservation of these symbols of historical and social identity is a challenge that could be overcome only with an interdisciplinary approach, creating new partnerships and collaborations, using new conservation technologies and promoting their diffusion.

The aim of conservation is to obviate damage liable to be caused by environmental or accidental factors which pose a threat in the immediate surroundings of the object to be conserved. The materials making up the cultural property are subjected to changes along time, due to the interaction between the object and the physical factors (light, temperature, relative humidity, etc…), the chemical factors (atmospheric oxygen, various pollutants) and the biological agents (bacteria, fungi, insects etc...). It is very important the monitoring of the artifact along time in order to alert the administrator or the conservator when dangerous situations are taking place.

The Archaeometry is an experimental discipline that uses chemical-physical and computer methods to conduct multidisciplinary research in various fields of art;

it is also able to guide, with real-time diagnostics, operations of maintenance and restoration of cultural heritage objects.

Many of these investigative techniques were optimized and interconnected in order to be able to carry out a diagnostic action, without requiring the movement of the object to examine from the place where it is usually preserved; the technique of investigation must usually have certain requirements: fast, economic, and especially it should not require invasive sampling (non-destructive analysis).

The results of all surveys are transferred to conservator, art historian researchers and archaeologists who, according to the diagnostic results obtained, reconstruct a "medical chart" of the object, complete with detailed information about the technique used by the artist, any previous restoration, the current state of conservation, art historical observations, comparisons with other similar works by the same author or authors of the same period.

In the last years the targets of the research in this field has concerned the development of monitoring methodologies that not only do not damage the object of art, leaving it unchanged for successive examinations, but that were also respectful of the museum or the environment in which the appropriate equipment must operate.

The technological innovations in electronic components and in laser and fiber-optic technology enabled the development of non-invasive methodologies and portable instrumentation for in situ studies of artwork.

The aim of this doctoral thesis is the development and application of analytical and statistical techniques for the non-invasive monitoring and analysis of cultural heritage. In particular, my research focused on the development and application of non-invasive imaging techniques for monitoring the conservation state of artwork and the development of non-invasive methods for the characterization of objects of art by using direct analysis in real time mass

spectrometry (DART-MS) and diffuse reflectance infrared Fourier transform spectroscopy (DRIFT).

2. MONITORING OF ARTWORKS USING IMAGING TECHNIQUES AND STATISTICS

2.1 MONITORING PRINCIPLES

Multivariate techniques are able to extract systematic information from complex datasets. Coupled with statistical process control tools[1, 2] these techniques can be very useful in the field of cultural heritage to monitor the conservation state of artifacts.

Multivariate Statistical Process Control (SPC)

Statistical process control is widely used in industrial applications, but can also be advantageously applied to cultural heritage monitoring[3, 4]. The aim of this research is automatic detection of a deterioration process in the substrate, as well as its localization and identification (i.e., which wavelengths are involved) before the human eye can detect the damage.

Collecting a multispectral or 3D images and using multivariate analysis allows the user to build control charts treating the object as a process to be monitored and controlled. The first step, as with implementing industrial process control, is to collect the data to build a training set to measure the system's natural variability, and the process is then monitored over time. If the natural variability of the imaging system is not correctly assessed at the outset, false/erroneous alarms or insufficiently sensitive charts will be obtained.

Diagram of the monitoring approach

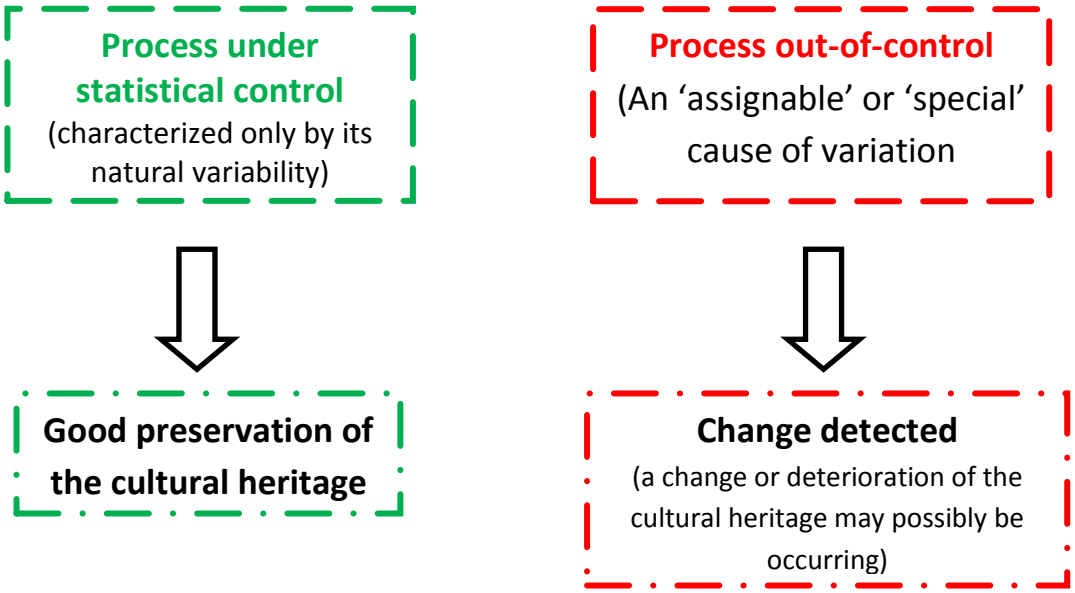

Principal Component Analysis (PCA)

The multivariate approach represents the only possible choice when datasets are characterized by a large number of variables and/or objects. In the present case, when multispectral images are used, the dataset is challenging, due to complex correlation patterns related to the use of a spectral description of the surface (obtained from the spectral imaging)[5, 6]. A rationalization of the problem can be obtained by means of Principal Component Analysis (PCA). PCA may enhance the ability to separate the systematic information from the experimental noise and the natural fluctuations. PCA provides a new set of orthogonal variables, a linear combination of the original components, to describe the system under investigation in a very compact and efficient way. This analysis can provide several types of information useful for pattern recognition analyses. The most important are: the *scores* (**T** matrix), namely the projections of the objects onto the space given by the relevant PCs and the *loadings* or *weights* (**L** matrix), the coefficients of each original variables in the linear combination

defining each PC. In the present paper PCA is performed on the characterization data providing information on the sources of variability that characterize the dataset. The degradation images are then projected onto the relevant PCs from the original characterization data. The analysis of the scores of the degraded images allows the identification of the presence of relevant changes caused by the degradation process, while the analysis of the loadings (calculated on the characterization dataset) may suggest the potential causes that produced the changes.

Using the subset of relevant PCs it is possible to rebuild the original dataset (matrix **X'**). In this way it is possible to filter, for example, the experimental noise or the unnecessary information:

$$\mathbf{X'} = \mathbf{T} \cdot \mathbf{L} \qquad \text{(eq. 1)}$$

The difference between the original data and the re-calculated data from the relevant PCs is called *matrix of the Residuals* (**R**) and contains the information not accounted for by the PCs used to recalculate **X'**. Normally the residual matrix is expected to contain only noise and random fluctuations. In the present case it may contain systematic information connected to the eventual presence of new species that were not present during the characterization step, species originated from the degradation process. These species were not present during the characterization phase so that they cannot be accounted for by the PCs. They represent new information[7, 8] that will be present in the **R** matrix. In this case the **R** matrix will contain systematic information, beside the expected random noise and natural system fluctuations: this systematic information can be detected by performing a further PCA on the residual matrix.

Multivariate Shewhart Chart

Shewhart control charts are a powerful tools for monitoring industrial processes and identifying the presence of assignable causes of variation. Anomalous process behaviors can be identified either when any point falls outside the ±3σ region, corresponding to a confidence level of more than 99% or when systematic trends are present. The control limits of this region are the upper control limits (UCL) and the lower control limits (LCL), which are calculated using the respective formulas:

$$UCL_{\bar{x}} = \bar{x} + 3 * sd(\bar{x}) \quad \text{(eq. 2)}$$

$$LCL_{\bar{x}} = \bar{x} + 3 * sd(\bar{x}) \quad \text{(eq. 3)}$$

where $\bar{x}$ is the mean score of a pixel at a defined PC and *sd* is its standard deviation. For multispectral methods the Shewhart control charts were constructed using the scores of the relevant PCs, instead for 3D imaging control charts were built using the Cartesian coordinates of the surface normal vector, as will be discuss in the next chapters. In this way if a sample violates the natural correlation structure characterizing the dataset, this sample will show anomalous score values or residuals and will be recognized from their analysis[9, 10].

IMAGE REGISTRATION

Image registration is critical, since mis-registered pixels between imaging sessions would show up as spectral changes, indicating a change on the surface. Our methods requires registering and comparing the same pixel for each imaging session with the *before* pixel. We used an extensive series of images taken sequentially to investigate methods for image registration, determine

registration errors and measure their effect on the sensitivity of the method and false positives. Since it is not possible to repeatedly replace and image an object on the spatial scale of a pixel (~20 microns), the burden falls to software. Registration errors show up most easily at the edges of the object. This makes sense specially in multispectral images: i.e. the biggest spectral difference is between ink and parchment, so a mis-aligned pixel that is (ink-parchment) when it should be (ink-ink) will show up as a changed pixel since it now has very different spectrum than the previous image. After all, an ink pixel is much closer spectrally to the ink pixel next door than to any parchment pixel (likewise for the parchment), so registration errors in areas of *all* ink and *all* parchment away from edges are reduced. Binning the data significantly reduces the effect of registration errors and also reduces the number of false positives.

To register images taken in different imaging session we used an open source image processing packaged based on imageJ called FIJI[11].
In particular we used Turboreg and bunwarpj tools, to align images, which are briefly described below.

TURBOREG

Turboreg is an automatic sub-pixel registration algorithm that minimizes the mean square difference of intensities between a reference and a test data set, which can be either tri-dimensional (3-D) volumes or bi-dimensional (2-D) images. It uses spline processing, is based on a coarse-to-fine strategy (pyramid approach), and performs minimization according to a new variation of the iterative Marquardt-Levenberg algorithm for non-linear least-square optimization (MLA). The geometric deformation model is a global 3-D affine transformation, which one may restrict to the case of rigid-body motion

(isometric scale, rotation and translation). It may also include a parameter to adjust for image contrast differences[12].

BUNWARPJ

bunwarpj is an algorithm for elastic and consistent image registration developed as an ImageJ plugin. It performs a simultaneous registration of two images, A and B. This image registration algorithm is based on the minimization of an energy functional that includes the dissimilarity between the source and target images that have to be registered. We use the standard SIFT algorithm for automatic features extraction, which allows for both rigid body (rotation and translation) as well elastic deformation of images[13].

2.2 MONITORING SURFACES USING MULTISPECTRAL IMAGING

Multispectral imaging or imaging spectroscopy has been developed by combing digital imaging and spectroscopy. Modern imaging technologies have had a significant impact on archaeology. Spectral imaging of manuscripts has been applied to improve the readability of documents and to assist in the assessment of their condition[14]. The technique is well accepted in biology, medicine, atmospheric studies, marine ecology and pollution control[15-17]. Caltech/NASA's Jet Propulsion Laboratory (JPL) has long been a leader in the application of this technology. Much research was originally conducted by remote sensing aircraft or orbiting spacecraft, but there is considerable a body of literature documenting its laboratory use for improving document legibility[18], unscrambling palimpsests[19], and analyzing the materials of paintings[20, 21].
Imaging spectroscopy is a non-destructive, portable, fast and economical technique that can represent a powerful tool for the study of cultural heritage.

2.2.1 Imaging techniques: state of art

The spectral imaging process obtains a complete spectrum for each pixel of the image. The potential applications are innumerable.
There are two main methods of capturing spectral imaging data: one is to illuminate the sample with broadband light and filter the image detection, separating wavebands by filtering between the object and the camera, while the other method is to filter the illumination or use narrow waveband illumination in conjunction with an unfiltered camera. This second method has conservation advantages due to reduced light levels and heat compared to the former.

There are many interesting studies that use imaging spectroscopy methodologies in cultural heritage: in table 1 are listed the main characteristics of the systems used [22].

Detectors	Illumination system	Spectral range	Dispersing element	Spectral resolution/number of filters	Applications	Ref.
CCD	Quartz halogen floodlights	650 - 1050	LCTF	10 nm	Inks, pen drawings, paintings	[23, 24, 25]
PbO-PbS Vidicon	150W quartz tungsten-halogen placed at 45°	420 - 1550	Narrow-band Optical filters	29 (20nm from 420-700nm, 50nm from 750-1200nm and at 1300, 1400, 1445 and 1550nm)	paintings	[26, 27, 28]
PbO-PbS Vidicon	150W quartz W-halogen at 45° with UV-cutting glass	400 - 1700	Narrow-band Optical filters	32 (20nm on the VIS region and 50nm on the NIR region)	drawings in paper	[29]
CCD	3200K 150W QTH-lamp 2fiber-optics 45°/0°/45°	400 - 900	Prism-grating-prism Line spectrograph	Spectral pitch of 0.89 nm	Historic surfaces, wall painting	[30]
CCD	Polychromatic UV-Vis-IR	400 - 1000	Imaging monochromator	2nm tuning step	manuscripts	[31]
CCD	Polychromatic UV-Vis-IR	380 - 1000	Imaging monochromator	3nm tuning step	palimpsests	[32]
CCD	Polychromatic UV-Vis-IR	360 - 1150	Tunable optical filter	34 spectral band	palimpsests	[33]
CCD (VIS-NIR) PtSi (SWIR)	500W, 3200Kquartz halogen lamps	450 - 1600	Optical filters	8 VIS-NIR and 3 SWIR	painting	[34]
CCD (VIS-NIR) InGaAs (SWIR) CCD (luminescence)	1000W halogen lamps at 50° Slide projectors with 380-520 nm filters at 45° (luminescence)	417 - 973 VIS-NIR 895 - 1749 SWIR 650 – 900 luminescence	Grating spectrometer Interference pass Bands filters (luminescence)	2.25 nm VIS-NIR 10nm SWIR 6 spectral bands luminescence	paintings	[35]
/	/	400-2500	Optical filters	15 spectral bands VIS-IR reflectance 7 spectral bands luminescence	Illuminated manuscripts	[36]

2.2.2 Multispectral imaging for monitoring of parchment

The monitoring of cultural heritage objects over time is critically important in order to alert the conservator when potentially damaging changes are occurring. The method described follows a new approach in the context of cultural heritage aimed at the automatic and fast detection of a developing deterioration process, and its localization and identification. This requires the direct measurement of the reflectance spectrum of the artifact through a non-invasive method, leaving the object unchanged for successive examinations. While our current work involves texts on parchment and papyrus, the method is extensible to other objects.

The utilization of multispectral imaging and digital image processing can be beneficial for the preservation of cultural heritage objects. For the case of the Dead Sea Scrolls, mostly on parchment, it is known that the changes in legibility are driven by changes in the parchment reflectance in the visible. Spectral imaging showed that the easy to read scrolls show significant differences between the ink and parchment spectra in the visible, while they are very similar for hard to read ones. However, for the illegible scrolls, the parchment reflectance increases significantly relative to the ink in the IR, which is why infrared photography of the scrolls, done in the early 1950s was successful[37, 38]. These changes in reflectance suggest a natural way to monitor the scrolls for changes, namely monitor the reflectance through repeated imaging, analysis and comparison.

A method based on multispectral imaging coupled to multivariate analysis is proposed for monitoring the state of health of cultural heritage objects surfaces and, in general, for every kind of surface whose conservation state needs to be monitored.

2.2.3 Monitoring virtual degradation

To test the algorithms a multispectral image of a DSS parchment, IAA inventory plate # 279, 4Q501 Apocryphal Lamentations B (dated between 50-25 BCE[39]) was used (Fig. 1). The applicability of the approach and its limitations were studied by generating virtual images of the parchment containing the artificially degraded region.

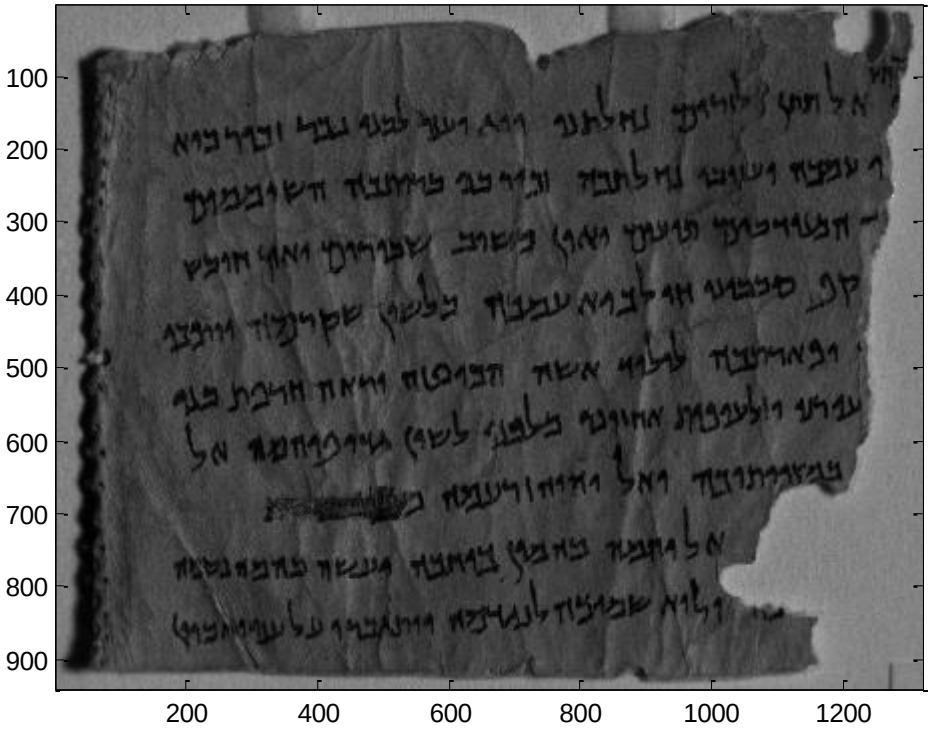

Fig. 1: Dead Sea Scrolls image at 960 nm.

Experimental

The multispectral image of a Dead Sea Scroll parchment (4Q501-279, Apocryphal Lamentations B) shown in figure 1 was chosen for the simulation.

The parchment imaging was performed at 35 wavelengths from 650-990 nm in 10 nm steps. Data was captured using a CRI Nuance Imaging Spectrophotometer (CRI, MA,USA) and normalized by dividing for a white

reference cubes obtained acquiring a 99% reflecting lambertian reflector (Spectralon®) in order to have reflectance spectra between 0 and 1.
All the algorithms necessary for the treatment of the data were developed using MATLAB (R2007b, The MathWork, USA).

The applied procedure

The procedure applied in this research was to evaluate the applicability and the limitations of spectral imaging by utilizing and manipulating simulated data. The following steps constitute the range of factors under consideration.

(1) *Addition of noise* – In order to be able to characterize what can be considered a natural variability of the images, it is necessary to have several images of the same objects, recorded over time while no degradation changes have occurred to the object. These images must account for all the natural variability sources, for example: instrumental noise, small alignment errors, normal hysteresis of the object, etc. In the present case noise was artificially added to the spectral images in order to simulate the natural experimental variability. A white noise was employed to this purpose. Different images were generated with the addition of a random white noise and the images were successively used to evaluate the control limits of the Shewhart charts built on the relevant principal components. In agreement with experimental evidence, the maximum white noise level was established to be 0.01 reflectance units with respect to the spectral intensity measured in each pixel for each different wavelength. This procedure was applied to obtain five different replications of the starting image of the DSS, obtaining at the end five image cubes of the DSS in presence of the white noise. These cubes were used for calculating the relevant PCs and the control charts limits.

(2) *CUBEs unfolding* - The cubes are unfolded into a bi-dimensional matrix (**X**) where the columns are the 35 wavelengths and the rows are the pixels of the different images. The columns are mean centered prior to any statistical analysis (auto-scaled).

(3) *Sampling of the dataset* - A good characterization of the in-control natural variability needs several cubes to be processed simultaneously, a process that requires a large volume of memory (in the level of the Giga- or Tera-bytes). A random selection of individual pixels that preserves both the macro and micro information present in the cubes was then tested. This sampling was performed on the rows of the data matrix and provided a representative dataset. Different percentages of the number of pixels present in the images (sampling percentages) were compared to select the best compromise between memory requirements and quality of the results. For every cubes of characterization were then sampled the same random pixels. A PCA was performed on six different datasets obtained by randomly selecting six different percentages of pixels. The loadings were compared with the aim to identify the minimum percentage of pixels that preserves the information present in the cubes.

(4) *Principal component analysis* - PCA was performed on the 5 CUBES of the dataset. This step enables the description of the in-control natural variability by means of the relevant PCs that take into account the systematic relationships present in the data. These relationships may include the covariance structure and the different sources of systematic information, like the presence of different figures or different colors.

(5) *Multivariate control chart* - Multivariate Shewhart charts are then calculated using the scores of the relevant PCs obtained in the characterization phase. It is possible from the training set data to calculate

the upper and lower control limits (UCL and LCL) that permit to identify the pixels that show anomalous behaviors along time.

(6) *Deterioration of the parchment* - The deterioration of the parchment was simulated by degrading the data cubes that had previously had white noise included. A Gaussian shape modification with predetermined size was added to each multispectral image of the cube. All wavelengths were interested by the degradation: the intensity of the Gaussian shape increased from Visible to IR in order to simulate the parchment deterioration spectra described by Bearman et al[40]. The Gaussian shape was used in order to evaluate how the control charts detect a vanishing effect of the degradation at the border of the Gaussian shape.

(7) *Monitoring of the parchment* - The "virtually aged" cubes were unfolded and centered using the mean calculated in the training session and the new data were projected onto the PC space previously obtained. The scores of the new image created were then compared with the LCL and UCL to identify the pixels whose variation exceeds the control limits. Contribution plots show the contributions of each wavelength to the aged image for a defined pixel. These plots allow the assessment of which wavelengths were most affected by a significant degradation.

(8) *Analysis of the residuals* - As previously indicated, a further principal component analysis of the residuals matrix obtained after re-projection of the degradation images along the relevant PCs provided information on the eventual presence of new sources of variation, namely the formation of new compounds of the surface.

Results and discussion

During this work the main assumption was that the experimental noise present in different replicated shots comes uniquely from instrumental noise (white noise).

Before starting the simulation, a preliminary study was performed to identify the optimal percentage of pixels of the images that needed to be sampled in order to obtain stable and reliable results: preserving both the macro and micro information present in the cubes.

Six different percentages of pixels randomly sampled from the 5 cubes, namely 100%, 10%, 1%, 0.1%, 0.01% and 0.001% were compared with the original image. PCA was performed on the 6 auto-scaled (mean centered) datasets obtained from the different random samplings and the original image. Figure 2a shows the loadings of the first principal component for the different samplings: it is evident that the loadings preserves the information present in the cubes down to a 0.1% sampling.

The pattern of the 0.01% and 0.001% samplings are different from the others and show that these choices produce results that differ significantly from the raw images. As a consequence of these results we used a 0.1% sampling.

Training set

The results of PCA performed on the auto-scaled simulated characterization images show that the first two PCs account for almost the total amount of the original variance (99.21%).

The score-plot of PC_1 and PC_2 is showed in figure 3b: the pixels (the objects) are well separated along PC_1 in two clusters that represent text (black pixels) and background (white pixels). We must conclude that the first principal component explains the differences between text and background.

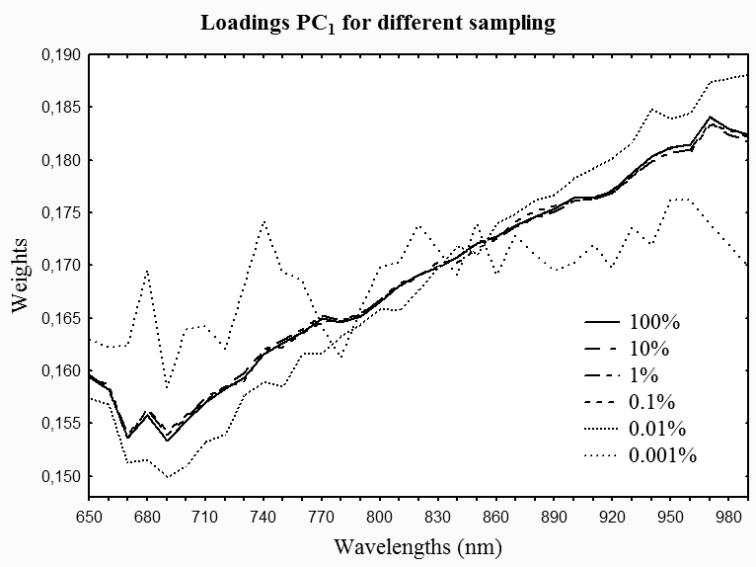

(a)

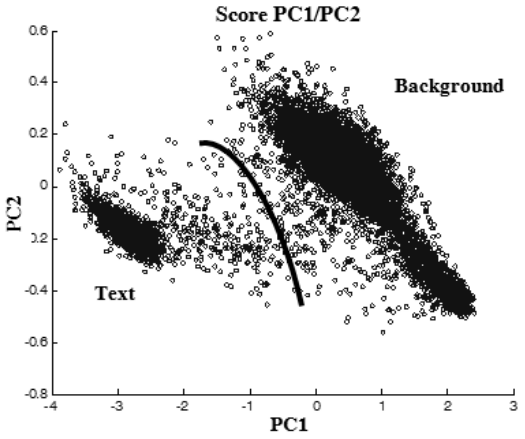

(b)

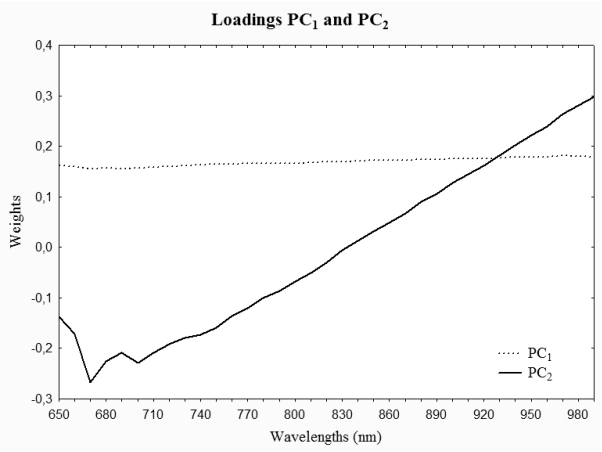

(c)

Fig. 2: loading of PC_1 for different sampling (a), score-plot of PC_1 and PC_2 (b), loading plot of PC_1 and PC_2 from IR (left) to UV (right) (c).

The differences observed in the score plot can be explained using the loading plot showed in figure 2c. The information accounted for by the first component is characterized by an equal contribution of all wavelengths. Instead PC_2 has a typical contrast effect since the contribution of the farthest IR and Visible wavelengths are opposed: it has a positive contribution particularly at 970, 980 and 990 nm and a negative contribution particularly at 670 nm.

Each cube was then projected onto the PC space using the loadings of the first and the second PC. The result is a matrix of scores filtered to account for the information corresponding to the first two PCs respectively where the 35 original channels (35 wavelengths) have been compressed into two new orthogonal channels (PC_1, PC_2). The image obtained from the scores along PC_1 (Fig. 3a) is very similar to the original image (Fig. 1) as only differences related to pigmented and clear areas are accounted for. Figure 3b illustrates the scores of the second component where PC_2 accounts for a significant part of the dataset information.

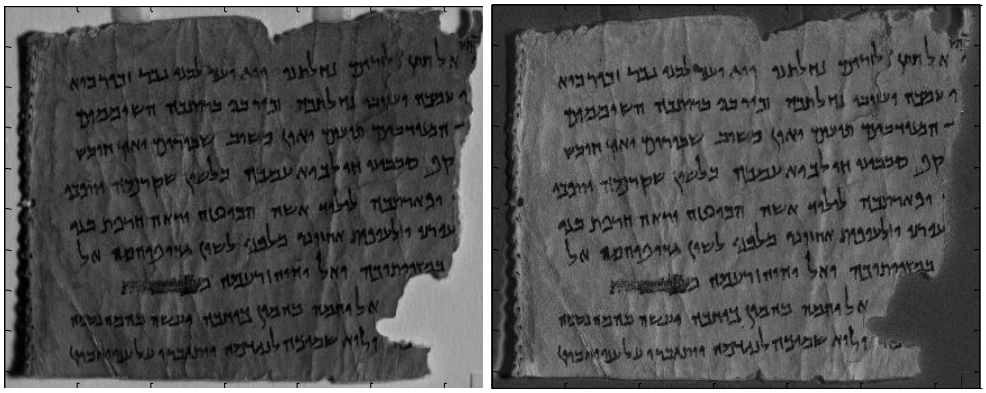

a b

Fig. 3a and b: projection of the score of the PC_1 (a) and PC_2 (b).

Monitoring the deterioration

The deterioration of part of the parchment was simulated by adding to the cubes already modified with the white noise, a Gaussian shape modification with predetermined size. The area of the degradation covered 1600 pixels of the original image and all the wavelengths were interested by the degradation: the intensity of the modification increased from Visible to IR (figure 4b). The spatial intensity of the degradation is a Gaussian surface whose maximum intensity is located in the pixel of coordinates x=400 and y=400 of the original image as shown in figure 4a**.** Parchment degradation was spatially modulated as a Gaussian surface since we want to focus the degradation within a region of

interest, with an effect decreasing homogeneously from the center of the Gaussian surface to the borders; in this way it is possible to evaluate if control charts can detect increasing levels of degradation and how they behave at the border.

In the simulation of the degradation process, the intensity and the area of the Gaussian surface were linearly increased over time, providing three new cubes of progressively more deteriorated images (fig. 4a).

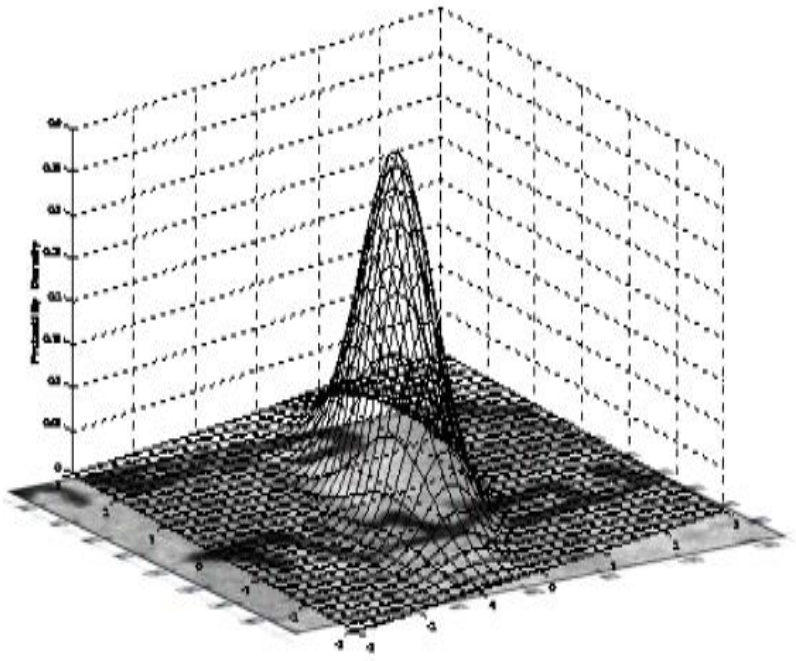

a

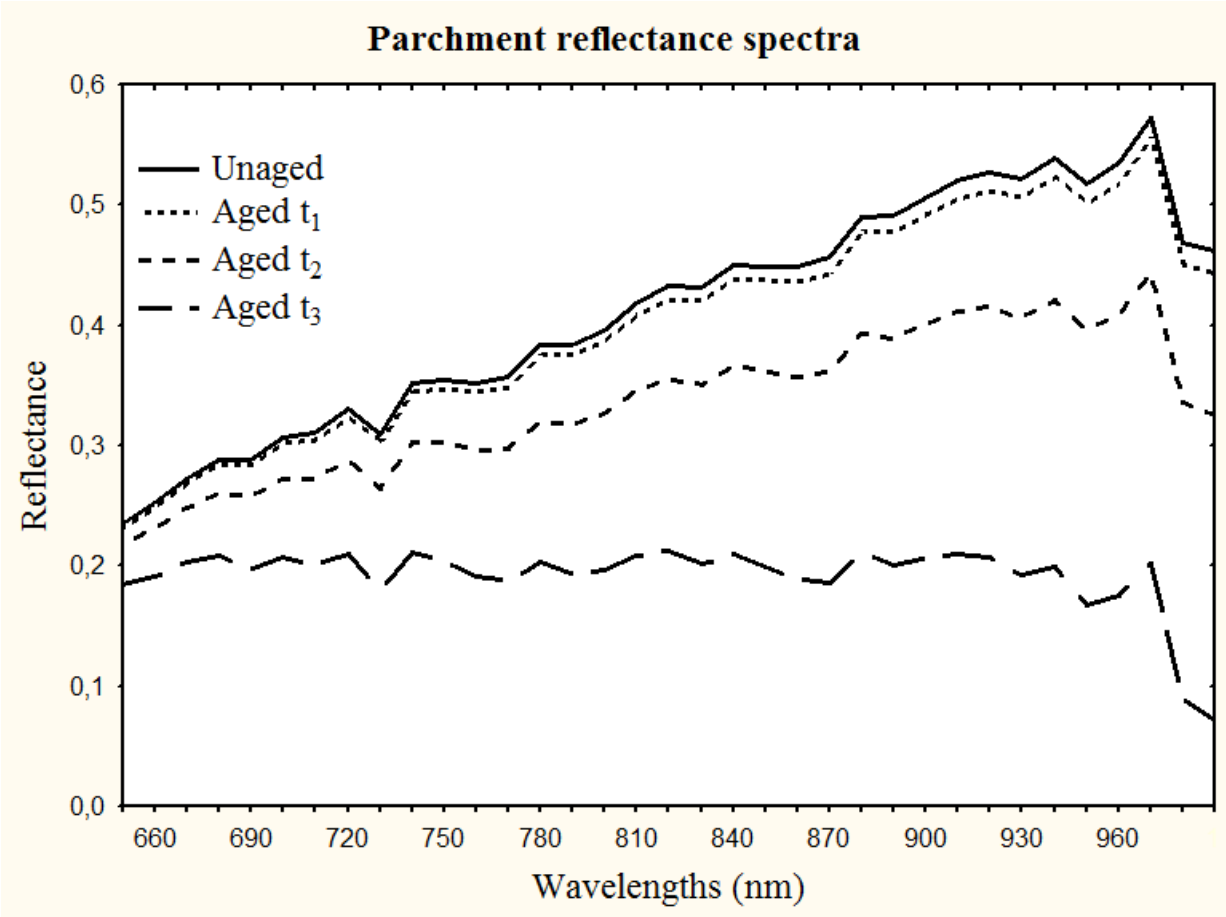

b

Figure 4a and b: degradation shape applied at the images surface of the cube(a), reflectance spectra of un-aged (the upper) and aged parchment over time (b).

Each degraded cube was projected onto the PC space previously calculated from the characterization images and the scores of the PCs were compared with the UCL and LCL limits. The Shewhart control charts for PC_1 and PC_2 are reported in fig. 5b and 5c respectively. These images show how that the control chart is able to precisely identify the degradation process, either with respect to PC_1 and PC_2: black pixels correspond to out-of-control pixel, namely pixels beyond the LCL for PC_2 and the UCL for PC_1. The highlighted areas in the control charts correspond perfectly to the simulated degraded areas, and the charts show how the degradation correctly increases along time.

There are few out-of-control pixels outside the degraded area. These are false alarms and are caused by the natural variability of the imaging system. Since the number of analysed pixels in the image is very large (n=1240800), the probability that few false alarms are present is also quite large. Nevertheless the false alarms do not show a systematic behaviour and they are typically spread all along the image. This explains the importance of controlling very precisely the acquisition of the images and the matching and characterization steps, that permit an accurate account of all sources of natural variability in the experimental system when it is *in-control* conditions.

The contribution plots in figure 5d show which wavelengths are affected by the degradation process of a specific pixel. They can be calculated for each pixel of the image. In the present case, most of the wavelengths contribute to the perceived degradation. This is illustrated in figure 5d, which shows the contribution plot for the pixel of coordinates x=400 and y=400, namely the center of the degradation ellipsoid. Observing the contribution plots (figure 5d) it is evident that the contribution plot of degraded pixel have the same trend of the degraded spectrum (fig 4b).

As the reflectance spectrum decreases the higher the values observed on the contribution plot.

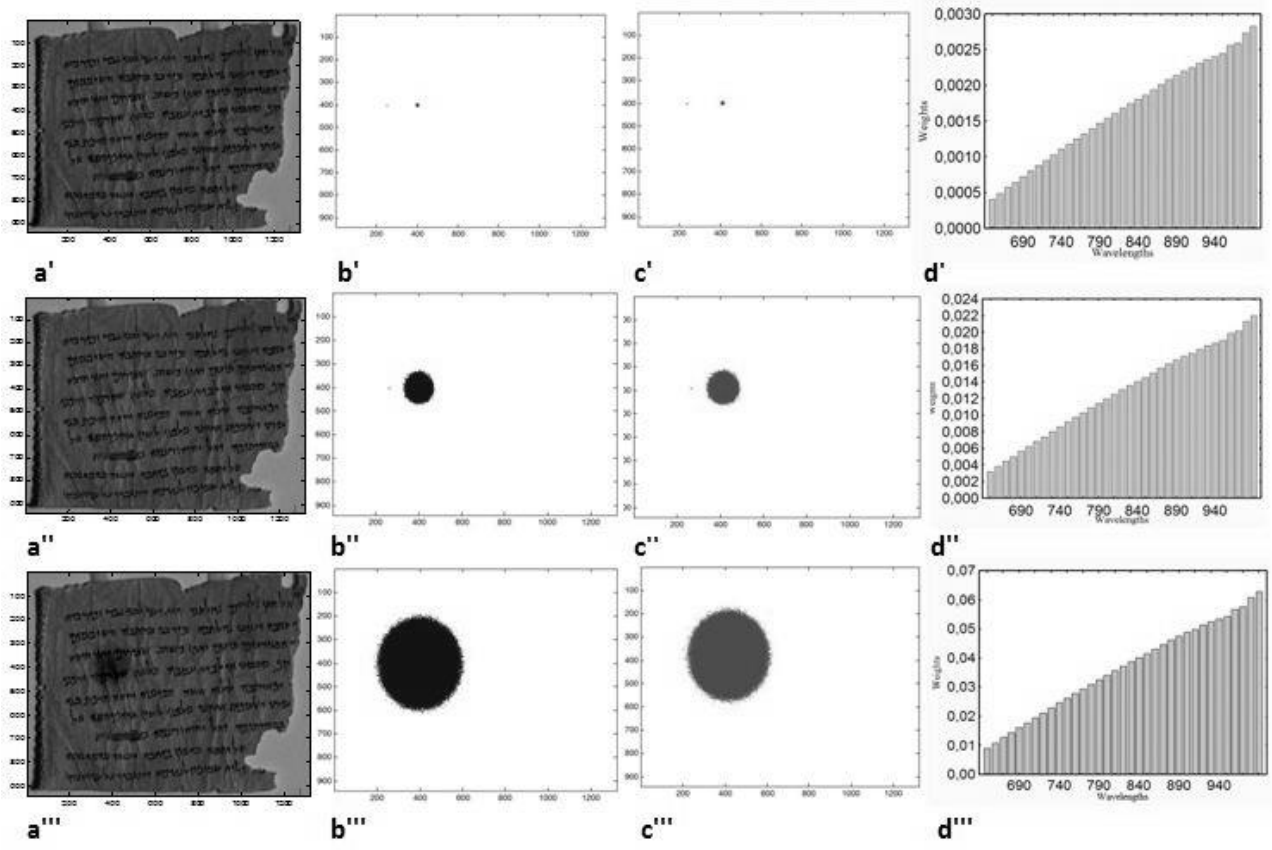

Figure 5a: images of the degraded parchment; 5b: PC_1 control chart; 5c: PC_2 control chart; 5d contribution plot of the pixel in the center of the degraded area.

Control charts also detected the vanishing of the degradation effect at the border of the Gaussian shape used. Figure 6 reports a particular of PC_1 control chart of the degradation at t3: grey pixels correspond to out of control pixels, i.e. beyond UCL, while black pixels represent pixels that are close to the UCL but which are still in control, i.e. beyond 2/3*UCL.

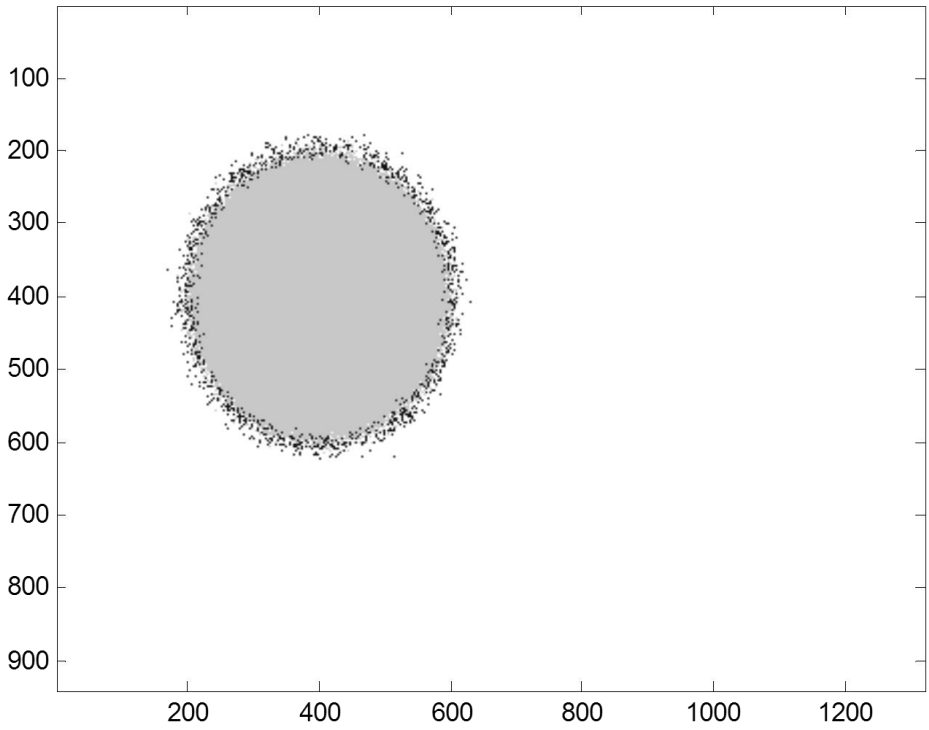

Figure 6: PC_1 control chart of the third degradation with the vanished effect detected (black pixels).

Principal component analysis of the residuals of the degradation analyses

With the aim of further investigating the effects of the degradation process, a new PCA was performed on the residuals data matrix obtained by subtracting the information accounted for by the first two PCs from the degraded images. As previously stated, the residuals contain the information not accounted by the two PCs that contain the systematic information.

The first principal component accounts for 62% of the original variance and was considered the only relevant PC. PC_1 is mainly constituted by the IR wavelengths at 990 and 950 nm. The analysis of the residuals identifies degraded areas only for the third virtual degradation where the ageing process was more intense. The first and the second cases do not evidence unusual distribution of the residuals. Figure 7 illustrates the projection of the scores of

the first principal component of the residuals for the degradation image at t3. As it can be observed, the only information present is related to the degradation. The other part of the image does not show structured information and, for example, the symbols present on the original DSS are not represented as their information is accounted for by the first two PCs employed for the monitoring. The elliptical spot present in the figure that corresponds to the degraded area, is due to changes of the spectra that are not accounted for by the two PCs calculated on the characterization images. This area shows that a new shape of the spectra has originated from the simulated degradation. This new shape of the spectra can normally be associated with the formation of new species on the degraded surface. In the present case, the change of the shape corresponds to the spectra of the gaussian surface that was artificially added to the original image to simulate the degradation.

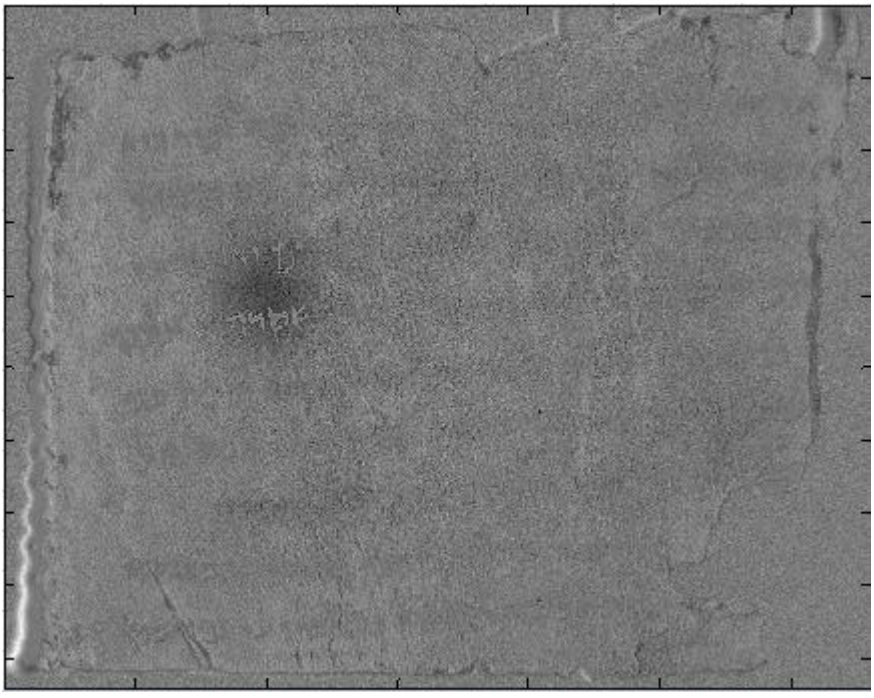

Fig 7: scores of the first component of residuals of the third degradation.

Conclusions

The aim of this research was the development of a non-invasive technique based on multispectral imaging for monitoring the conservation of cultural heritage objects.

The simulation shows that the control charts built on the relevant PCs are able to accurately detect the degradation process. In the first four simulated data scenarios, the degradation was not visible to the human eye, but could be detected by the algorithm. The contribution plots help the analyst to determine which wavelengths are involved in the assessment of the degradation process.

PCA performed on the residuals matrix enabled the identification of effects on the surface not accounted for by the PCs previously calculated, i.e. spectral evidence related to the possible occurrence of structural changes of the sample surface because of the ageing treatment and not just a decrease/increase of the intensity related to the species originally present on the surface.

A crucial step to making this methodology work in a real application is to collect an appropriate training set to measure the system's natural variability: if the natural variability is not correctly assessed false alarm will be obtained.

2.2.4 Monitoring parchment degradation

This study proposes a new method, based on LED multispectral imaging coupled with multivariate analysis, for monitoring the state of the health of parchment surfaces. Therefore, monitoring of the parchment reflectance suggests itself as a natural way to detect changes in the parchment. Our aim is to detect a degradation process of the parchment *before* its effects are visually recognizable, which indicates that significant damage has occurred. Advantages of our method include obtaining large-format images (39 MP), in about a minute with no thermal exposure to the object from lighting.

Spectral imaging acquires samples of the reflectance spectrum for each pixel of the image: the resulting dataset is a three dimensional matrix where the coordinates of pixels are on the x and y axes and the third-dimension is the reflectance of each pixel at a defined waveband. For this work, spectral images were obtained with a 39-megapixel monochrome camera and two LED illumination panels. The system has been extensively tested for thermal effects, and its data acquisition performance is well documented [40, 41].

The Parchment

Parchment is a semi-tanned skin used as a writing surface in Asia Minor as far back as 200 BCE. Of all the components that make up living skin, only insoluble proteins (collagen) and water remain present in parchment. The proteins are grouped together, forming fibers of considerable physical consistency and excellent hydration capacity. Water is the only binding agent, which, as in paper, forms intermolecular bonds that join the fibers by means of hydrogen-bond bridges. The protein fibers are held together cohesively as long as the hygrometric balance is not disrupted. This means that the role of water and, more specifically, humidity, is of prime importance in the conservation of parchments [42-44] . Abrupt changes in humidity and temperature are

parchment's worst enemies. High humidity can degrade the parchment by hydrolysis of the collagen as well as by denaturizing, so there are multiple processes at work. Low humidity and/or elevated temperature can dry out the parchment, locking in any gelatinization of the surface as well as promoting shrinkage and tearing by differential contraction.

The skin is flexible thanks to the natural disposal of its protein fibers, but when the hygrometric balance is lost due to lack of humidity, the skin becomes rigid; desiccation leads to isolation of the protein filaments (linking by means of hydrogen bonds is lost) and this separation reduces flexibility, promoting cracking, exfoliation and even disintegration of the support. In the case of complete saturation with water, the excessive number of water molecules transform the fibers into aggravated gelatins; decomposition of the parchment will be further aggravated by the effect of hydrolysis [45, 46].

Procedure

The procedure developed for monitoring the conservation state of parchment consisted of the following steps:

(1) *Imaging system setup.* A preliminary study of the imaging system in order to identify the best instrumental conditions and the most sensitive operative parameters to be kept under control during the imaging sessions for the sake of data quality and reproducibility.

(2) *Sample Characterization.* The sample's natural variability, including the natural variability of the imaging system must be evaluated and described. The description is accomplished by recording replicated images in multiple wavelengths (cubes) of the surface, before application of any conservation. In our case, the baseline image cubes set the timeline to zero. The set of images obtained in this phase constitute the training set. The parchment in this phase can be considered "in statistical control,"

as no degradation process is active. The baseline cubes also are used to set the standard deviation of the data that serves as a classification parameter for the control charts. Naturally, the larger the variance of the baseline cubes, the less sensitive the method is. For this reason, we have spent considerable time on characterizing system stability and quantitative results. This method *explicitly* requires a stable and repeatable spectral imager that provides excellent quantitative results.

(3) *Cube Registration.* While the individual wavelength images for each cube are naturally registered, it is important that image cubes collected during different imaging sessions be registered

(4) *Unfolding Cubes.* The cubes are unfolded into a bi-dimensional matrix (**X**) where the columns are the 13 wavelengths and the rows are the pixels of the different images. The columns are mean-centered prior to any statistical analysis.

(5) Dataset Sampling. A good characterization of the in-control natural variability requires that several cubes be treated together so that a large amount of memory (several GBs) is necessary. A random sampling must preserve both the macro and micro information present in the cubes. The sampling was performed on the rows of the data matrix, and provided a representative dataset.

(6) *Principal Component Analysis* of the sampled baseline dataset. This enables the description of the in-control situation natural variability by means of the relevant PCs that take into account the systematic relationships present in the data, example its covariance structure.

(7) *Multivariate control chart*. Multivariate Shewhart charts are calculated using the scores of the relevant PCs obtained in the characterization phase. In particular from the training set data it is possible to calculate the upper and lower control limits (UCL and LCL)

that permit identification of the pixels that show anomalous behaviors along time.

(8) *Parchment Monitoring*. The image of the parchment after application of temperature shock is aligned to the characterization images; the cube is then unfolded and centered using the mean calculated in the training session, and the new data are projected onto the PC space previously obtained. The scores of the new image are then compared with the LCL and UCL to identify which pixels variance exceeds the control limits. Contribution plots, which show the contribution of each wavelength to the aging process for a defined pixel, enable us to determine which wavelengths are affected by degradation.

(9) *Residuals Analysis.* As previously indicated, a further principal component analysis of the residuals matrix obtained after re-projection of the degradation images along the relevant PCs provides information on the eventual development of new sources of variation.

Experimental

LED Multispectral Imaging and Parchment.

We used a Eureka Vision LED system from Megavision, CA, USA. The system has a 39-megapixel Kodak CCD monochrome sensor array, size of 49 mm – 37 mm, with 7216 x 5412 pixels, 6.8micron – 6.8 micron, and two EurekaLight™ LED illumination panels. In this method the spectral component is provided by fixed wavelength light emitting diodes (LEDs) that emit in narrow spectral bands over ranges of wavelengths from the near ultraviolet to the near infrared. The LED bandwidth ranges from ~10 nm in UV to 40 nm in the IR. The LED emissions are centered on the following wavelengths: 365, 450, 465, 505, 535, 592, 625, 638, 700, 735, 780, 870 and 940 nm. For principal component analysis, control charts and all other computations, we used the following:

MATLAB (The MathWorks Version R2007b) and Photoshoot (Version 4.0, MegaVision, CA, USA).

Our approach requires a well-characterized, quantitative system that returns absolute reflectance spectra regardless of the imaging setup. Rather than relying on keeping everything the same for each imaging session, we simply measure the absolute reflectance accurately each time. We correct for illumination gradients, LED power variations and camera noise. The system performance and stability have been measured in several ways. One is retrospective, by happenstance: the system has been set up for imaging by Megavision at three locations in the last year and calibration images taken with color standard targets; in each case we obtained the standard color space values and CIE spectral values to within a few percent. We also measured the LED performance-central wavelength, bandwidth and power, and modeled how those changes affected measured reflectance. All of these factors have negligible effect and the system is very stable and reproducible. Results of the measurements and modeling have been reported in the literature [37].

Parchment

A new 15cm x 20cm calfskin parchment (Figure 1a) was used in the present study (Pergamena Parchment LLC, NY, USA). The parchment was marked using a special ink (carbon black, lamp black, Natural Pigments, USA): fourteen symbols were painted on the page. The parchment was aged in a temperature and humidity-controlled oven model 9121 (PGC, NC, USA).

Methodology

Image cubes were corrected, "flattened" for illumination gradients by dividing the image cube by a white reference cube of a standard uniform white balance card (although actually grey). Due to system stability we needed to take

reference cubes only infrequently. The data were then corrected for dark noise, normalized to unit exposure time and unit illumination power and converted to absolute reflectance. The latter is done with a known NIST traceable reflectance standard in the image. With this approach, variables such as location of the light panels, the camera height, the f/stop, etc., are corrected and calibrated out, thus reducing the burden on imaging. However, as noted above, bad quantitative results for reflectance will lead to bad results with this method.

Results and discussion

The choice of instrumental conditions is important for obtaining high-quality spectral images. The resolution used for the imaging session was 599 dpi, the highest resolution available for the size, and the pixels size at the artwork plane was of 0.04 mm.

The light exposure of each waveband depends on the reflectance of the sample in that band and must be set individually for each band. The exposure times were determined by the Photoshoot software to set the maximum signal at a specified percentage of the CCD well depth.

(a)

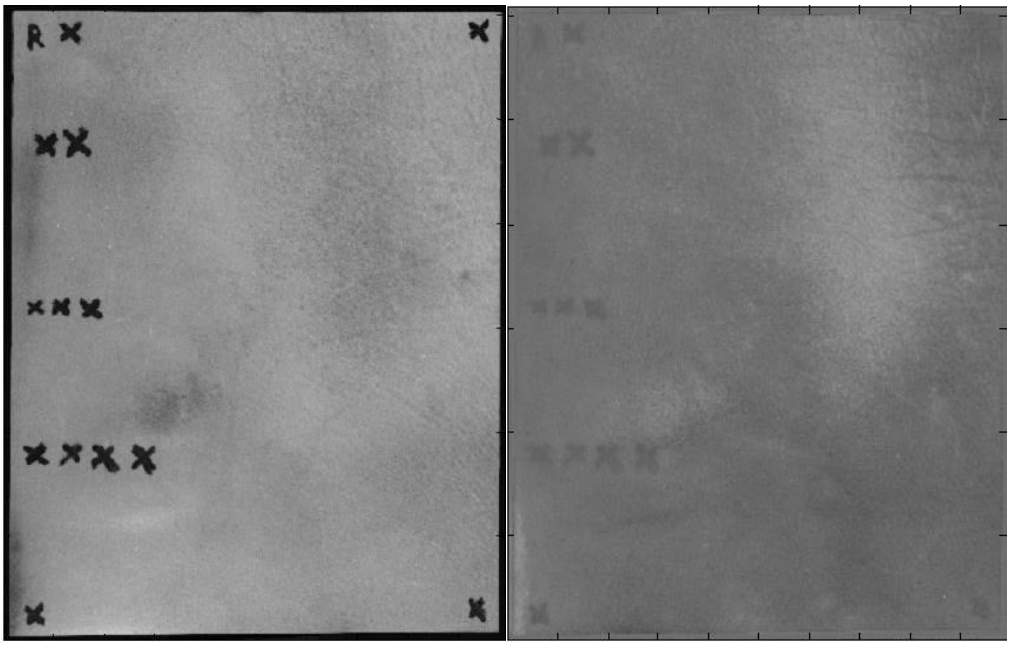

(b) (c)

Figure 8: Color image of the parchment used in the present study (a); projection of the score of the PC_1 (b) and PC_2 (c).

This was chosen to be 75% for these samples, which provides adequate dynamic range without clipping either extremum. The increase in temperature of illuminated LEDs changes the central wavelength and bandwidth, though their small thermal mass ensures that the temperature difference relative to the much larger heat sink is rapidly reduced. The camera software allows insertion of a delay between turning on the LED and acquiring the image.

We determined that a 100 ms delay was sufficient when shooting at f/8 to allow the LEDs to thermalize and stabilize [47].

Training set - A set of multispectral images was recorded and used as training set to characterize system variability for statistical control, i.e., before any aging. This was achieved by replicating the multispectral imaging acquisition of the parchment surface. The effect of some operative factors, such as the location of parchment, instrument settings, time of day, and location of LED panels, were tested to account for sources of variability that could affect monitoring over time. These factors were intentionally varied during the characterization step:

moving the parchment in different positions; switching the instruments on/off; changing the instrumental conditions and returning them to the original setting; simulating other imaging sessions during the characterization; recording the images at different times of day; moving the panels of LEDs and returning them to the original position. Thirty-three cubes were recorded in optimal instrumental conditions as previously defined.

Each field of view contained a 99% reflecting lambertian reflector (Spectralon®) and mini-color checker by X-Rite for post-processing normalization of the incident LED power and to provide an absolute reflectance standards. The CIE spectral values of the X-Rite color checker were measured separately as part of the calibration program and provided references for creating high-fidelity images using the 6 visible bands.

Each cube included 13 wavebands with 7216 x 5412 pixels, and was flattened by dividing the cube images by the textured flat field in the Photoshoot software.

Monitoring: deterioration of parchment - The parchment was aged in a special oven, under controlled conditions, at 80°C and 50% relative humidity, for 2 and 6 hours. One hour after the degradation process was finished, the parchment was imaged under the same instrumental conditions used for characterization of the process. The parchment did not show changes detectable by the human eye.

The first five principal components calculated using auto-scaled characterization measurements account for approximately 96.43 %, 2.79 %, 0.28 %, 0.15 % and 0.06 % of original variance; The first two alone (PC_1 and PC_2 respectively) account for 99.22% of the variance of the image bands. PC_1 and PC_2 were considered the only two significant principal components.

The score plot of PC_2 vs. PC_1 (Figure 9a): the pixels (the objects) are well separated along PC_1 in two clusters that represent the text (black pixels) and the background (white pixels). We must conclude that the first component explains the differences between text and background.

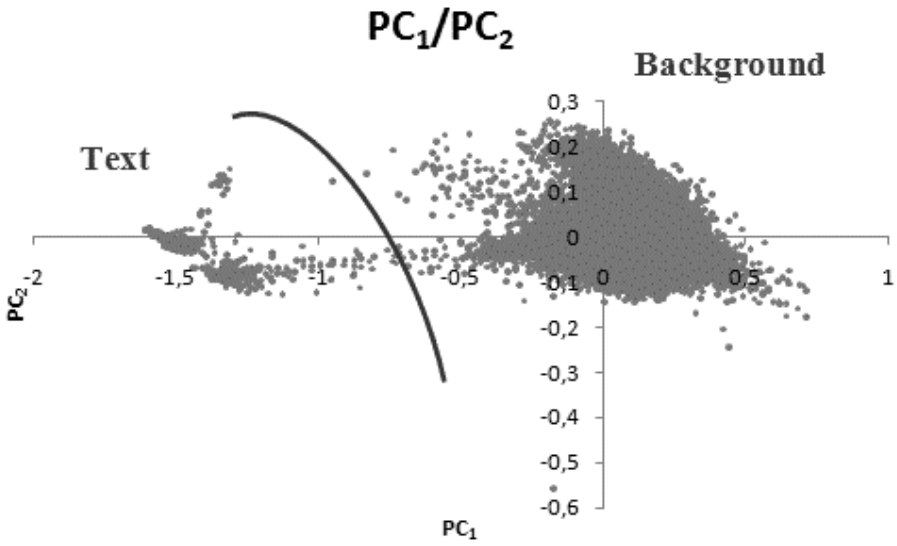

(a)

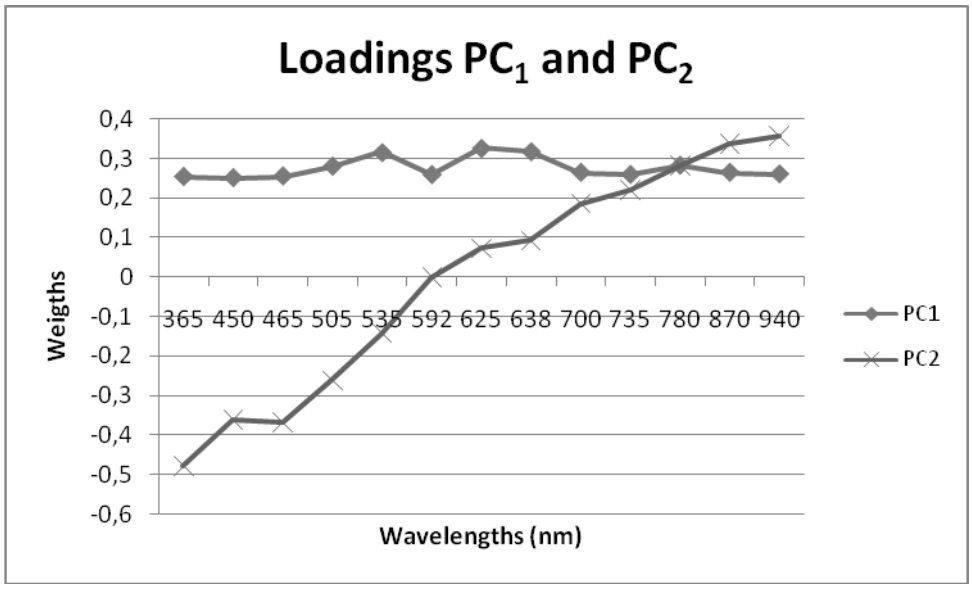

(b)

Figure 9: Score plot of PC_1 and PC_2 (a). The pixels are separated along PC_1 in two clusters that represent the text and the background. Loading plot of PC_1 and PC_2 (b): the first component accounts for the information of all channels instead the second component mainly accounts for the information of UV and of the last two IR channels.

The differences observed in the score plot can be explained using the loading plot showed in figure 9b: the first component accounts for the information of all the channels. The second PC mainly accounts for the information of UV (450 nm and 465 nm channels with negative weights) and of the last two IR channels (870 and 940 nm with positive weights). This means that along PC_2, those pixels

with large reflectances at infrared wavelengths will have positive scores while those with large reflectances in the ultraviolet region will have negative scores. PC_2 has the meaning of a typical contrast effect between high and low wavelengths that exhibit opposite loadings.

Each cube was projected onto the PC space using the loadings of the first and second PC; the result is a series of scores that compress the information from all the 13 channels into two orthogonal channels. The image obtained from the scores along PC_1 (Figure 8b) is very similar to the original image (Figure 8a), as only the differences related to pigmented and clean areas are accounted for. So PC_1 acts as a filter and could be used also for increasing the document readability. In supporting information (Figure 8c) the image rebuilt using the information accounted for by PC_2.

The scores of the first PC of degraded parchment were compared with the UCL and LCL limits: figures 10a and b show the Shewhart control charts for PC_1.

Blue and red pixels in the charts are the out-of-control points of the parchment: blue pixels represent regions that exceed the LCL and red pixels are the regions that exceed the UCL.

The two blue circles in the upper side of the charts represent the holes that were made, after the characterization, to put the parchment in the oven for the degradation. Wide areas of both images present values that exceed the LCL; this phenomenon is interpretable with a darkening of the parchment, not detectable by the human eye but recognized by the spectral imaging. The contribution plot (Fig. 11a) of the blue pixel (x =604, y =880) of the background of parchment shows that the first (365 nm, UV) and the tenth (735 nm, IR) channels are the main responsible for the out-of-control event. The absence of significant variations in the visible region explains why the human eyes cannot yet recognize it, in fact the visible wavelengths (450 nm, 465 nm, 505 nm, 535 nm, 592 nm, 625, and 638 nm) are the less affected by the degradation process.

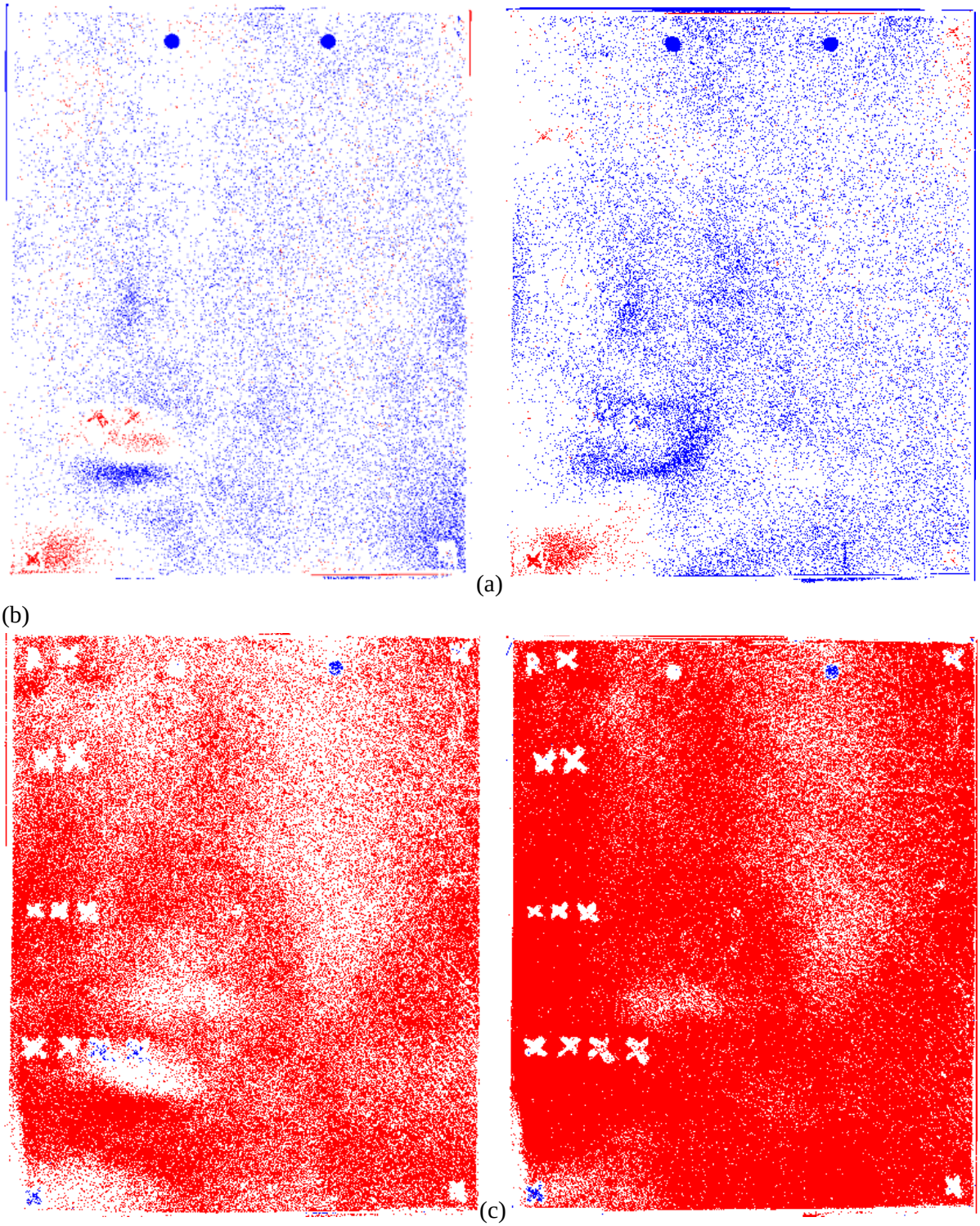

Figure 10: Control charts of PC_1 2 hours (a) and 6 hours aged (b). Control charts of PC_2 2 hours (c) and 6 hours aged (d). Blue and red pixels in the charts are the out-of-control points of the parchment: blue pixels represent regions that exceed the LCL and red pixels are the regions that exceed the UCL.

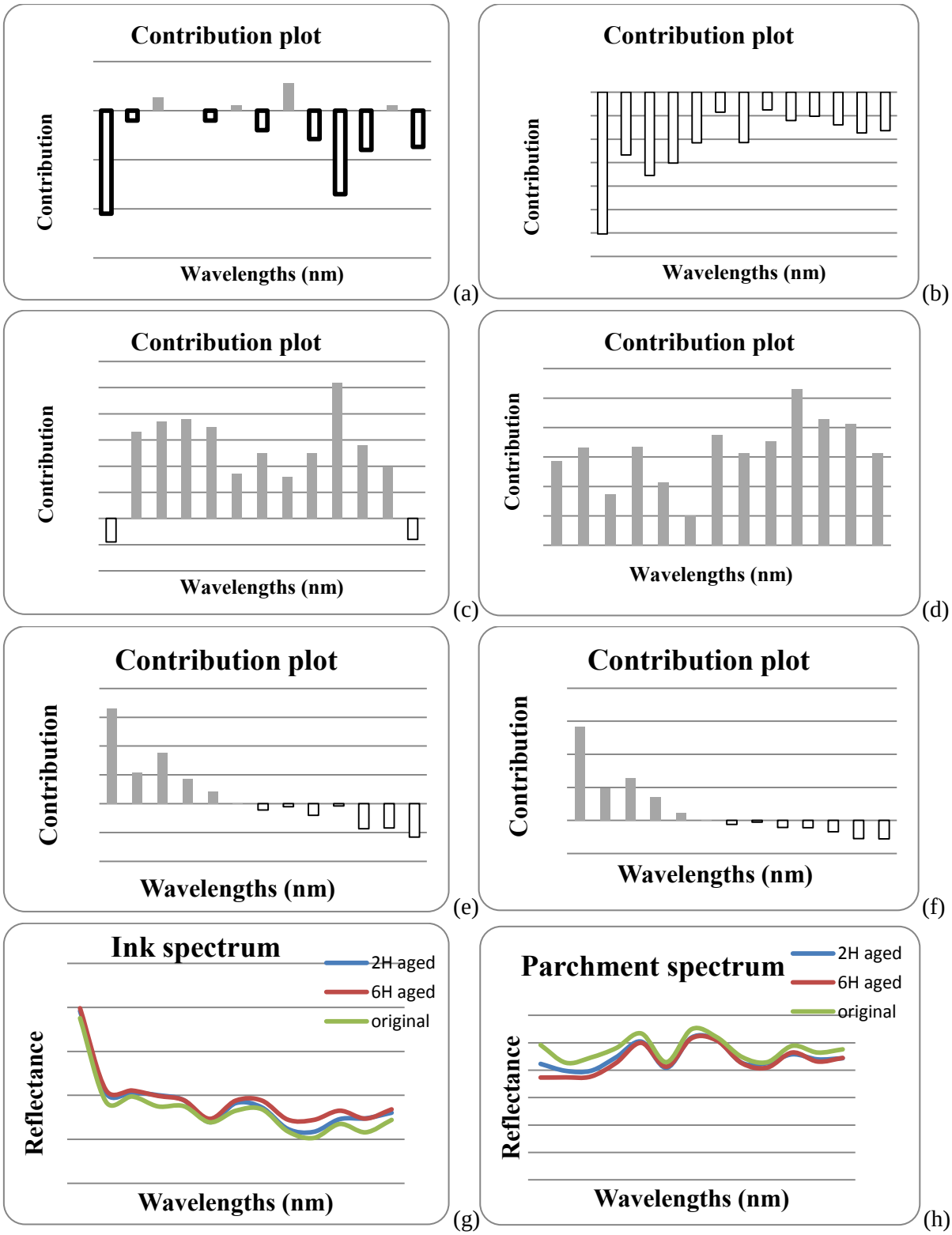

Figure11: Contribution plots for $PC_1$of the pixel x=604 and y =880 2h aged (a) and 6h aged (b): the first and the tenth channels are the main responsible for the out-of-control event of the background pixels. Contribution plots for PC_1 of pixel x=150 and y =200 2h aged (c) and 6h aged (d): the visible bands in the blue and green (450, 465, 505, 535 nm) and the infrared

band at λ=735 nm appear to be primarily responsible for the changes in the ink pixels. Contribution plot for PC_2 of the pixel x=604 and y =880 (background) 2h aged (e) and 6h aged (f): the first channel (λ=365 nm) is the primarily responsible for the out-of-control event. Original, 2 hours and 6 hours aged ink (g) and parchment (h) spectra. In general, the absolute value of the contribution of each wavelength increases from 2 to 6 hours of aging as showed by the spectra.

Some pixels that exceed the UCL are present in the control chart of figure 10a and b; these pixels present a whitening effect. In particular some areas with a diffuse presence of red pixels are present in the lower left corner of the charts aged 2 hours. Here, two important regions that alternate blue and red pixels are present: in this part of the parchment a wave is present that formed during heating. The upper side of the wave is the most exposed to the incident light and it presents greater intensity values: the opposite is true on the opposite side of the wave: in fact the lower side of the wave is the dark area and it is characterized by pixels that exceed the LCL values.

Figure 11c shows a contribution plot of a typical out-of-control ink pixel (x= 150 y =200). The contribution plot shows that the degradation of the ink exceeds that of the parchment: the visible bands in the blue and green (450, 465, 505, 535 nm) and the infrared band at λ=735 nm appear to be primarily responsible for the changes. Figure 11b and 11d show contribution plots of parchment and inked pixels (x= 150 y =200) aged 6 hours, which are out of control. The contribution plots show that the degradation is greater than at 2 hours of aging: the absolute value of the contribution of each wavelength increases from 2 to 6 hours of aging.

The charts based on the scores of PC_2 are shown in figure 10c and d. Again blue and red pixels in the charts indicate the out-of-control points of the parchment in the degraded cubes.

Wide areas of the image contain values that exceed the UCL. The contribution plot in Figure 11e and Figure 11f of a red pixel at coordinates x =604, y =880 shows that the first channel (λ=365 nm) is the primarily responsible for the out-of-control event.

Figure 11g and h show the spectrum of original, 2-hour and 6-hour aged ink and parchment. The reflectance of the ink spectrum progressively increases during the degradation process and the reflectance of the parchment spectrum progressively decreases during the aging process. For the parchment, we see that the reflectance decreases as aging time in the oven, consistent with our notion that environmentally induced changes in the parchment decrease legibility by reducing reflectance. Why the ink also shows changes is unknown, perhaps because the very recently applied inks still contain binder and solutes that are continuing to evaporate as we age them. The inks on the scrolls do not contain such materials; though while we cannot meaningfully compare the relative absolute reflectance of the inks on the scrolls, we do know that the ink spectra for both legible or illegible fragments are relatively flat, so it is the parchment reflectance that drives the ink contrast and therefore the legibility.

We also measured the L*a*b color coordinates for all image pixels using the X-Rite color checker as the standard. We created the transformation that converts gray values of the six visible bands to a high-fidelity color image in L*a*b color space [35]. Using these values, we calculated the color difference between un-aged and aged parchment using ΔE_{2000}, the standard color difference metric accepted by the International Commission on Illumination (CIE). We find that ΔE_{2000} between the original and the result of 2 and 4 hours of aging are respectively 1.18 and 1.69. A ΔE_{2000} of less than 2 is typically considered not perceptible by the human eye, so we are indeed detecting changes before they are visible. Note that the method is sensitive: we find 1880368 changed pixels after only 2 hours of aging.

Principal component analysis of the residuals of the degradation analyses

To further investigate the effects of the applied aging treatment, a new PCA was performed on the residuals data matrix obtained by subtracting the information accounted for by the first two PCs of un-aged parchment from the degraded image.

The resulting residuals contain the information regarding formation of new species or events on the parchment surface that are not accounted in the first two principal components of the un-aged parchment.

The first principal component accounts for 60% of the original variance and was deemed the only relevant PC. This information is probably due to changes occurring on the pigment surface during the aging treatment. The UV channel suggest the potential formation of new compounds (Figure 12). A pattern apparently due to the pigment may be recognized in the image of the PCA residuals of the un-aged parchment (Figure 13, upper), which indicates that the residuals convey information about the aging process. No systematic pattern may be identified after subtracting PC_1, which appears to indicate that only PC_1 contains information about the aging treatment (Figure 13, lower).

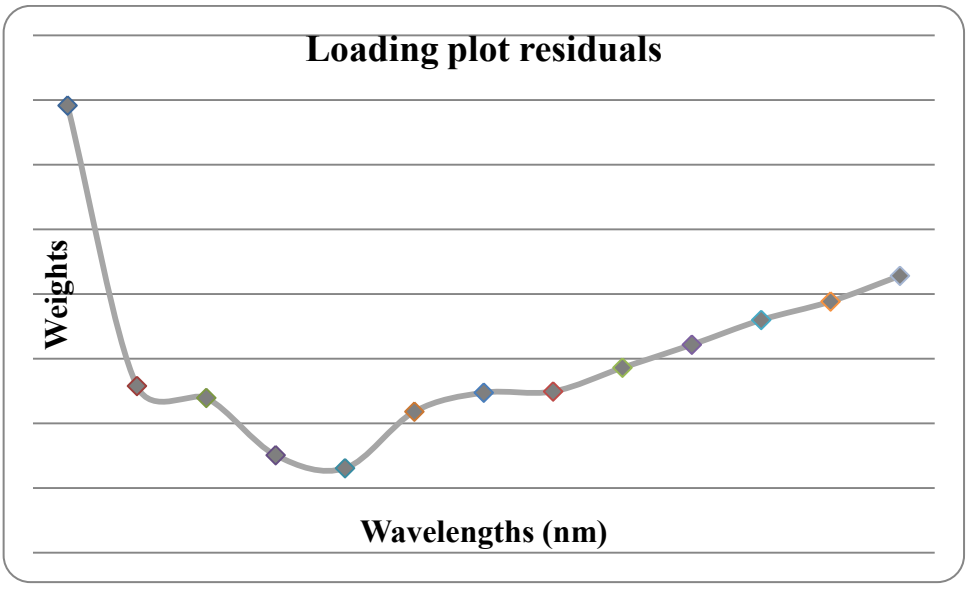

Figure 12: Loading plot of the residuals. The UV channel is the primirily responsible of the formation of new compounds or phenomena.

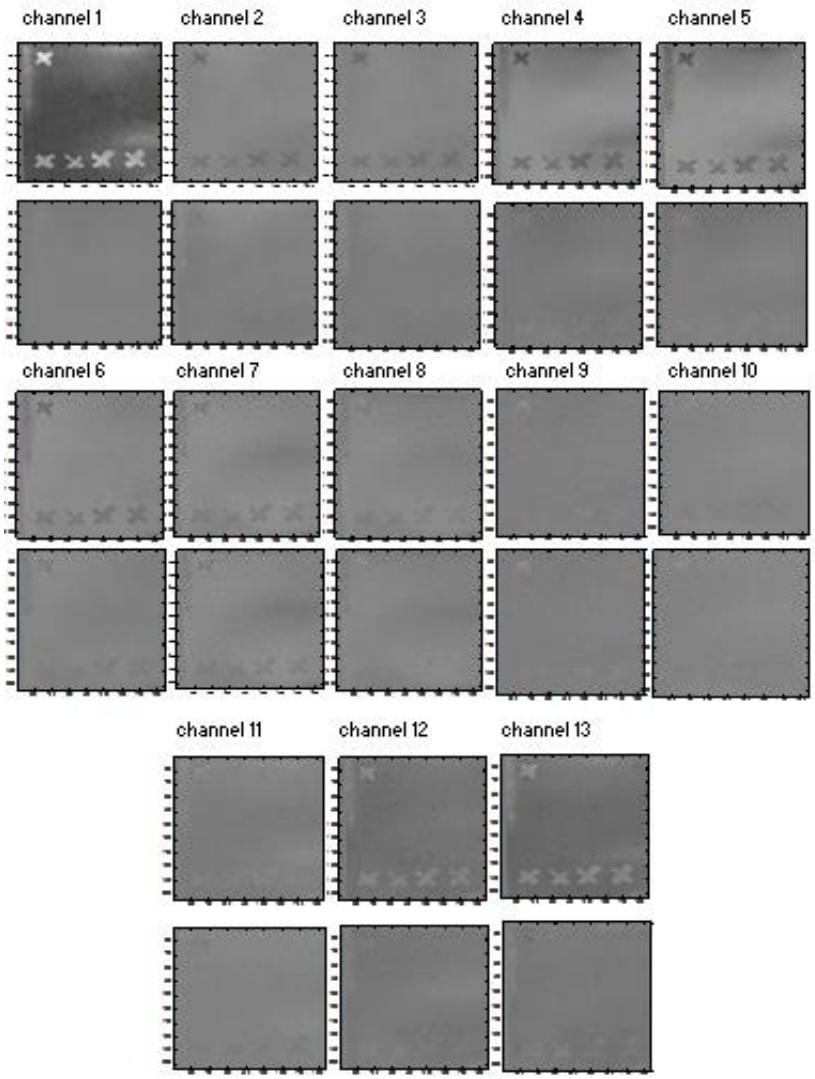

Figure 13: residuals images of all 13 channels (up) and residuals images of all 13 images without the information accounted by the PC_1 (down). No systematic pattern may be identified after subtracting PC_1: PC_1 contains information about the aging process.

Conclusions

The aim of this project is the development of a non-invasive technique based on LED multispectral imaging for monitoring the conservation of cultural heritage objects, particularly parchment.

A LED multispectral imaging system analyzed a sample of parchment before and after applying a degradation treatment. Our algorithms are able to detect degradation of the parchment before visually detectable damage has occurred. The chart also detects the presence of a wave on the surface of the parchment

that was generated by the heating in the oven. In addition, the method shows that the spectra of changing pixels and that the visible reflectance of parchment decreases, as would be expected based on previous observation of ancient manuscripts. A future publication will consider artificial aging and degradation that is visible to the eye.

Out-of-control events may be interpreted from a contribution plot, and the channels responsible for the alarm may be isolated and analyzed to interpret the chemical and physical processes that account for the event. The evolution of the damage during the degradation process may be detected from the control charts. Surface effects not accounted for by the initial PCA could be identified from PCA of the matrix of residuals. In other words, the PCA of the residuals may show spectral evidence of structural changes of the surface due to the aging treatment. The proposed procedure is a pixel-by-pixel strategy and it is dependent on image alignment, which is a crucial step in the algorithm workflow; this is the most critical step in the procedure. Our current images are aligned to one pixel with custom software. We have modeled the effects of mis-registration and binning on the control charts; these results will appear in a future publication. However, the short message is that one pixel registration is acceptable, and we can easily do one pixel with current software (less than a pixel with centroiding).

Binning reduces the effects of mis-registration while still leaving a high-resolution image to interrogate for changes. Since physical alignment of the images is not a simple task, we are aligning them using software (each IFOV on the parchment is 40 μm). Aside from the issues with positioning an object to that resolution, the fragments have poorly defined edges where the parchment is torn or cut.

In conclusion, we affirm that the proposed approach may yield rapid and accurate measurements of the preservation state of manuscripts. The technique

also may be useful for other cultural heritage objects, such as frescoes and paintings. Industrial applications for the control of surfaces can also be envisaged.

2.2.5 Quantitative monitoring of parchment aged by light

There are many studies concerning the application of various analytical methods in the characterization of parchment and ageing phenomena, some non-destructive (optical, SEM, XRD, spectral methods: IR,UV,-VIS) and others destructive (TG/DTG, DTA, DSC, DMA, TMA)[48-50].

The methods of thermal analysis were found to be very useful for assessment of the degradation degree of parchments and leathers[51, 52]. Most of the study focused on thermal ageing of collagen to investigate the variation induced by ageing on the thermodynamic parameters associated with both parchment denaturation and softening of collagen crystalline fraction[53-56].

It is known that photochemical reactions depend upon the structure of polymer chains, presence of chromophoric groups, impurities, temperature, pressure and wavelength. Moreover, parchment mass decrement, activation energy and entropy changes give some information about changes of water content and about structural transformation of protein after light irradiation[64].

The analysis of the emission of volatiles from parchment was used as tool for evaluation of parchment stability: the content of volatiles aldehydes was investigated using gas chromatography analysis of the atmosphere surrounding parchment during oxidation because they can be the products of lipids autoxidation. The presence of lipids leads to oxidative degradation of collagen[57]. The content of lipids strongly affects the decrease of shrinkage temperature of collagen during degradation, and thus its thermo-mechanical properties, confirming the high importance of lipid peroxidation during degradation of parchment[58].

The effects of drying and thermal treatment of collagen were observed by X-ray diffraction[59] and a new method of investigating variation of preservation within a parchment sample that uses microfocus X-ray beams was proposed[60] but it allows to work on a small region at time and is not of simple use. A non-invasive method for quantitative characterization of parchment deterioration based on spectral measurement was proposed but has the limit of being a punctual technique[61].

Most is known about parchment structure, ageing phenomena and damaging events but there is a lack of knowledge about the monitoring of degradation processes to anticipate irreversible damages and in particular on ageing effects caused by light exposure of parchment objects.

The effect of exposure of paper and parchment to UV light was investigated by using ATR-FT-IR spectroscopy and multivariate statistical tools[62].

Raman spectroscopy was applied in the assessment of changes in parchment glue and protein-based paint media after artificial ageing with exposure to visible light: changes in bands in the fingerprint region were associated with amino acid oxidation[63]. It is well known that light degradation promotes oxidation of parchment and its yellowing.

We present here a study on the use of quantitative multispectral imaging technique to monitoring the degradation of parchment caused by light exposure. The effect of UV radiation was also investigated using a UV filter. The degradation was monitored also by ATR-FTIR, GC-MS and TGA techniques in order to understand the ageing mechanism of parchment and to correlate the chemical information with imaging information.

EXPERIMENTAL

Materials

Our experiments were carried out on goat parchment samples made by an Orthodox Rabbi from Jerusalem (Israel). The samples were characterized and monitored over the ageing using LED multispectral imaging, ATR-FTIR, GC-MS and TGA and then aged for 24, 48, 72 and 120 hours in the weather-ometer ageing chamber (Company name, USA) with a light exposure of 700 Watt/m^2 to simulate light exposure. One sample was aged using a UV filter.

Methods

LED multispectral imaging

LED multispectral images of parchment were acquired at 1200 dpi with an Eureka Vision LED system from MegaVision, Santa Barbara, CA, USA. The system has a 39-megapixel Kodak CCD monochrome sensor array and the LED emissions are centered on the following wavelengths: 365, 450, 465, 505, 535, 592, 625, 638, 700, 735, 780, 870, and 940 nm. Following our previous papers[65, 66], the monitoring of the conservation state of parchment by means of LED Hyperspectral imaging and multivariate analysis was performed.

ATR-FT-IR

Fourier transform infrared spectral analysis of parchment was conducted using ATR-FT-IR. All spectra were obtained using a Thermo Nicolet 670 FT-IR Spectrometer. Sample spectra were obtained in absorption mode over a wavelength of 400 cm^{-1} to 4000 cm^{-1} at 64 scans per sample and a resolution of 4 cm^{-1}. Background readings of air were established prior to data collection. The background was subsequently subtracted from each spectrum before data output. All data was recorded using OMNIC software.

GC-MS

A strip of 4x13mm of each sample was subjected to a pre-oxidation treatment in a 1.5 mL sealed vial in a thermostated water bath at 85°C for 30 min; after

15min an headspace sampling was performed using SPME fibers (Supelco, Bellofonte) with a Carboxen/PDMS stationary phase, thickness 75 *u*m, for 15 min at 85°C and for 30 min at room temperature. Before each sampling the fiber was pre-conditioned at 250°C for 15 min. An Agilent Technologies 6890N gas chromatography, coupled to an Agilent Technologies 5975B quadrupole mass spectrometer equipped with a Agilent cooled injection system CIS 4 and a 30-m Agilent 19091S-433 HP 5-MS column, I.D. 0.25 mm and 0.25 um stationary phase thickness was used. The mobile phase used was helium (99.999%) at a flow of 1.3 mL m^{-1}. The following oven temperature were used: 1 min at 40°C, then heating to 130°C at the rate of 5 °C min^{-1}, after which the temperature is kept constant for 10 min.

Ionization was performed using standard EI mode applying 70 eV at 230°C. The interface is heated to 270 °C and the quadrupole analyzer to 150°C. The detection is performed using total ion current and the identification of the most abundant volatiles is performed using the NIST mass spectra library.

TGA

TGA and DTG measurements were performed on parchment samples using synthetic air (purity better than 99.999%, 20 mL min^{-1} flow rate) in the temperature range 25-500 °C at 10°C min^{-1} heating rate, with a Perkin Elmer Pyris 1 TGA.

TGA was used to assess the sample water. The non-isothermal thermo-oxidative degradation of parchment occurs through successive processes accompanied by mass losses.

RESULTS AND DISCUSSION

In order to understand the ageing mechanism of parchment caused by the light and to correlate this information with the degradation detected by quantitative

imaging technique (LED multispectral imaging) we characterized and monitored the ageing of parchment by using: Fourier Transform Infrared spectral analysis (ATR-FT-IR) to identify the formation/disappearance of chemical species in parchment samples; solid-phase micro-extraction and gas chromatography-mass spectrometry (SPME-GC-MS) to analyze the content of volatiles which provide an indication of lipid autoxidation in parchment which leads to the degradation of the collagenous phase; thermogravimetry analysis (TGA) to assess sample water release during the degradation which are strictly correlated with the thermo-oxidative degradation of parchment.

The parchment samples were aged for 24, 48, 72 and 120 hours in the weather-ometer ageing chamber with a light exposure of 700 Watt/m^2 to simulate light exposure. One sample was aged using a UV filter in order to study the effect of the UV radiation.

After the starting characterization, performed before the artificially ageing, parchment samples were analyzed after each ageing step and the results were compared with the baseline characterization.

The LED multispectral imaging characterization was performed following the methods described previously and in our previous works[65, 66] : the result is a model of the state of conservation of parchment before the light degradation. The outcome of the monitoring of the sample over the ageing is a control charts that is an image in which the position of each pixel of the parchment is rebuilt: blue and red pixels are the changed pixels, or out of control points, of the parchment. Blue pixels represent regions that are darkening instead red pixels represent regions that are whitening. Green pixels correspond to unchanged regions, or in control points.

Parchment characterization

Figure 14 shows the ATR-FTIR spectra of the parchment sample before the ageing. The strong and broad band centered near 3281 cm^{-1} is assigned to the stretching of OH and NH groups variously hydrogen bonded. NH groups are confirmed by the broad absorption between 500 and 600 cm^{-1} associated with the out of plane motions of the NH group. The characteristic doublet near 1632 cm^{-1} (amide I) and 1540 cm^{-1} (amide II) indicated the presence of the amide group -CONH-. At 2952, 2921 and 2851 cm^{-1} there are the medium-weak band originating from the C-H stretching modes of $–CH_2-$ and $–CH_3-$ groups occurring in the amino acid residues of the polypeptide chains.

At 1447 and 873 cm^{-1} there are the characteristic band of $CaCO_3$ that comes from the preparation process to which parchments was subjected.

Peak at 1034, 1199 and 1331 cm^{-1} are characteristic of tannins, in according to the manufacture procedures described by the producer: the first peak is due to the superimposition between stretching modes of the ester –C–O–C– and the carboxylic C–O– and instead the second to the superimposition between stretching mode of C–O–C and bending mode of C–H. Tannin peaks cover the amide III band near 1239 cm^{-1}.

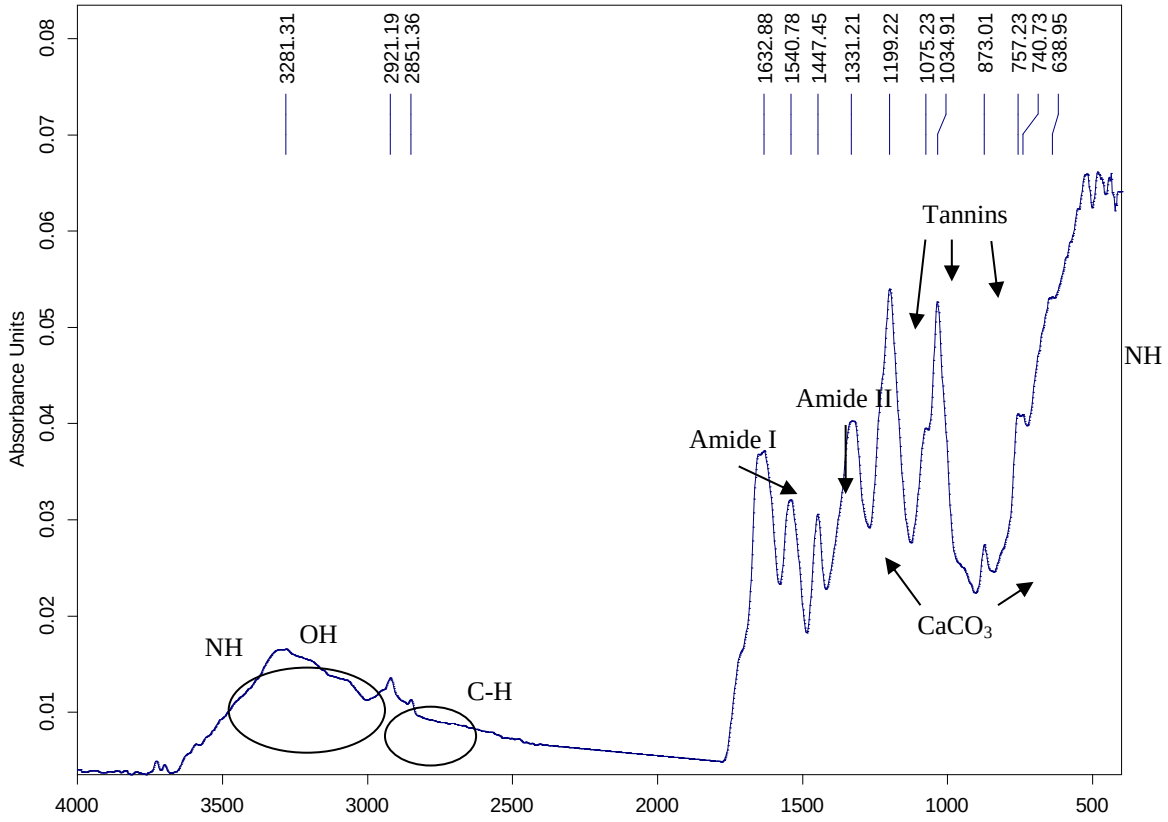

Fig. 14: ATR spectra of goat parchment, recto. cm^{-1}

The content of volatile aldehydes provides an indication of lipid autoxidation in parchment which leads to the degradation of the collagenous phase: we found secondary peroxidation products which came from a structural rearrangement of primary peroxidation products. The majority of chain-cleavage products are molecules belonging to short chain aldehydes: Hexanal, heptanal, Octanal, Nonanal, Decanal and 2-Decenal (Fig. 15).

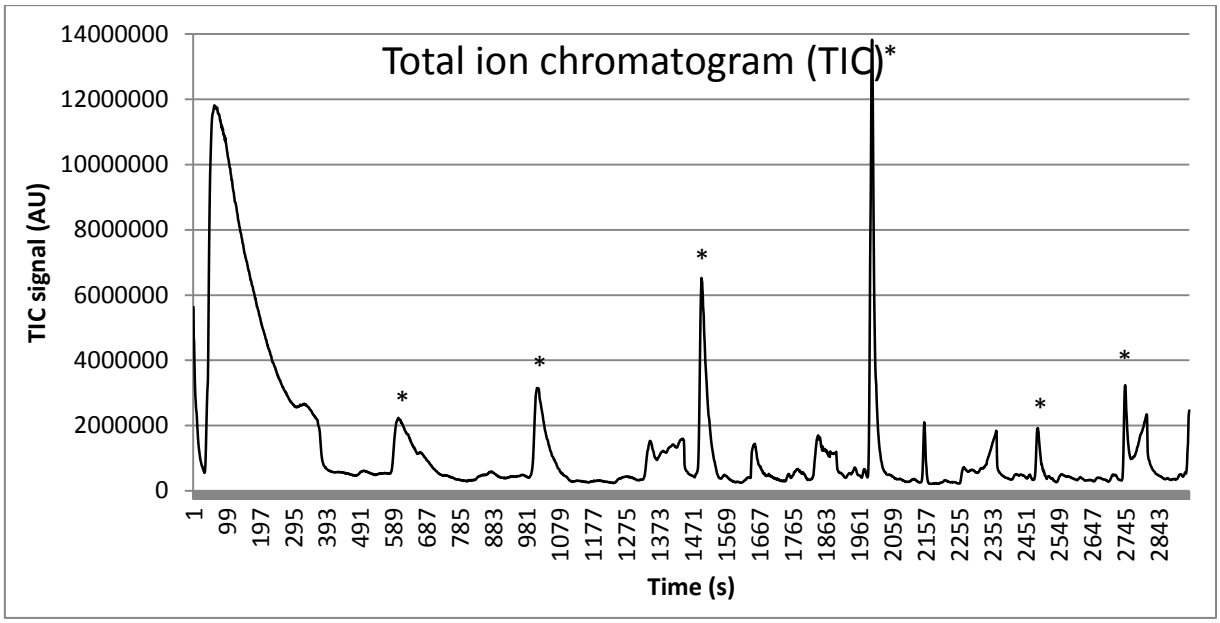

Fig. 15: Total ion chromatogram of volatiles desorbed from goat parchment sample: the detected compounds are marked with *.

The non-isothermal thermo-oxidative degradation of parchment occurs through successive processes accompanied by mass losses: TGA was used to assess the sample water release.

Figure 16a shows the TGA of the parchment sample: in the first process (I in Fig. 16b) the water was completely lost (dehydration). The next two steps (II and III in Fig. 16b) consist in the pyrolytic decomposition of parchment.

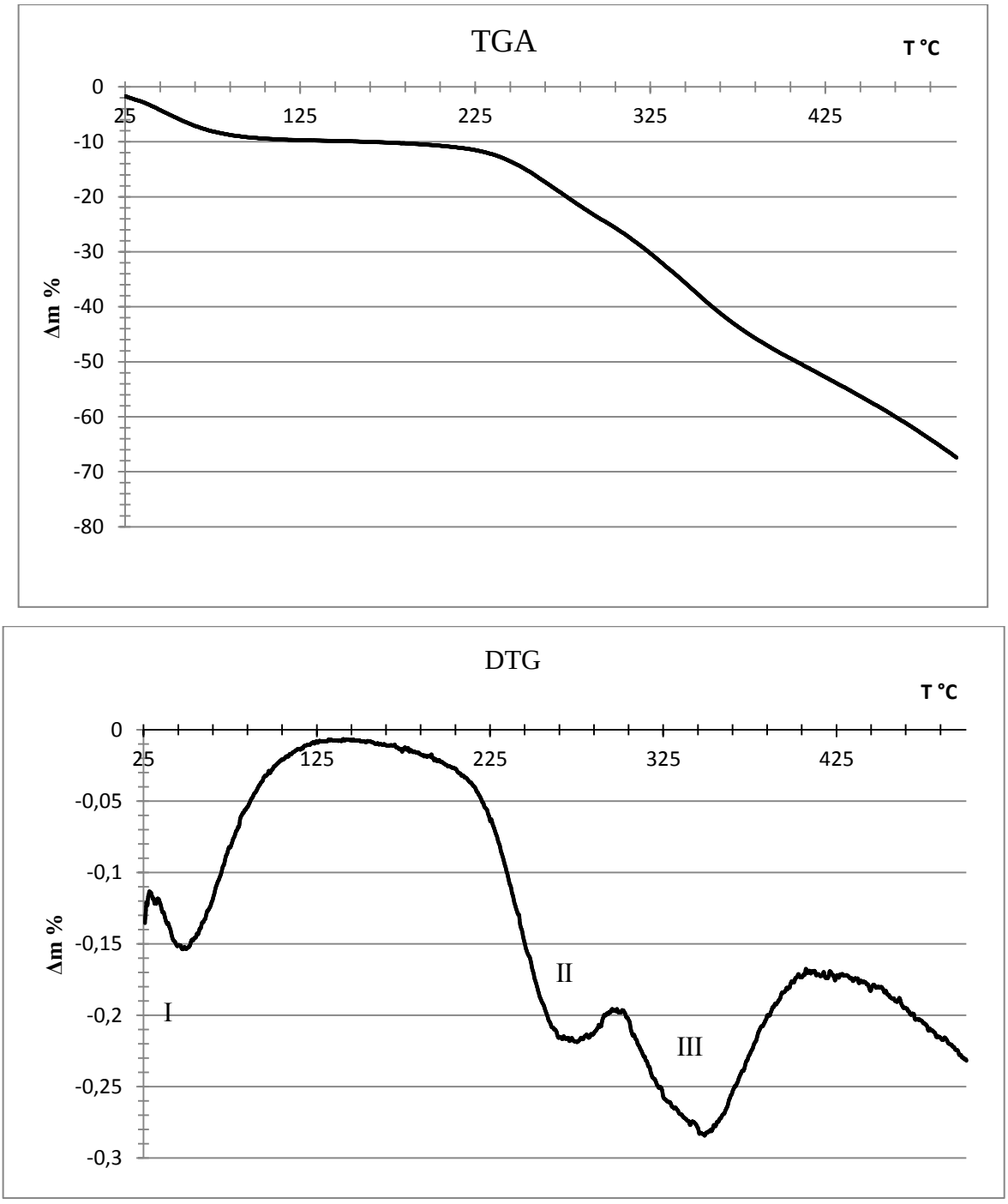

Fig. 16: TGA (fig. 16a) and DTG (fig. 16b) curves of goat parchment analyzed in syntethic air atmosphere.

The dehydration temperature is 43°C and the two characteristic pyrolytic temperatures are 260°C and 341°C.

Light ageing without UV filter

Figure 17 shows the color images of the parchment sample before ageing (a) and after the 24 hours ageing with light (b): both images were collected using the LED multispectral imaging system used for the monitoring. The control chart of the first PC of the parchment aged for 24 hours is represented in figure 17c: blue and red pixels in the charts indicate the point of the parchment that can be considered changed. Wide areas of the image contain blue pixels: these pixels represent areas that are darkening. In the upper and lower left corner there are two regions with both red and blue pixels: these regions were used to stick the parchment at the sampler using tape, so the surface was damaged and somewhere became lighter. The area on the right of the control chart is more concentrated by out of control pixels than the area on the left: this is mainly due to a different exposure angle of the sample, the right side was not fixed to the sampler and slightly detached from it, changing the exposure angle respect with the lamp. The red circle in the middle side of the chart represents a hole that was made before the characterization step. The large number of blue pixels explains the ability of the methodology to verify the presence of an ageing effect.

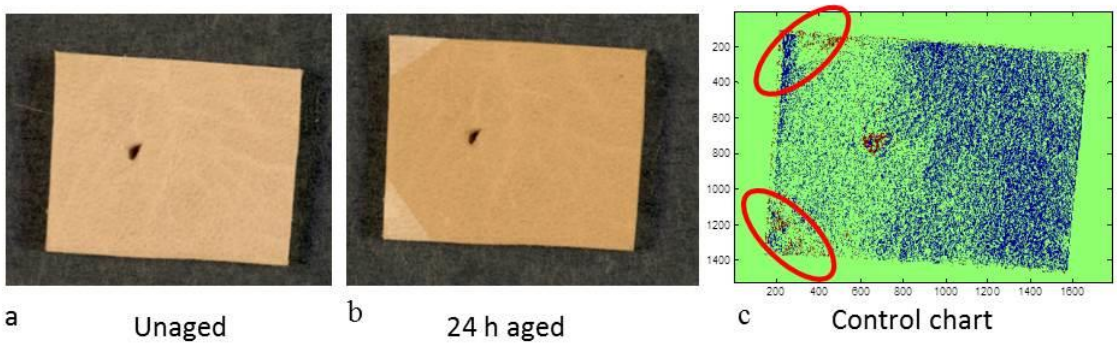

Fig. 17: color images of parchment sample before (a) and after 24 hours ageing(b); control chart of parchment aged for 24 hours: blue pixels represent the regions that can be statistically considered aged. The ageing detected by LED multispectral imaging is clearly visible by looking at the color image in figure 1a and b.

The infrared analysis of parchment sample aged simulating 24 hours of sun light exposure doesn't show any change (Fig. 18 blue line). The ageing for 48 and 72 hours showed a new band at 1733 cm^{-1} that slightly increases from 48 to 72 ageing hours. This band could be originated by a C=O groups. Moreover, the band at 2922 cm^{-1} and 2855 cm^{-1} increased in intensity. The degradation detected by LED multispectral imaging after 24 hours was not detected by the infrared analysis.

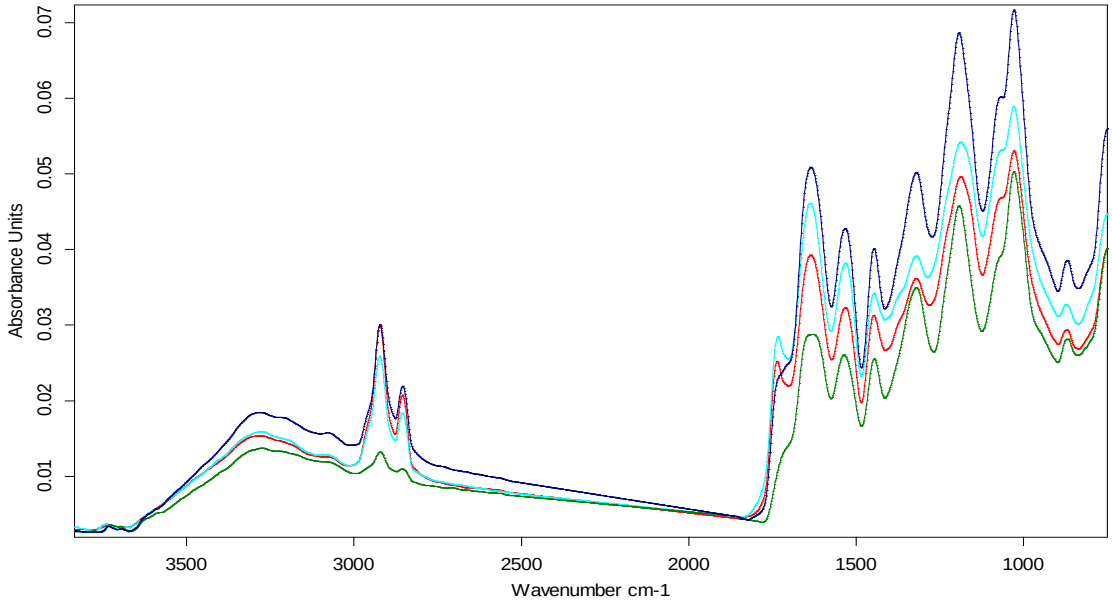

Figure 18: ATR spectra of goat parchment unaged (green), 24 (blue), 48 (red) and 72 hours aged (light blue). The infrared analysis of parchment sample aged simulating 24 hours of sun light exposure doesn't show any change.

The analysis of the content of volatiles in parchment samples, which can be very useful to provide an indication of degradation, doesn't show significant results: the content of the five aldehydes identified in the sample in characterization didn't significantly decrease during the degradation (Table 2).

Unaged	24 h aged	48 h aged	72 h aged
Hexanal	100%	99%	97%
Heptanal	100%	98%	97%

Octanal	100%	96%	94%
Nonanal	100%	97%	95%
Decanal	100%	96%	97%

Tab. 2: residual content of the 5 aldehydes during ageing.

Moreover, the dehydration and pyrolitic temperatures of parchment didn't significantly change over the ageing as shown in table 3.

The fact that the GC-MS and TGA analyses were not able to detect any change caused by the light ageing allows us to say that thermo-oxidative phenomena and degradation of collagenous phase linked to the autoxidation of lipids are not involved in the chemical-physical ageing process caused by the light.

Ageing hours	Dehydration T °C (I)	Pyrolitic decomposition T °C (II)	Pyrolitic decomposition T °C (III)
0	48	253	334
24	48	251	338
48	50	255	336
72	45	253	336

Tab 3: Dehydration and pyrolitic temperatures of parchment samples at different ageing steps.

Light ageing with UV filter

Figure 19 shows the color images of the parchment sample before ageing (a) and after the 24 (b), 48 (c) and 120 (d) hours of degradation with light with a UV filter: all the images were collected using the LED multispectral imaging system used for the monitoring.

The control charts of the first PC of the parchment aged for 24 (a), 48 (b) and 120 (c) hours are represented in figure 6 in the lower side: blue and red pixels in the charts indicate the point of the parchment that can be considered changed.

The effect of the light on the parchment when a UV filter is used is significantly smaller than when all the radiation is used to age: this is very clear both looking at the color images and looking at the number of out of control pixels that the LED multispectral imaging detected after 24 hours of ageing. The ageing is not visible to human eyes except where was used a tape to fix the parchment at the sampler where now slightly is lighter.

The LED multispectral imaging method was able to detect the progress of the degradation: the out of control pixels increased during the ageing.

The ATR ,the GC-MS and TGA analyses didn't show any significantly change over the ageing.

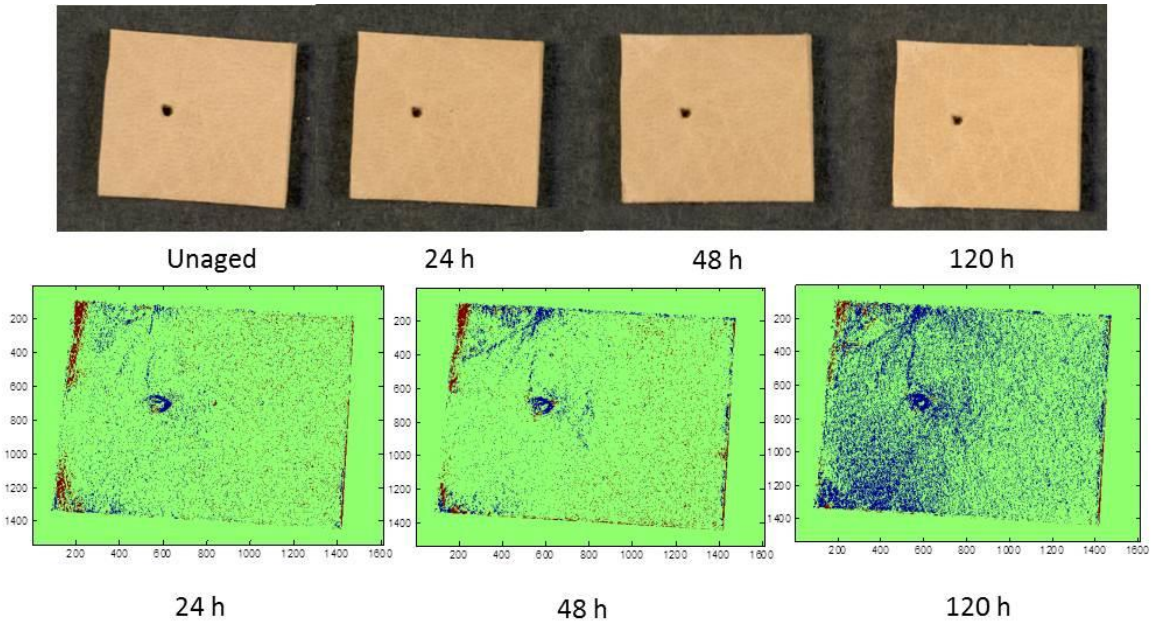

Fig. 19: color images of the parchment sample before ageing (a) and after the 24 (b), 48 (c) and 120 (d) hours of degradation with light with a UV filter; control charts of the first PC of the parchment aged for 24 (a), 48 (b) and 120 (c) hours: blue and red pixels in the charts indicate the point of the parchment that can be considered changed.

CONCLUSIONS

We used a quantitative multispectral imaging technique coupled to statistics, ATR-FTIR, GC-MS and TGA to monitoring the degradation of parchment caused by light to understand the ageing mechanism and to correlate this information with the degradation detected by quantitative imaging. Parchment samples were aged for 24, 48, 72 and 120 hours simulating a sunlight exposure. The degradation was done also using a UV filter.

The degradation performed including UV was detected by LED multispectral imaging technique after 24 ageing hours and the effect was clearly visible comparing color images before and after the degradation process. The large number of out of control pixels presented in the control chart confirms the ability of the methodology to verify the presence of an ageing effect. The infrared analysis after 24 ageing hours doesn't show any change: only after 48 hours a new band at 1733 cm^{-1}, originated by a C=O group, appeared and the bands at 2922 cm^{-1} and 2855 cm^{-1} increased in intensity. The content of the five aldehydes identified in parchment by GC-MS didn't decrease during the degradation and the TGA showed that the sample water release during the degradation didn't change.

The effect of light degradation on parchment when a UV filter is used is significantly smaller than when a UV filter is not used: the number of out of control pixels that the LED multispectral imaging detected after 24 hours of ageing is smaller and color images are pretty similar. Anyway, the LED multispectral imaging method was able to detect the progress of the degradation because the out of control pixels increased during the ageing. The ATR ,the GC-MS and TGA analyses didn't show any significantly change over the ageing.

In general, the fact that the GC-MS and TGA analyses were not able to detect any change caused by the light ageing allows us to say that thermo-oxidative phenomena and degradation of collagenous phase linked to the autoxidation of

lipids are not involved in the chemical-physical ageing process caused by the light. Moreover we can affirm that UV light definitely accelerates the ageing of parchment: the use of UV filter when parchment materials are exhibited is strong recommended.

In conclusion we can state that the LED multispectral imaging methods is able to detect the ageing effect of light before other common analytical techniques.

2.2.6 Real case 1: Monitoring the conservation of the Dead Sea Scrolls

The discovery of the Dead Sea Scrolls some sixty years ago is considered to be one of the greatest archaeological discoveries in modern times. The scrolls were written or copied in the Land of Israel between 250 BCE and 68 CE, and were rediscovered in 1947 in eleven caves in the Judean Desert [14]. The Scrolls represent the oldest written record of the Hebrew Bible, and contain the earliest copies of every book except Esther. This ancient library sheds insight into centuries of history that are pivotal to both Judaism and Christianity. Thanks to these remarkable finds, our knowledge of the people in the Land of Israel as well as the origins of Judaism and early Christianity has been greatly enriched.

The conservation, preservation and documentation of the DSS have concerned both scholars and conservators ever since their discovery. The constant and arid climate of the Dead Sea area, which is about 400 meters below sea level, was probably the major factor in the preservation of these precious documents for over two millennia: removal of the fragile scrolls from the caves interrupted that environmental stability.

Since their discovery, the scrolls have been damaged by the ravages of time and, in the early years, by inappropriate conservation methods in a poorly controlled environment. About 80% of the scrolls are written on skin and 20% on papyrus.

The skin is from sheep and goats, but it is neither leather nor parchment as we understand these terms today.

The Israel Antiquities Authority (IAA) is Israel's state authority in charge of its archaeological activities. It is in charge of the country's antiquities and antiquity sites, their excavation, preservation, conservation, study and publication. In 1991 the IAA, advised by the leading experts on issues relating to the conservation of manuscripts, parchment and papyrus, established a conservation laboratory dedicated solely to the DSS, and has since been in the forefront in conservation techniques. The task of conservation and preservation of the scrolls is ongoing, due to their extreme brittleness and the need to make use of the most up-to-date conservation methods known.

The IAA, in cooperation with international experts, has decided to reevaluate the state of the art of conservation techniques and to define processes for issues still unresolved. As part of its conservation efforts the IAA has initiated a digitization project both to monitor the well-being of the scrolls, and to enable universal access, while at the same time avoiding further damage to the scrolls from physical exposure. By creating high-quality images in color and infrared, and collecting multispectral data, the IAA is taking a leadership role in defining parameters for early detection of deterioration. These efforts will support and provide active conservation assessments, non-invasive testing and monitoring tools, and a better record and documentation of the physical state of the scrolls in real time. Further, the IAA will use the most advanced and innovative technologies available to reimage the entire corpus of 900 manuscripts, comprising c. 15,000 DSS fragments, in high resolution. With the assistance of Google-Israel, the IAA will support scholarship by creating and delivering to all who are interested the highest quality images of the DSS, coordinated with a new, usable integration of related scholarly resources, including transcriptions, translations, and bibliography.

The aim of conservation is to obviate damage caused by environmental or accidental factors. Materials of cultural property are subjected to changes over time, due to the interaction with physical factors such as light, temperature, relative humidity, etc; chemical factors such as atmospheric oxygen, pollutants, etc.; and biological agents, including bacteria, fungi, insects, etc. Monitoring of the artifact over time can alert the conservator of potentially damaging situations. The objective of this research is to develop a monitoring methodology, using imaging, that not only does not damage the historical artifact, but also automatically recognizes areas (i.e., pixels) that are changing.

The damaged state of the scrolls was a consequence of both the ravages of time, the mishandling and mistreatment they were exposed to during the four decades that had passed since their discovery in 1947. In 1991, the IAA established a unique conservation laboratory, dedicated to the conservation and preservation of the DSS.

The conservation and preservation of the scrolls is a continuous task due to their extreme brittleness and the need to make use of the most up-to-date, state-of-the-art, conservation methods known worldwide.

Imaging has been a mainstay of text study for decades, There are, in general, two goals of text imaging; content and conservation. The goal of imaging for content is concerned with legibility. Many texts have become illegible due to damages caused by age, the environment and handling. Some have faded, some have darkened and some have been reused - palimpsests. The imaging method serves both kinds of users, text scholars and scientists. The by-products – "best possible images" improve the legibility of the texts and open new horizons in scholarly research.

More generally, spectral imaging requires careful calibration to be useful. Calibrated systems offer a range of advantages to the research and conservation community, including: 1) easy comparison of data across groups and objects

(this is critical for works by the same artist or distributed texts/collections located in multiple institutions); 2) development of libraries of absolute spectra of pigments, inks, papers and so on; 3) use of spectral libraries for image segmentation, image processing and comparison of objects; 4) development of a journal literature. There is always a serendipity factor in having a lot of easily mined data that is based on the same physical calibration.

Imaging for monitoring

Many of the scroll fragments are difficult to read, either completely or in areas. It has long been known that near infrared photography (NIR) of ancient texts would often improve legibility, and the images of the scrolls to which scholars have had access were taken with infrared film in the early 1950s. Experiments with spectral imaging of the scrolls in 1993-1994 helped understand the whys and the hows of NIR photography. In the case of the Dead Sea Scrolls and of many papyri, spectral imaging showed that the reduction in visible contrast and consequently the transition from legibility to illegibility is due to changes in the reflectance of the parchment (or papyrus) substrate relative to that of the ink [67, 18].

The work on the Dead Sea Scrolls with spectral imaging showed that legibility issues are driven entirely by contrast between the ink and parchment. In a legible text, the ink and parchment have very different spectra, especially in the visible spectrum where the human eye and traditional film photography work. For an illegible text, while the ink and parchment have similar spectra in the visible, providing no contrast and the text is not readable. However, for the illegible scrolls, the parchment reflectance *increases* in the infrared, starting typically above ~ 700 nm [18]. That increase in reflectance brightens the parchment, and increasing the contrast makes the text legible.

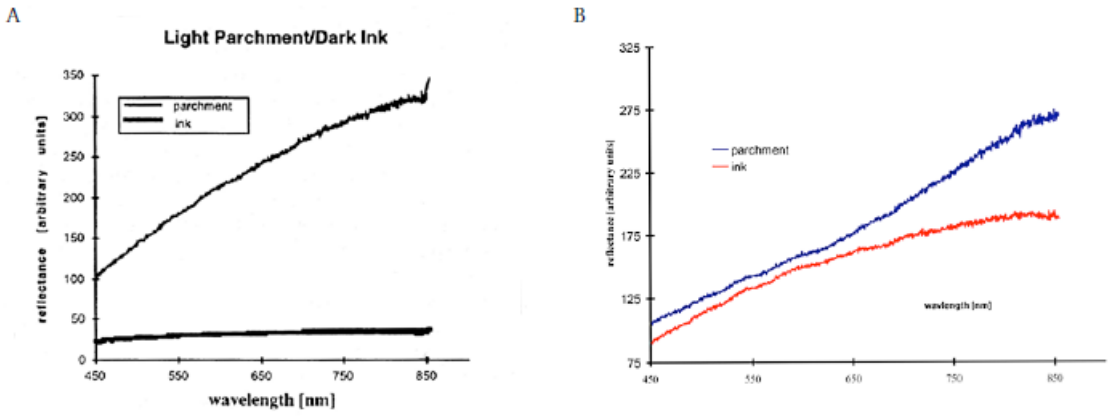

Figure 20: Reflectance spectra of two Dead Sea Scroll fragments. The fragment for the spectra on the left is easy to read both with the eye and in a b/w image while the right only becomes visible in the infrared.

Thus, monitoring reflectance suggests itself as a natural way to detect changes in the parchment. We will monitor changes in the parchment substrate, as that drives the transition from legible to illegible. The aim is to detect degradation *before* its effects become visually recognizable due to significant damage. At this moment, the cause of the change is unknown, but it surely reflects chemical or physical-chemical phenomena.

The conservation-monitoring plan

A number of fragments have been selected for periodic imaging and analysis. These are representative of the state of the scrolls as identified by the conservators. Issues include delamination, gelatinization, organic residues and cockling.

Note that we do not propose training across a large collection of fragments and then attempting to use this to measure changes. We are measuring a before and after for each fragment individually and not attempting to develop metrics across the entire collection.

Clearly, for this method to work, the imaging system must return accurate, repeatable and calibrated reflectance spectra. A noisy system would have an increased threshold of detection, so that larger spectral changes would be necessary before they could be recognized as "changed.". The system must be able to detect small changes; also false positives for the presence of changes must be avoided in data taken over time. This requirement for calibration and reproducibility has driven our technical decisions on the choice of imaging system.

Our approach to is to remove the imaging burden as much as possible by providing *calibrated, absolute* reflectance image cubes. We correct for variables, e.g., illumination gradients, illumination intensity variation and so on; as a result, *each time* an absolute reflectance cube is produced, and we can meaningfully compare the data with our multivariate methodology. We are measuring reflectance relative to a NIST white standard and obtain values between [0,1]; we are not calibrating the system into radiometric units. With this approach, spectral data quality and image registration between imaging sessions become the main factors that influence the sensitivity of the technique. The minimum spectral variation the technique can detect is strongly correlated to both sensitivity and technique. As we will show, binning the image is a good strategy to reduce the effects of registration and to increase the sensitivity, since the influence of a mis-registered pixel is now a smaller part of the binned (and larger) pixel.

The Imaging System

Only a few methods can produce medium format size spectral images, and we decided upon spectral illumination with narrow-band LEDs coupled with a 39 MP monochrome digital camera. High power LEDs (12) provide more than enough illumination to image a large field of view. We used λ=445, 475, 499,

540, 595, 638, 656, 706, 728, 772, 858, 925 nm. In general, one thinks that the more bands obtained, the better. In considering a method that yields 12 bands, not 40 or 50, a glance at Figure 1 shows that the spectra of the Dead Sea Scrolls are rather broad, featureless and highly correlated, rendering a dense spectral grid unnecessary. Practically speaking, one does not need *all* the spectral points. In any case, the first stage of analysis of spectral image data is to reduce the data dimensions via principal component analysis (PCA) or other methods.

The chosen system has the following advantages and features: 1) High-resolution color. We take the seven bands in the visible and create a color image, using a calibrated CIE mini-color checker chart from X-rite to create the proper transformation matrix. 2) Since one of the bands is 928 nm, we produce a high resolution IR image that provides legibility for text scholars. 3) A single image station can provide all three required imaging modes. 4) All images for any one image session or spectral cube are naturally co-registered across wavelength -- no refocusing or chromatic or lateral image shifts. 5) We are also taking low-angle raking illumination (~20^{o}) images to provide shadows and contrast that show surface topography.

Imaging Details

We are using an LED imaging system from MegaVision (Santa Barbara, CA, USA) [www.mega-vision.com], permanently installed in the IAA's dedicated imaging lab in Jerusalem. A critical component of the system is the 120 mm lens newly designed for broadband correction across the visible and NIR so there are neither chromatic aberrations nor lateral shifts as we change wavelengths (http://mega-vision.com/UV-IR_120mm_lens_130101.pdf). As a result, the images are naturally registered across wavelengths and there is no post-processing to align image planes of the same cube, a standard problem with band sequential imaging. The four panels of LED lights are arrayed in two

panels on each side, one with visible LEDs and the other with NIR. We did this to reduce NIR exposure times; since the Si camera sensitivity rolls off, moving the LEDs closer considerably reduces the exposure times. The panels hanging between the LED panels and the copy-stand base are plastic sheet diffusers that spread the illumination pool across the camera field of view and reduce hot spots. To permanently fix the illumination pool, the LED panels are fixed to the ceiling, the camera stand is bolted to the table and the table is bolted to the floor.

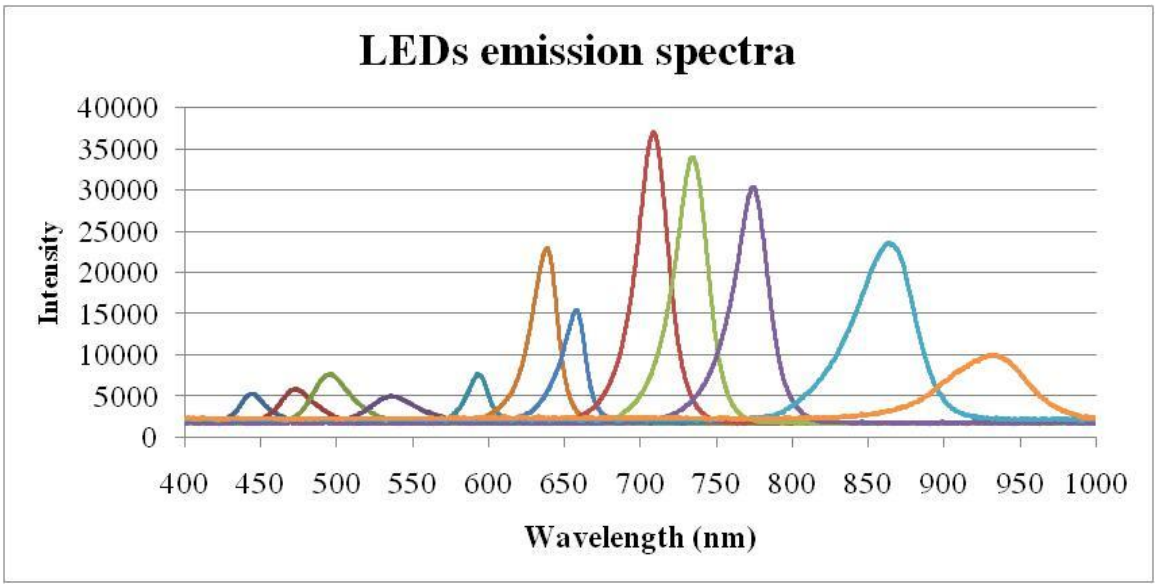

Figure 21: emission spectra of the 12 LEDs

Spectral data quality

Spectral data quality and image registration are the main drivers of the success of this approach. We have approached spectral data in two ways; 1) measurement of the illumination LEDs' performance separately; and 2) an extensive program of calibrated target measurements.

We are addressing two issues with the system calibration: 1) absolute reflectance, i.e., how well do we do with known targets; and 2) stability and reproducibility; i.e., even if we had systemic errors that prevented us from hitting the calibration values, how stable and reproducible is the system? Since

we are interested in changes, reproducibility is more important. *In precision vs. accuracy, we need precision.*

There are two ways to look at calibration and spectral data. One is to leave everything the same, i.e., target in same place, and take repeated measurements. This measures the stability of the system itself. We find that variations in the LED center wavelength are ~0.05%, variations in the bandwidth are ~0.24 % and power variations ~ 1%. Power changes are always calibrated out from a standard white. The other is more complicated. The feature that makes this conservation approach work, is that no matter where we put down a target and no matter how the LED panels are arranged, etc., we get the same absolute reflectance results within some error that we quantify. We use four separate targets to test for repeatability and absolute results: 1) the Xrite mini-color checker; 2) Imaging Sciences Golden Thread linear color target (http://www.imagescienceassociates.com/mm5/merchant.mvc?Screen=PROD&Store_Code=ISA001&Product_Code=OL5&Category_Code=TARGETS); 3) a custom calibrated target with seven patches, red/green/blue/yellow and 3 greys (Avian Technologies); and 4) individual Spectralon targets (red/green/blue/yellow and 4 greys) from Labsphere with NIST traceable reflectance measurements.

Since the project is required to create high fidelity color images we have also tested its color performance. Indirectly, this is a proxy for the spectral calibration since the L*a*b color space data is a weighted sum of the spectrum by the CIE XYZ values and so closely tied to spectra.

Calibration results

We measured the more important consideration, *repeatability*, in several ways. For one set of data, we moved the targets around in the field of view and measured the reflectance for different imaging locations. Figure 22 shows the

ratioed reflectance for three separate locations of the green Labsphere target; since the values are so close, the ratios are plotted to illustrate the differences. Remember that while we have absolute calibration of the Xrite color checker only out to 730 nm (the maximum wavelength of the CIE standard), we can still use the *entire* spectral range of the system to look at reproduciblity.

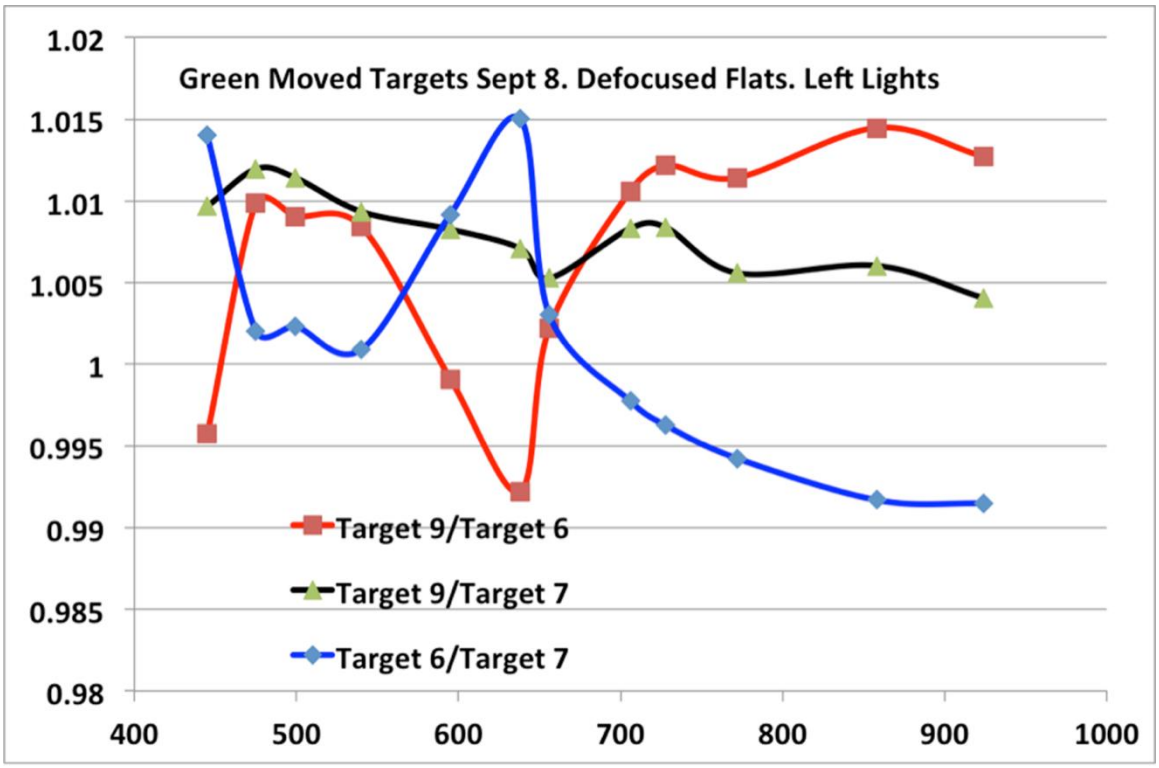

Figure 22. Measured reflectance for three separate locations of the target within the field of view; in general they were right, middle, left across a ~7" field of view.

Absolute values for the reflectance for the blue NIST traceable Labsphere reflectance standard are shown in Figure 23.

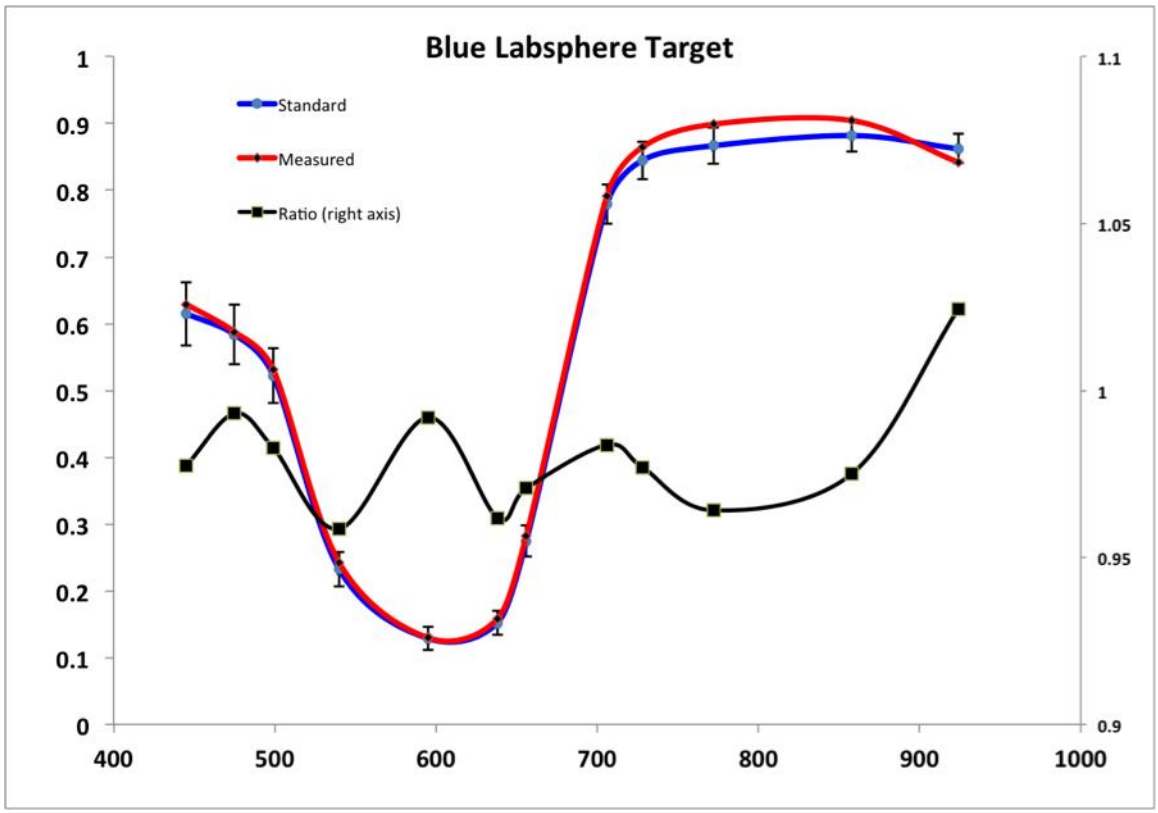

Figure 23. Comparison of measured and standard reflectance for blue target. The ratio of the standard/measured is plotted on the right hand axis.

Perhaps the best way to look at the stability and reproducibilty of the system is to look at data taken under very different conditions. Target data taken August 2 2010 and June 29 2010, are presented in Figure 24, for a custom gray target. In this case, the system had been taken down and reassembled in another location (another city, actually). Everything was different --LED illumination angle, resolution, focus, exposure times and so on -- however, we obtained the same values to ~0.02 absolute reflectance units.

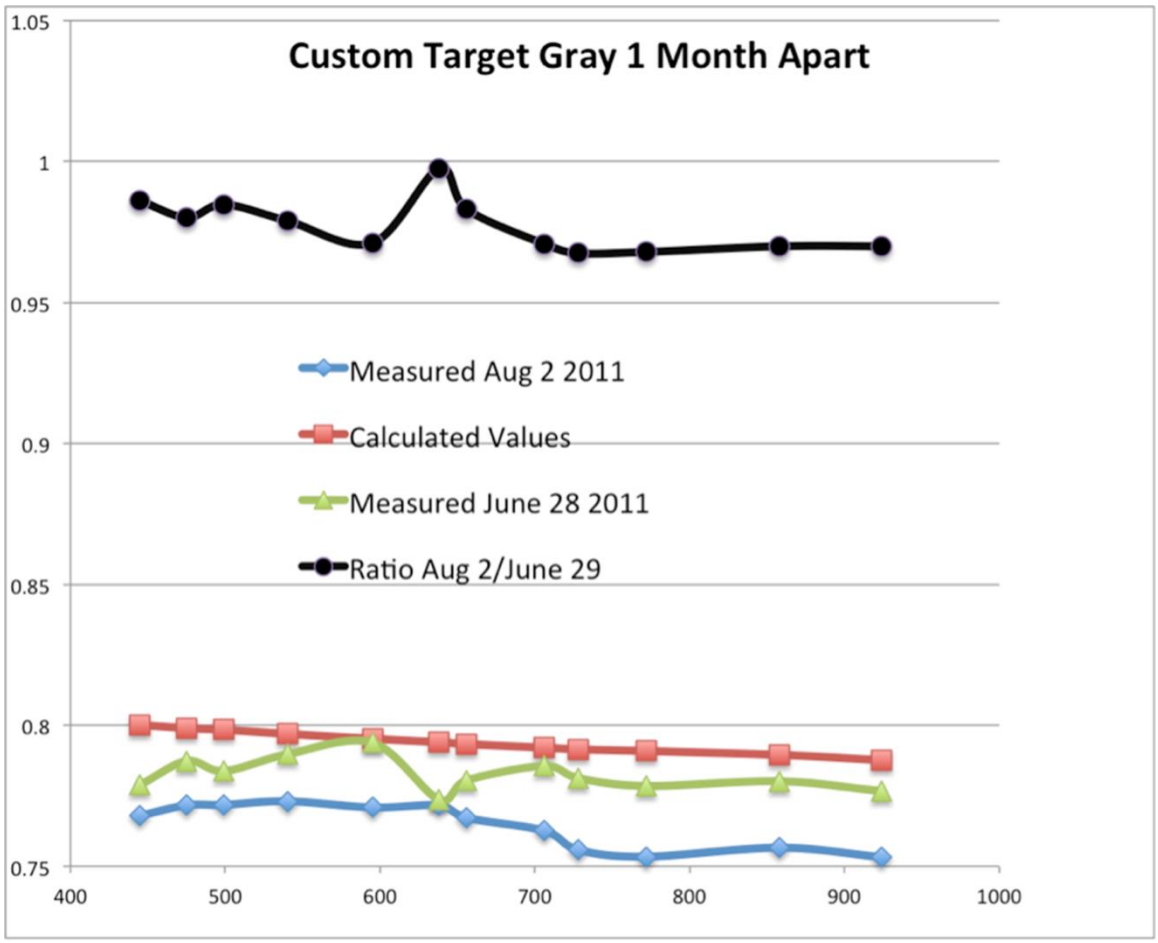

Figure 24. Measured values of a custom grey target taken over a month apart; the sytem had been dissassembled, moved to another city and reassembled inbetween.

The Dead Sea Scrolls are a universal cultural heritage. As such, the IAA is committed to safeguard the scrolls, preserve them for future generations and share them with the public and scholarly community worldwide.

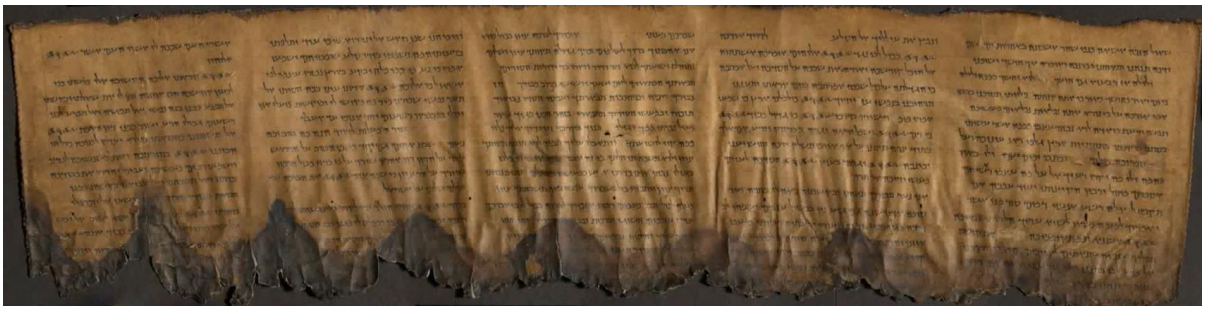

Figure 25: The Ten Commandments Deuteronomy scroll, 4QDeut^{n}, Spectral image in near infra red - 924 nanometers. (Photographers: Yair Medina & Shai Halevi, Courtesy of IAA)

2.2.7 Real case 2: Monitoring the conservation of S. Maria di Castello frescoes

Fresco painting is a method of ornamenting the walls and ceilings of buildings by painting designs in colors ground in water and mixed with lime upon the freshly laid plaster. Sometimes, in presence of walls crumbling by decay, old frescoes are detached, transferred to canvas and thus preserved.

In the ancient deconsecrated church of Santa Maria di Castello, located in Valle Lomellina (PV) Italy, are preserved five frescoes, now detached and framed, accidentally discovered inside the building under the plaster during the last restoration works in the seventies. The history of the church is linked to the mediaeval Strada's family, already present in Valle in the fifteenth century. The frescoes were painted in the first middle of the '400 and are therefore one of the oldest and most interesting of the Lomellina[68] (Figure 26).

Fig. 26: Saint Lucia and Saint Antonio Abate fresco.

Detached frescoes are more sensitive to temperature and humidity variations because they are attached on a linen support: their long term conservation is a challenge that can be overcome developing integrated research methodologies for the non-destructive monitoring of their conservation state.

The conservation work of cultural heritage, and in particular of wall paintings, has developed over time: from documents to drawings until photographs to record the information of the frescoes.

The applications of spectral imaging in cultural heritage sciences has been focused both on qualitative examination of artwork and, only recently with new advance of NIR imaging, also on quantitative chemical information[69].

Nowadays, methods belonging to digital image processing can help even in the restoration of historical artwork: digital image processing and computing has been used to give to conservator and restorers a better insight into the evolution of the fresco ageing[70].

Monitoring the conservation state of frescoes and, in general, of cultural heritage objects over time is very important in order to alert the conservator when potentially damaging changes are occurring.

The method described here follows a new approach aimed at the automatic detection of a deterioration process, its localization and identification. This method has been developed and applied with success on parchment samples and other supports and is actually used for monitoring the conservation state of the Dead Sea Scrolls in Israel. The technique is based on multispectral imaging coupled to multivariate analysis[66, 67].

For this project we developed a portable multispectral imager made by a CCD Monochrome camera and by two LEDs panels with 8 wavelengths from UV to IR.

EXPERIMENTAL

LED Multispectral Imaging. We developed a portable multispectral imaging (Figure 27) where the fresco is actively illuminated by light-emitting diodes (LEDs) generating different spectral bands while the reflected light is captured by a monochrome camera synchronized with LED. We used LEDs as light source because they are stable, highly monochromatic and non-invasive as there is no heat and stress for the imaged objects. We used two identical panels (Equipoise Imaging LLC, MD, USA), each consisting of 8 different LEDs centered on the following wavelengths: 370, 444, 466, 598, 521, 600, 640 and 923 nm. The LED bandwidth ranges from ~10 nm in UV to 40 nm in the IR. A CCD camera with a 8.3-megapixel Kodak CCD monochrome sensor array (ST-8300M, Santa Barbara Instrument Group, CA, USA), 17.96 x 13.52, with 3326 x 2504 pixels, 5.4 x 5.4 μm was employed.

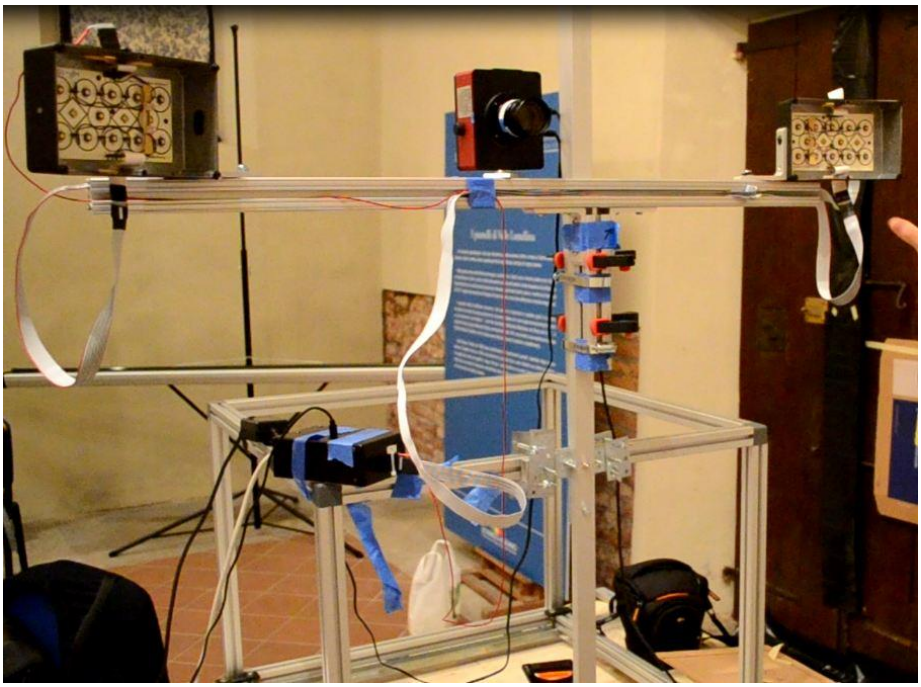

Fig. 27: Portable LED Multispectral Imaging system.

For principal component analysis, control charts and all other computations, we used the following software: MATLAB (The MathWorks, version R2007b) and

the open source software ImajeJ. We correct for illumination gradients, LED power variations and camera noise.

The power spectra of the different LEDs were measured using a spectrometer (Fig. 28).

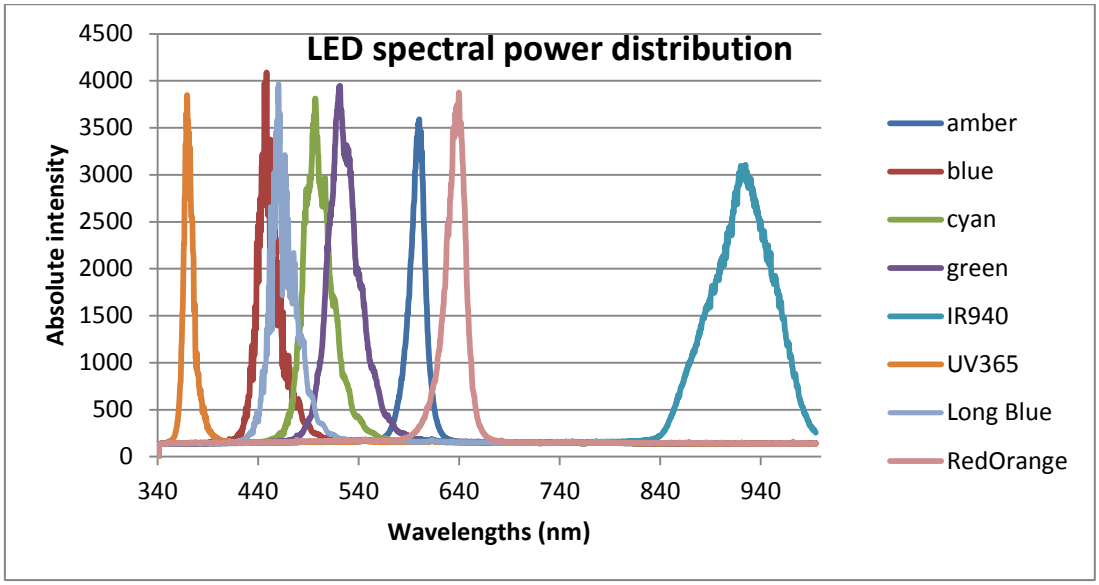

Figure 28: LEDs spectra power distributions.

The monitoring protocol

The procedure developed and used for monitoring the conservation state of frescoes consists of the following steps:

1. Fresco characterization: all the natural variability must be evaluated by recording five replicated images in multiple wavelengths (cubes) of the surface of the wall painting: in our case, the baseline image cubes set the timeline to zero.
2. Cube registration: image cubes collected during different imaging sessions have to be registered in order to compare always the same pixels.
3. Unfolding cubes. The cubes are unfolded into a bi-dimensional matrix (X) in which the columns are the 8 wavelengths and the rows are the pixels of

the different images. The columns are mean-centered prior to any statistical analysis.

4. Data set sampling. A good characterization of the natural variability requires that several cubes be treated together so that a large amount of memory (several GBs) is necessary. A random sampling must preserve both the macro and micro information present in the cubes.
5. Principal component analysis of the sampled baseline data set: this enables the description of the in-control situation natural variability by means of the relevant PCs.
6. Shewhart control chart: multivariate Shewhart charts are calculated using the scores of the relevant PCs obtained in the characterization phase. it is possible to calculate the limits (UCL and LCL) that permit identification of the pixels that show anomalous behaviors along time.
7. Fresco monitoring. The fresco is then monitored just acquiring a multispectral image cube: the cube is then unfolded and centered using the mean calculated in the training session, and the new data are projected onto the PC space previously obtained. The scores of the new image are then compared with the LCL and UCL to identify which pixels' variance exceeds the control limits. Contribution plots, which show the contribution of each wavelength to the aging process for a defined pixel, enable us to determine which wavelengths are affected by degradation.

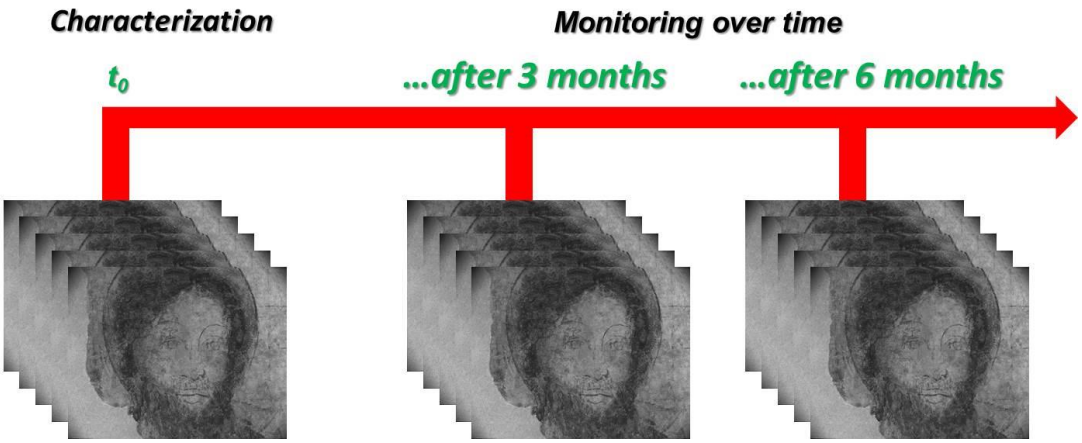

Fig. 29: monitoring steps. The procedure consist of a first characterization of status quo of the wall painting and then of the monitoring over time of the conservation state of the artwork.

RESULTS AND DISCUSSION

For this paper we focus on the fresco called Saint George and the Princess and in particular in a region that was not well conserved with some cracks, lacuna and discoloration as represented in the macro in figure 30.

The wall painting was monitored for 6 months: after the starting characterization, which serves as baseline of the frescoes conservation state, the painting was monitored three and six months later.

Fig. 30: Saint George and the Princess fresco and a macro of the area on which we focused our attention.

Principal Component Analysis. The first components calculated using centered multispectral image account approximately 74.2 %, 16.3 %, and 5.18 % of original variance. The first two alone account for 90.5 % of the variance and were considered the only two significant principal components. Figure 31 shows a particular of the score of the first (a) and second (b) principal component of Saint George and the Princess fresco: PC_1 is very similar to the original image and the second component accounts for a significant part of the dataset.

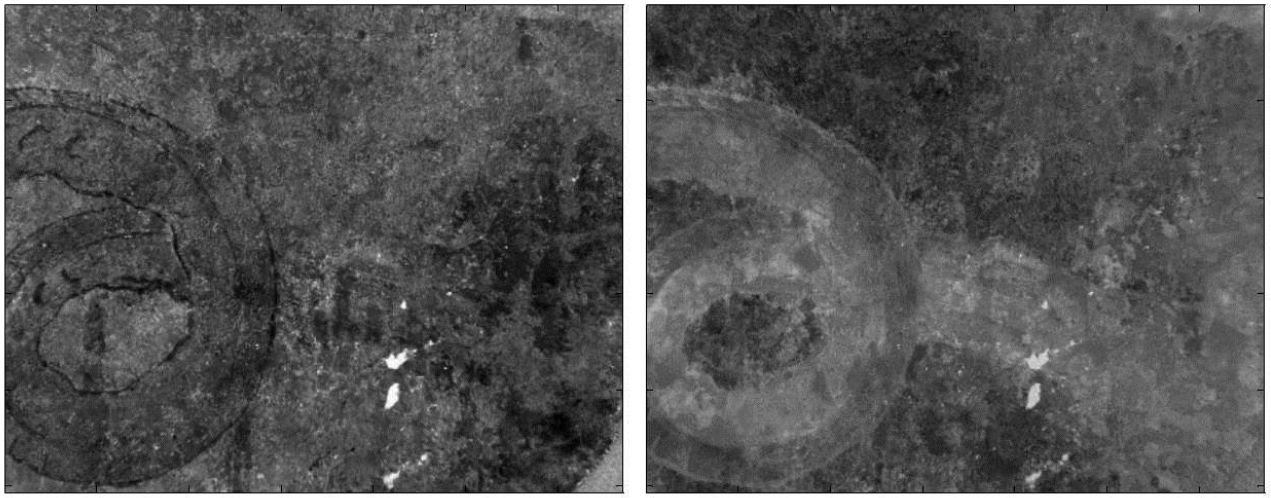

Figure 31: a particular of the score of the first (a) and second (b) principal component of Saint George and the Princess fresco.

Control chart is a map, related to the monitored region, that indicates the areas where the reflectance spectra of the fresco is changed respect with the starting characterization. Red and blue pixels represent the regions that are statistically changed and so where a degradation is probably in act. Green pixels correspond to the 'in control' areas: here the conservation state of the object is good.

Figure 32 shows the control chart of the first PC (a) of the monitored area of the fresco after 6 months: most of the pixels are green which means that the wall painting is in good state of conservation and the reflectance spectra didn't change after 6 months. There are only few out of control pixels (red and blue pixels) in correspondence of the corners of the control chart. They are caused by the aberration of the camera lens that is not able to get a good focus near the corners: this pixels can't be considered changed/degraded. Figure 32b is another representations of the out of control pixels (white) overlapped to the black and white image of the fresco.

The analysis of the control chart of the second component didn't show particular situation: all the pixels were in control.

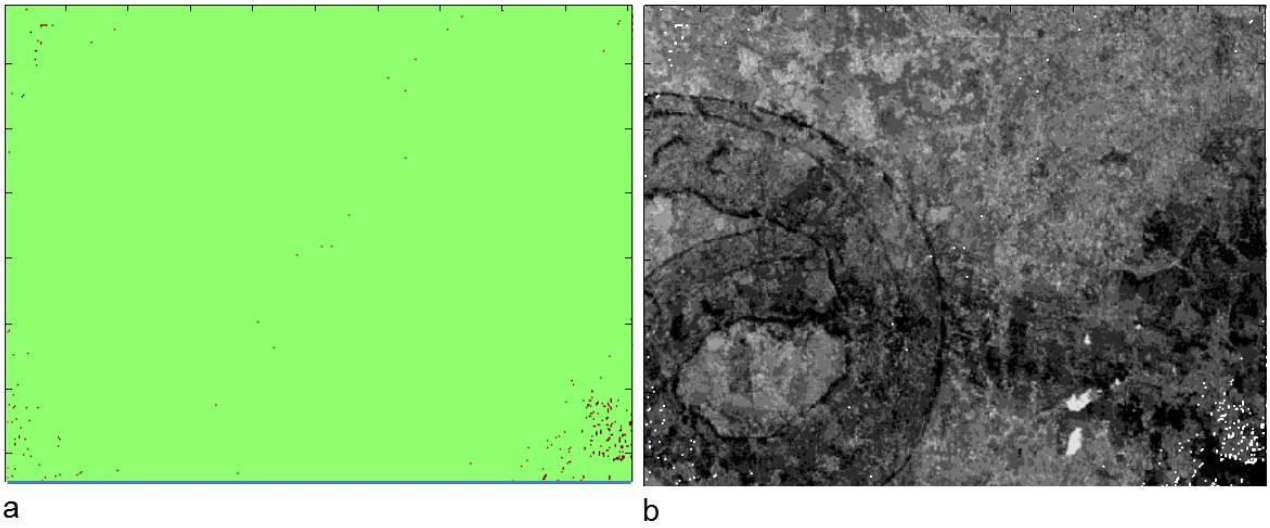

Fig. 32: control chart of a region of the Saint George and the Princess fresco (a), the fresco can be considered in good state of conservation; red and blue pixels, that usually represent the changed areas, are caused by the aberration of the camera lens that is not able to get a good focus near the corners; figure b is another representations of the out of control pixels (white) overlapped to the black and white image of the fresco.

CONCLUSIONS

The aim of this project was the development of a non-invasive tool based on a portable LED multispectral coupled to statistics imaging for monitoring the conservation state of frescoes.

The objective was to detect degradation of frescoes before visually detectable damage has occurred. The technique here presented is actually in use for monitoring the conservation of the Dead Sea Scrolls (parchment) in Jerusalem.

A portable LED multispectral imaging system was used to characterize the conservation and set the timeline to zero of Santa Maria di Castello frescoes (Italy).

We focused the monitoring on the fresco called Saint George and the Princess and in particular in a region that was not well conserved with some cracks, lacuna and discoloration. The wall painting was monitored, after the starting characterization, three and six months later. After six months the fresco was in

good state of conservation: the method was able to detect some changed areas in correspondence of the corners of the monitored region that were caused by the aberration of the camera lens. This instrumental problem can be overcome by using a bigger camera sensor or by introducing some sort of image correction.

In conclusion we can affirm that this method could be a useful tool for the monitoring of conservation state of frescoes: the advantages of been non-invasive, fast and a surface-analysis instrument makes this quantitative imaging approach the future of conservation monitoring.

2.3 MONITORING SURFACES USING IMAGING 3D

Imaging 3D

Optical instrumentation allows the acquisition of complex virtual models from the original artwork with high accuracy. These models permit the study of the structure without a direct handling on the artwork, avoiding damages due to the process.

The construction of 3D surface models of the objects for detailed 3D measurements is a field of ongoing research for some decades[72].

In recent years, the demand for optical 3D imaging sensors has become increasingly relevant. The miniaturization and integration of optical light sources, detectors and components, in the electronic equipment and the mechanical structure of the sensors has led. In the last decade, the availability of techniques and components has led to the production of a wide spectrum of commercially available devices, with measurement resolution from a few nanometers to fractions of a meter[73].

The objects typically measured are size, surface texture and shape of the artwork, for whole and partial scans for reverse engineering of art restoration and for reproduction of artworks.

2.3.1 Imaging 3D: state of art

3D imaging techniques generally operate by projecting (in the active form) or acquiring (in the passive form) electromagnetic energy onto/from an object followed by recording the transmitted or reflected energy.

Reflection sensors for shape acquisition can be subdivided into non-optical and optical sensing. Non-optical sensing includes acoustic sensors (ultrasonic,

seismic), electromagnetic (infrared, ultraviolet, microwave radar, etc...) and others. These techniques typically measure distances to objects by measuring the time required for a pulse of sound or microwave energy to bounce back from an object. In reflection optical sensing, light carries the measurement information.

The 3D techniques are based on optical triangulation, on time delay, and on the use of monocular images. They are classified into passive and active methods. In passive methods, the reflectance of the object and the illumination of the scene are used to derive the shape information: no active device is necessary. In the active form, suitable light sources are used as the internal vector of information. A distinction is also made between direct and indirect measurements. Direct techniques result in range data, i.e., into a set of distances between the unknown surface and the range sensor. Indirect measurements are inferred from monocular images and from prior knowledge of the target properties.

Laser triangulators

Both single-point triangulators and laser stripes belong to this category. They are all based on the active triangulation principle. The laser source generates a narrow beam, impinging the object, the back scattered beam is imaged and the measurement of the surface is achieved by scanning.

One of the most significant advantages of laser triangulators is their accuracy, and their relative insensitivity to illumination conditions and surface texture effects. Single-point laser triangulators are widely used in the industrial field, for the measurement of distances, diameters, thicknesses, as well as in surface quality control applications.

Structured light

Structured light based sensors share the active triangulation approach above mentioned. However, instead of scanning the surface, they project bi-

dimensional patterns of non-coherent light, and elaborate them to obtain the range information for each viewed point simultaneously. A single pattern as well as multiple patterns can be projected.

Stereo vision

The stereo vision method represents the passive version of structured light techniques. Two or more cameras concurrently capture the same scene. The reconstruction by stereo approach expected the following steps: image acquisition, camera modeling, feature extractions, correspondence analysis and triangulation. No further equipment (e.g. specific light sources) and no special projections are required. The remarkable advantages of the stereo approach are the simplicity and the low cost; the major problem is the identification of common points within the image pairs, i.e., the solution of the well-known correspondence problem. Moreover, the quality of the shape extraction depends on the sharpness of the surface texture (affected by variations in surface reflectance).

Photogrammetry

Photogrammetry obtains reliable 3D models by means of photographs. The elaboration pipeline consists of: camera calibration and orientation, image point measurements, 3D point cloud generation, surface generation and texture mapping. Camera calibration is crucial in view of obtaining accurate models. Image measurement can be performed by means of automatic or semi-automatic procedures.

Time of Flight

Surface range measurement can be made directly using the radar time-of-flight principle. The emitter unit generates a laser pulse, which impinges onto the

target surface. A receiver detects the reflected pulse, and suitable electronics measures the roundtrip travel time of the returning signal and its intensity. Single point sensors perform point-to-point distance measurement, and scanning devices are combined to the optical head to cover large bi-dimensional scenes. Large range sensors allow measurement ranges from 15 m to 100 m.

Interferometry

Interferometric methods operate by projecting a spatially or temporally varying periodic pattern onto a surface, followed by mixing the reflected light with a reference pattern. The reference pattern demodulates the signal to reveal the variation in surface geometry. The measurement resolution is very high, since it is a fraction of the wavelength of the laser radiation. For this reason, surface quality control and microprofilometry are the most explored applications.

Shape from shadows

This technique is a variant of the structured light approach. The 3D model of the unknown object is rebuilt by capturing the shadow of a known object projected onto the target when the light is moving. Low cost and simple hardware are the main advantages of this approach, even if at the expense of low accuracy.

Shape from shading

Shape-from-shading requires the acquisition of the object from one viewing angle and varying the position of the light source, which results in varying the shading on the target surface. The acquisition hardware is very simple, and low cost. The technique is better known as reflectance transformation imaging (RTI)[73].

2.3.2 Reflectance Transformation Imaging (RTI)

Malzbender et al. introduced a novel image-based relighting technique for visualizing the appearance of a surface under a spatially variable source of illumination. RTI is an image-based recording methods in which information about surface reflectance is captured per pixel. RTI images are created from information derived from multiple digital photographs of an object shot from a stationary camera position: in each image, light is projected from a different known, or knowable, direction. This process produces a series of images of the same subject with varying highlights and shadows. Lighting information from the images is mathematically synthesized to generate a mathematical model of the surface, in the form of surface normals for each pixel, and used for enhancing detail[74-76]. A surface normal is a vector perpendicular to the surface at any given pixel. One of the products of the method is the surface normal for each pixel and we focused on that for measuring change[77].

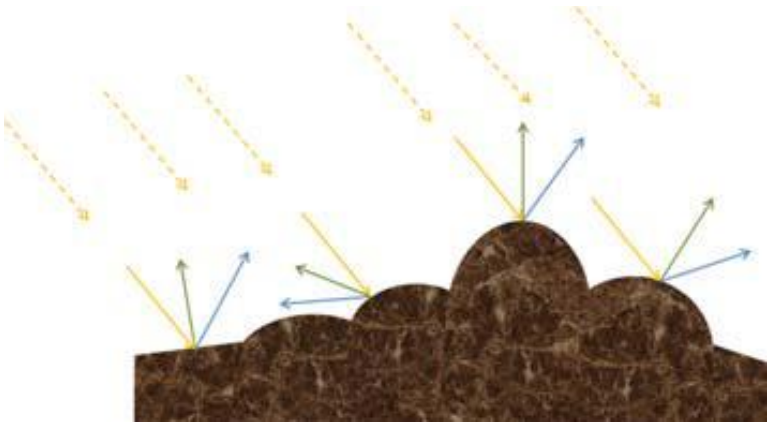

Fig 33: Surface normal representation: the green arrows represent surface normal. the surface normal data provide information about the 3D shape of the surface.

Three-dimensional virtual reality processing software is able to utilize surface normal information in order to calculate the deflection of light rays on a virtual 3D surface.

RTI is a non-invasive and non-contact recording method, and therefore protects the heritage resource being recorded. RTI captures information about surface texture using a series of digital photographs, thus eliminating the need for contact or destructive sampling. Although this is a 2D recording technique, it is often described as 2½D because of the high-level visual information provided by highlighting and shadowing 3D objects. In particular, it approximates the surface orientation at each pixel, providing a relative measure of curvature known as a surface normal.

Using color data stored per pixel, as well as the captured surface normal information, this technique reveals surface texture and fine detail sometimes not captured by static photography or even obvious to the naked eye. RTI is cost effective, as it can be carried

out using a relatively inexpensive tool kit and freely available software.

The software processes the multiple images into a single file that derives all possible light positions within the virtual hemisphere of light. The final image looks like a 2D photograph, but is actually the documentation of the subject's surface interaction with the light positions, at the individual pixel level. By moving a mouse (or other pointing device), the viewer can control the light direction, zoom in and out, and select data enhancement options that increase sharpness and contrast and even change surface properties. For instance, non-reflective surfaces such as paper can be given a metallic surface quality to increase legibility and remove color and stains[77].

Generating surface normal

A surface normal of a pixel is a vector perpendicular to the local surface that provides information about 3D shape of the surface. Irradiance signals can be represented using low-order basis functions due to their low-frequency nature. Spherical harmonics (SH) have been used to provide such basis. However the

incident light at any surface point is defined on the upper hemisphere; full spherical representation is not needed. In literature exists two main ways to describe the reflectance function: one using polynomial texture map (PTM)[75] and another one using Hemispherical Harmonics (HSH)[79]. Is well known that HSH approach is superior in term of 3D rendering because PTM use only 6 coefficients of a biquadratic polynomial to describe the surface normal and a third order HSH uses 16 coefficients.

After capturing all images for RTI, each with a different light position and the same camera position, all the pictures, and respective light direction, for each single pixel is collected from all the images and fitted to the Hemispherical Harmonics function or Polynomial Texture Map[78].

Change detection principles

Change measurement requires quantitative imaging methods: measuring change requires a before and an after image, quantitated well enough, with low noise, to make useful comparisons. The objective of this research was to define how reproducible and accurate RTI methods are in order to develop a monitoring methodology to automatically recognize areas that have changed. By monitoring the normals over time it is possible to detect the small-scale morphological and physical changes in an object.

Low reproducibility and accuracy mean that any comparison method has poor sensitivity to change, since we cannot differentiate image change from uncertainly in the measurement.

Statistical process control is widely used in industrial applications but has been advantageously applied to cultural heritage monitoring. The general principle is to consider the conservation state as a process in its “in-control” condition, that is, when no deterioration effect is acting. Each further deviation from this initial condition is attributable to a damaging effect acting on the artistic object. The

basic idea is that monitoring the normals over time it is possible to detect the small-scale morphological and physical changes in an object.

A normal can be considered changed only if the value exceeds the region of statistical control which is defined by 3σ around the average value of each pixel. This region corresponds to a confidence level of more than 99%. The average normal of each pixel and the region of statistical control have to be accomplished by recording several replicates of RTI of the monitored object: this baseline of normals set the timeline to zero and constitutes the characterization of the object. In this phase the object can be considered "in statistical control".

The absolute sensitivity of the method is the minimum variation of the normal that can be considered a statistically relevant change of the object: the larger the variance of the baseline normals, the less sensitive the method is.

In the present research the region of joint probability of x, y and z (Cartesian coordinate of the surface normal vector) corresponding to the hyper ellipsoidal volume defined by the multivariate Gaussian probability function was approximated by the volume reported in figure 1: this approximation is sufficiently conservative to provide reliable results. A normal is considered changed only if the monitored vector is outside the control volume.

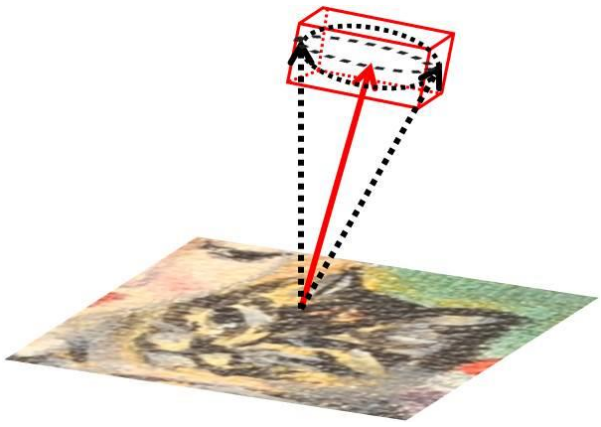

Fig. 34. Cone with ellipsoid base (dot lines) that represents the region of the statistical limit within which a normal can be considered not changed.

2.3.3 Case study 1: monitoring of a drawing

The past decade has seen the rapid evolution and application of computational photography methods to document important works of human heritage, from art and architecture to archives and archaeology. The next logical step involves defining just how reproducible and precise these methods are in order to use them to measure rates of change for important works of cultural heritage. The need is to move to calibrated, quantitative image datasets for reproducible imaging.

The aim of this research was the development of a reliable RTI imaging method for monitoring changes in cultural heritage objects. We measured the precision of computed surface normals, which define the basic repeatability of RTI and the sensitivity of the method.

EXPERIMENTAL

Camera – We used Nikon D3X DSLR camera with a 50 mm macro lens. The images are 6048 x 4032 pixels. The camera was operated tethered to a PC.

Reflective sphere – We used a black reflective sphere to locate the lighting angle in each photograph. The processing software is able to identify automatically the light direction on the sphere.

Light – A wireless synched flash light source illuminated the surface of the object to produce the highlight point in the reflective target. The object was illuminated from multiple light positions, creating a virtual dome, using 15°, 30°, 45° and 60° lighting angles and moving the flash following a pattern with radial spokes. The power of the flash light was set to illuminate the surface of the object enough. The light was separated from the surface of the object at a consistent distance of 2× the object's diameter.

RTI REPEATIBILITY AND SENSITIVITY

For this research we imaged a model drawing (Fig. 35a).

We measured the repeatability of computed surface normals by recording in five separate imaging sessions all the images. We computed the normals both using PTM and HSH and we calculated the average variability. The normal is described representing the vector using Cartesian coordinates *x*, *y*, and *z*: the average variability is calculated as standard deviation/mean*100 for each pixel. The average variability for PTM is 26%, 17%, 3% for *x*, *y* and *z*, instead for HSH is 0.8%, 1.9% and 1.9% for *x*, *y* and *z* (table 4).

RTI average variability: PTM and HSH			
variables	PTM	HSH	diff
x	26%	0.8%	-97%
y	17%	1.9%	-87%
z	3%	1.9%	-37%
phi	19%	1.7%	-91%
theta	6%	0.7%	-88%
rho	58%	1%	-98%

Table. 4. RTI average variability computed using PTM and HSH polynomial functions: the variability was calculated both using Cartesian and spherical coordinates.

We calculated the sensitivity of the method, which is the minimum variation that can be statistically considered a change of the object and which is directly correlated to the repeatability of the method. The statistical limits of each normal are represented as a cone, as described before: the absolute sensitivity is measured in steradians percentage and is calculated dividing the solid angle of

the cone by the hemispherical space (4π) which represents the all possible positions that a normal can have. The average included solid angle of the cone is 0.003 steradians for HSH, while for PTM method is 0.5 steradians, much less sensitive (Table. 5).

We also calculated the absolute sensitivity of phi and theta as angle: for PTM the sensitivity is 17.4% and 1.6% for phi and theta instead for HSH the sensitivity is 0.5% and 0.8% for phi and theta.

Absolute sensitivity of PTM and HSH		
variables	**PTM**	**HSH**
average solid angle	**0.5%**	**0.003%**
phi	**17.4%**	**0.5%**
theta	**1.6%**	**0.8%**

Table. 5. Absolute sensitivity of PTM and HSH computed normals.

We also measured the repeatability of RTI dome method in which each highlight position is provided by a different light source. Table 6 shows the average variability for HSH using movable flash light and a dome: the average variability for flash light is 0.8%, 1.9% and 1.9% for *x*, *y* and *z* and for the dome is 1.2%, 1.8% and 1.2% for *x*, *y* and *z*.

The repeatability of the RTI dome is pretty much the same of the movable flash light technique but one of the advantages of this approach is that the light position is fixed and the acquisition time is cut down.

RTI average variability: flash light and dome		
variables	Flash light	Dome
x	0.8%	1.2%
y	1.9%	1.8%
z	1.9%	1.2%

Table. 6. RTI average variability computed using HSH from movable flash light technique and RTI dome method.

DAMAGE DETECTION IN A DRAWING

The derived statistical limits from variance of the five RTI replicates have been used to compare the normals before and after damage. Figure 35 shows the color image of the drawing we used for this research: figure 35a represents the undamaged drawing and figure 35b represents the drawing after damage. After characterizing the natural variability of the method and of the object, we damaged the drawing by creating two small holes (red circles) and a scratch (red arrow).

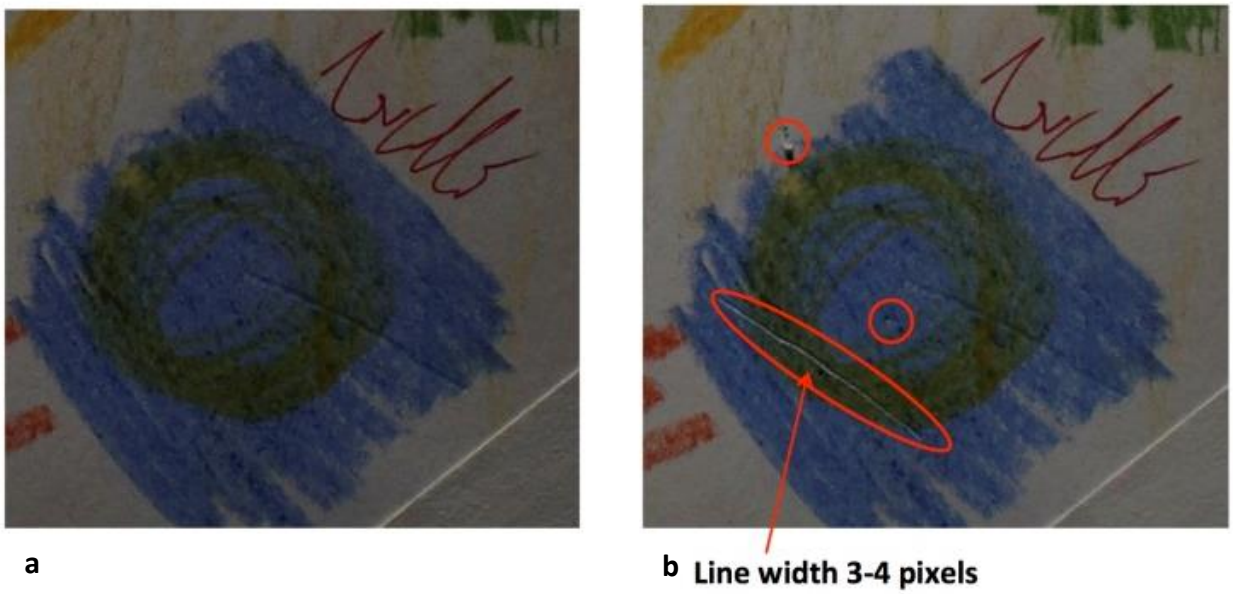

Fig. 35. Color images of the drawing used for this research before (a) and after (b) damage.

Then we captured the RTI again, we calculated the surface normals of the damaged drawing and we built a map of change by comparing the normal of each damaged pixel with the statistical limits. The normal image of the damaged drawing was aligned with the normal images of the undamaged drawing before the comparison.

Figure 37b shows the map of change for the y values of the normal: red and blue pixels represent the areas where the normals are statistically changed. In figure 37b there is the color image of the drawing: white pixels are the changed pixels. Figure 37a represents the bi-dimensional projection of the y value of the normals of the damaged drawing: the two holes and the scratch are clearly seen. They show up as changes in the normals as the act of scratching and punching the paper distorts the paper surface a bit.

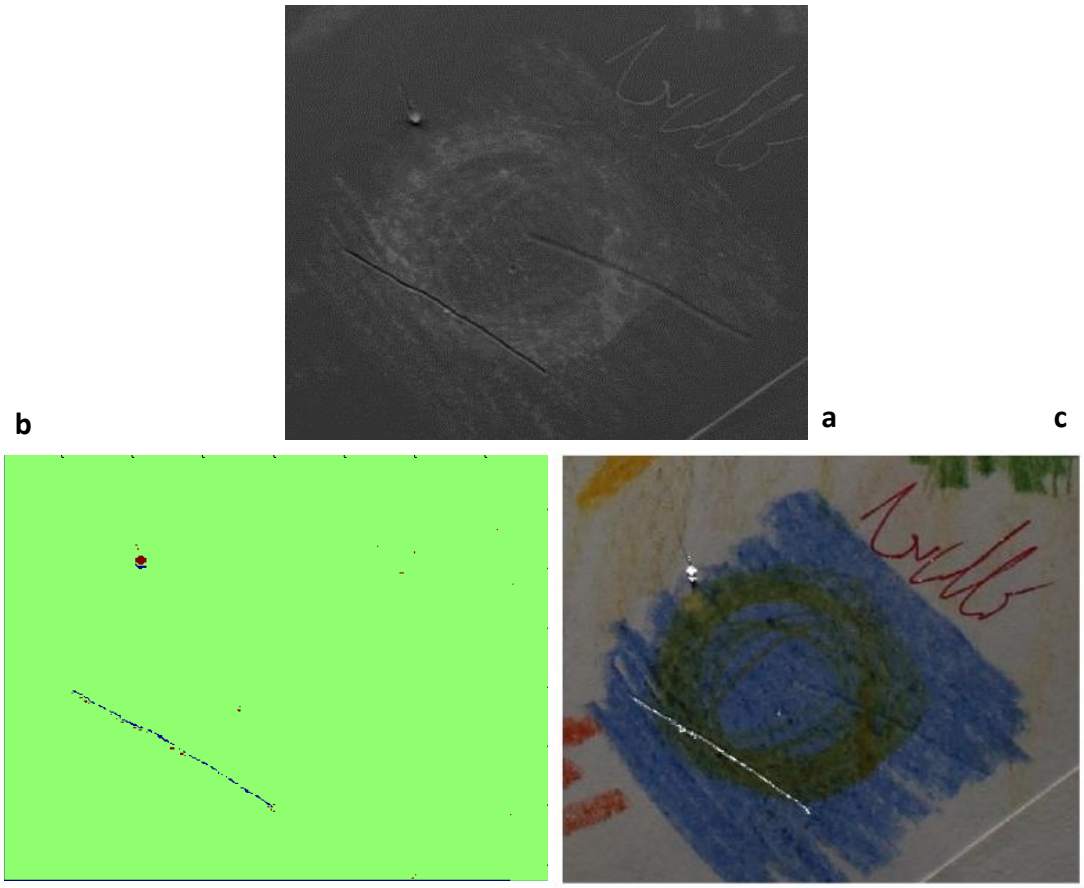

Fig. 37. Maps of change for the y value of the normal (b), red and blue pixels represent the damaged areas. In figure 37b is represented the map of change (white pixels) overlapped to the color image of the drawing. Figure 37a shows the bi-dimensional image of the y values of the normal of the damaged drawing.

Figure 38a shows the map of change of the normal in presence of a new wave on the drawing (fig. 38c): red and blue pixels represent the areas where the normals are changed. The behavior of the two sides of the wave is different (blue and red areas) because the directions of the normal are the opposite respect with the camera. At the top of the wave (green area) the normal didn't change because is still flat. Figure 38b represents the intensity map of change of each pixel.

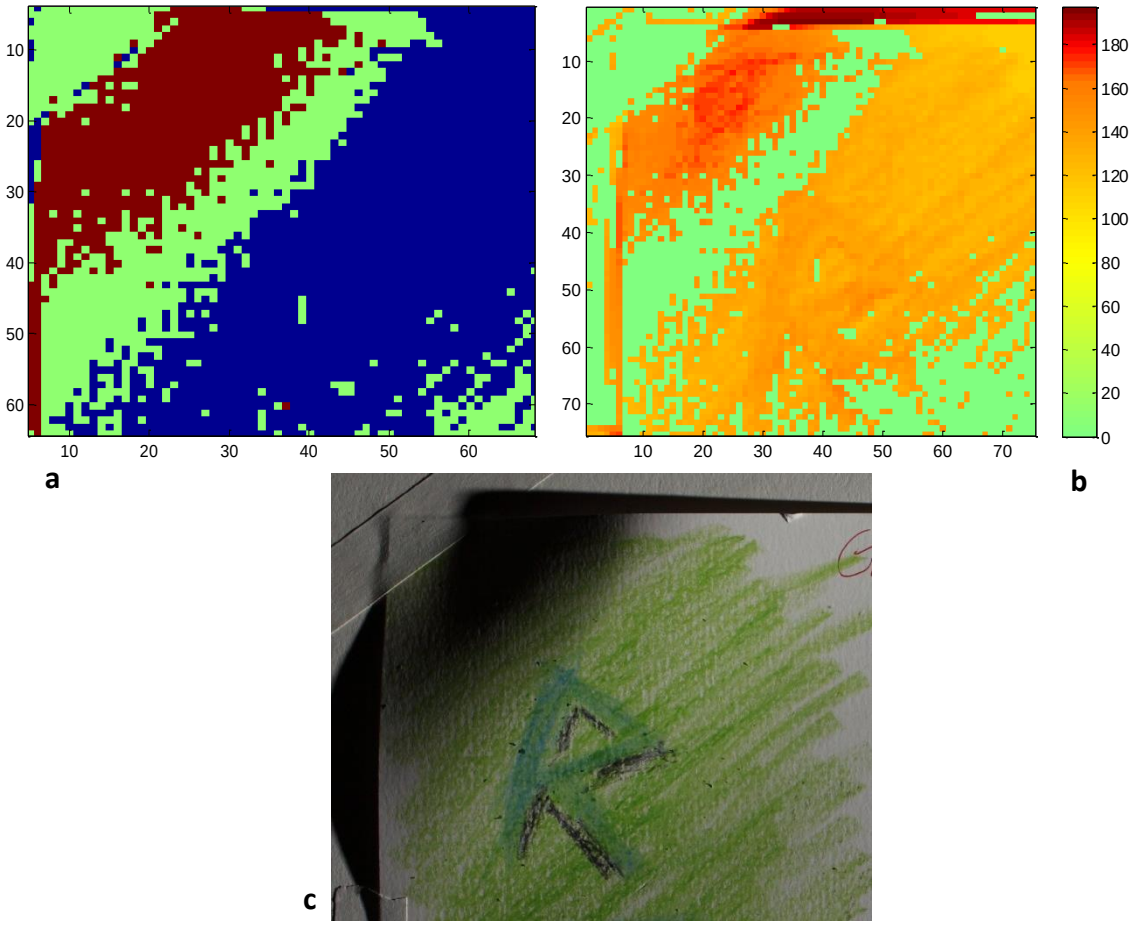

Fig. 38. Maps of change of normal in presence of a wave of the paper.

CONCLUSIONS

The aim of this research was the development of a reliable RTI imaging method for monitoring changes in cultural heritage objects. RTI provides detailed information on the geometry of the object surface. We showed that RTI can be reproducible and quantified to the level where it can be used as practical method for measuring change in objects.

We found that computing surface normals by using the HSH polynomial function is more reproducible than using the older PTM method, and is therefore more sensitive to changes.

We developed a monitoring protocol which includes an imaging protocol, the extraction of the normals and comparison within statistical limits.
We characterized the variability of a drawing, computed the statistical limits and then damaged the object. We then captured the RTI and compared the normals to the limits: the method was able to detect the damage automatically.
In conclusion, this new approach to RTI offers a useful strategy for monitoring physical change in important cultural heritage objects.

2.3.4 Case study 2: monitoring of a painting

Paintings are made by different layers of material, which roughly are support, primer, different layers of paint and varnish. Other layers such as glue, a preparatory drawing, an imprimatur and additional layers of paint can complement the painting composition. Moreover, the material composition of paintings is often dominated by composite materials of different chemical substances. In general, a damage or defect can be defined as an adversely change to an original state.
Deterioration of paintings can be caused by environmental factors such as temperature fluctuations, relative humidity variations, light radiation and biological factors. In addition transportation can be another source of damage: vibration, environmental climate change and bad handling can add up and damage the transported. The effects of all these factors produce changes in both the painting structure and chemical composition[80, 81].
In traditional conservation techniques the evaluation and quantification of smallest changes and defects results mostly from an optical and subjective assessment, comparison of the previous and the subsequent state of conservation and by means of condition reports. Conservators and specialists are not always able to distinguish a new defect from an old one or detect its expansion.

Several paintings have been examined and it is shown that RTI is able to record surface features including craquelure, planar distortion, wood grain and canvas weave.

RTI renderings made before and after physical changes to painting were compared and showed how promising the technique is for the examination of alterations in texture and shape of paintings[82].

In this paper we propose a reliable RTI imaging method for the non-invasive detection of morphological and physical changes in painting: the method includes an imaging protocol, the extraction of the surface normal and comparison with statistical limits. In order to have a reproducible and quantitative method that can be used as practical method for measuring change in objects we developed a custom semi arch arm with LED lights to illuminate the surface of the painting. Our method is a completely non-invasive monitoring technique: we obtained an accurate and quantitative measure of the deterioration and degradation present in the painting after artificial damages.

EXPERIMENTAL

Camera - We used Nikon D3100 camera with a 18 mm macro lens, F-stop f/8 and exposure time 0.62 seconds: both F-stop and the exposure time were fixed for all the acquisitions. The images are made by 4608 x 3072 pixels. The camera was operated tethered to a PC.

Light - We used a semi arch arm on which were placed four LEDs (20 Watt) at 15°, 30°, 45° and 60° lighting angles (Figure 39) to illuminate the surface of the painting to produce the highlight point in the reflective target. The object was illuminated from multiple light positions moving the arm following a pattern with radial spokes, creating a virtual dome. The power of the light lamps was set to illuminate the surface of the object enough and was the same for each lamp.

The lights were located from the surface of the object at a consistent distance of 3 times the object's diameter.

Fig. 39: instrument setup: semi arc arm with LEDs and RGB camera working on a painting.

Reflective sphere - We used a black reflective sphere to locate the lighting angle in each photograph. The processing software is able to identify automatically the light direction on the sphere.

Image processing - We used open source software to build the RTI images from the raw image set RTI Builder from Cultural Heritage Imaging (culturalheritageimaging.org) and then calculated the normals separately using both Python version 2.7.3 and Matlab R2010a (The MathWorks, USA).

Painting - Paintings are made by different layers of material and by composite materials of several chemical substances. In general, a damage or defect can be defined as an adversely change to an original state. Deterioration of paintings can be caused by many factors that may produce changes in both the painting

structure and the chemical composition, some are: cracks, abrasion, craquelure, general and point surface deformations, canvas waves, stretching, crazing and sinking.

A painting on canvas of 10 cm x 7 cm size was created. The canvas was painted with acrylic colors.

RTI REPEATABILITY AND SENSITIVITY

For this research we imaged a model painting (Fig. 40a). We measured the repeatability of computed surface normals by recording in five separate imaging sessions all the images. We computed the normal using HSH and we calculated the average variability. The normal is described representing the vector using Cartesian coordinates x, y, and z: the average variability is calculated as standard deviation/mean*100 for each pixel. The average variability is 5.8%, 6.9% and 3.8% for x, y and z. The variability of the measure is very important because is strictly correlated to the sensitivity of the method which is the minimum variation that can be statistically considered a change of the object. Our repeatability is higher than the one we calculated in our previous work even if we used a semi arc arm to reduce the variability of light positions and to save time during imaging sessions. In the previous work we used a DSLR camera which is well known has better performance than the camera we used for this work.

DAMAGE DETECTION IN PAINTING

The five RTI replicates recorded to calculate the repeatability were used as a training set to characterize the system "natural" variability for building the control chart, that is, before any aging. The statistical limits were calculated as 3σ around the average value of each pixel and have been used to compare the normals before and after damage. Figure 40 shows the color image of the

painting we used for this research: figure 40a represents the undamaged painting and figure 40b represents the drawing after damage. After characterizing the natural variability of the method and of the object, we damaged the drawing by creating different types of damages: some small holes, three cracks and one abrasion (red circles).

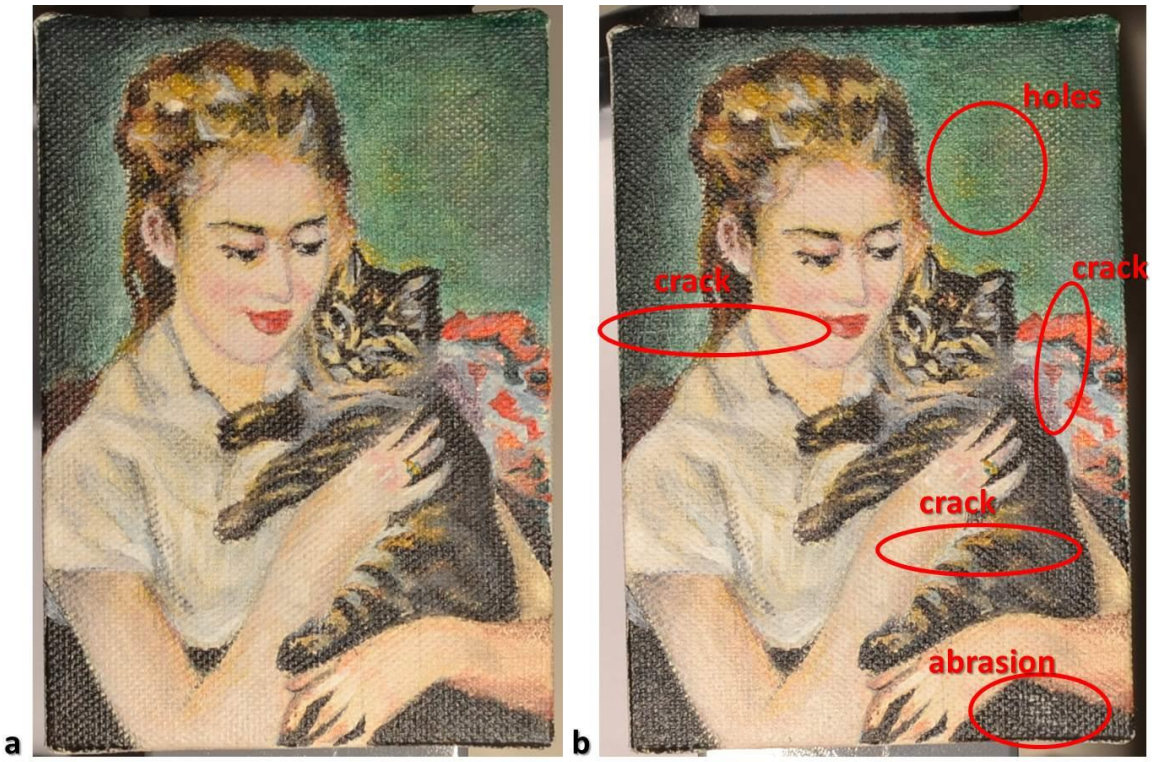

Figure 40: color images of the painting before (a) and after the damage (b).

Then we captured the RTI again, we calculated the surface normals of the damaged painting and we built a map of change by comparing the normal of each damaged pixel with the statistical limits. The normal image of the damaged painting was aligned with the normal images of the undamaged painting before the comparison.

Figure 41 shows three different ways to visualize the results: figure 4a shows the map of change for the x values of the normal: red and blue pixels represent the areas where the normals are statistically changed; the map of change for the y

values of the normal is represented in figure 4c. In figure 4b there is the color image of the painting: white pixels are the changed pixels.
Maps of change detected all the damages (red circles) that had been artificially done: the method was able to identify the changed area.

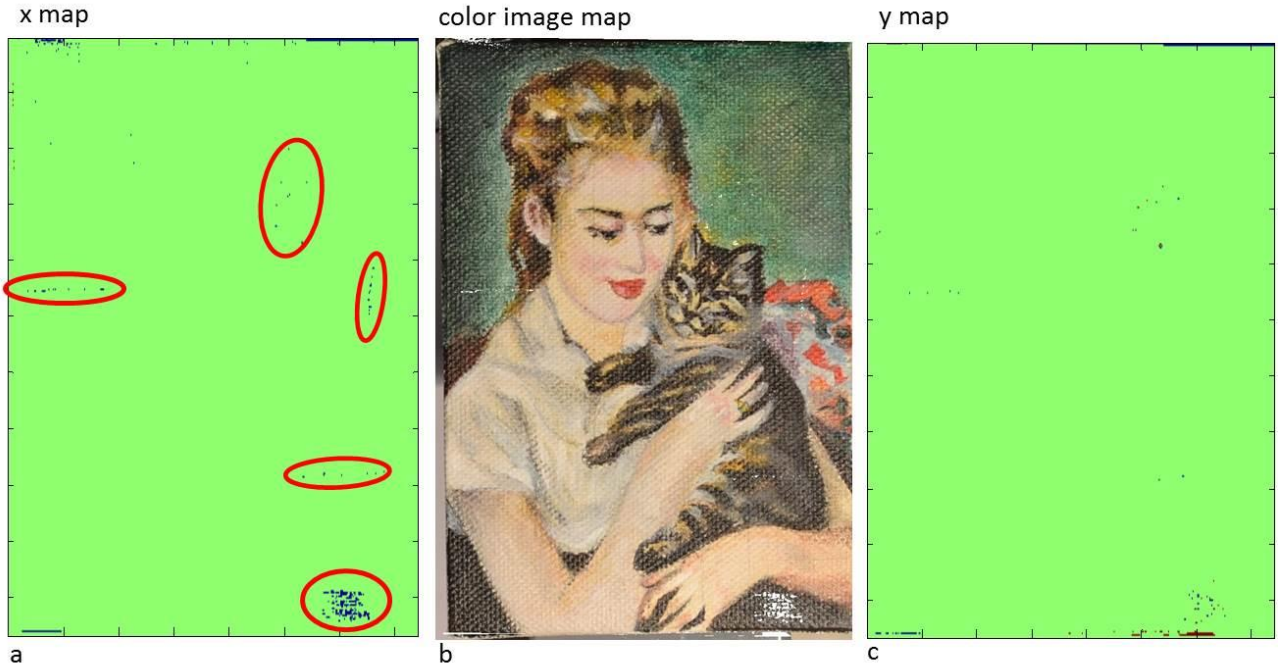

Fig. 41: Maps of change for the x (a) and y (c) values of the normal, red and blue pixels represent the damaged areas. In figure 4b is represented the color image map of change where map of changes (white pixels) are overlapped to the color image of the painting.

Figure 42a represents the bi-dimensional projection of the y value of the normals of the damaged painting: figure 42b and c are respectively the macro of an area before and after the abrasion. We can affirm that we are detecting morphological changes and not color changes because the abrasion of the canvas is clearly seen and represented by the normal vector represented in figure 42c.

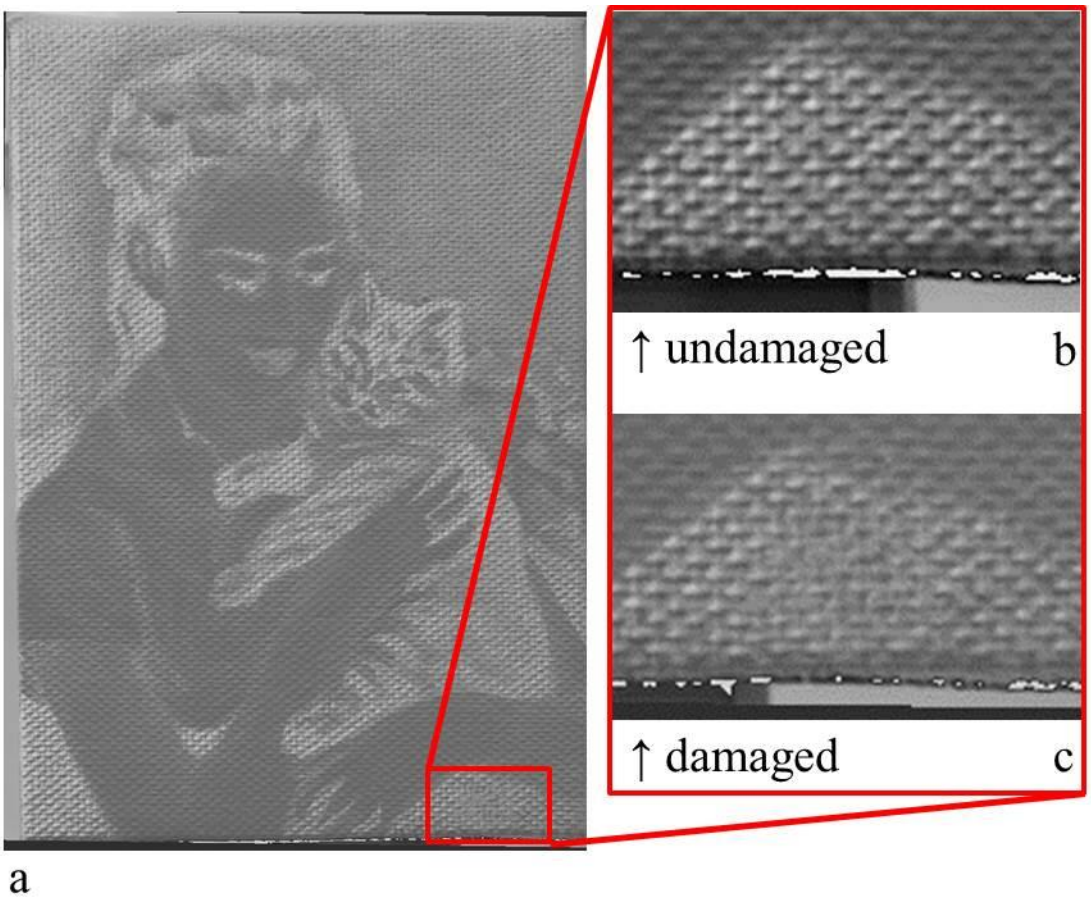

Fig. 43: bi-dimensional image of the y values of the normal of the damaged painting; figure 43b and c show the macro of a damaged area before and after of the abrasion.

Figure 44a represents the intensity map of changes of the damaged painting. The map represent the distance of each pixels from the region of statistical control: this region represents the good conservation and was calculated on the starting characterization of the painting. The limits within which the pixel is considered in control, and so the area can be considered unchanged, is three: over this limit the pixels can be considered changed.

Figure 44b represents a macro of the intensity map of the area damaged with some holes: the method is clearly able to detect small holes and the intensity map of change was able to points out and describes the physical changes caused by holes. Figure 44c shows the color image of the damaged area: the holes are not recognizable.

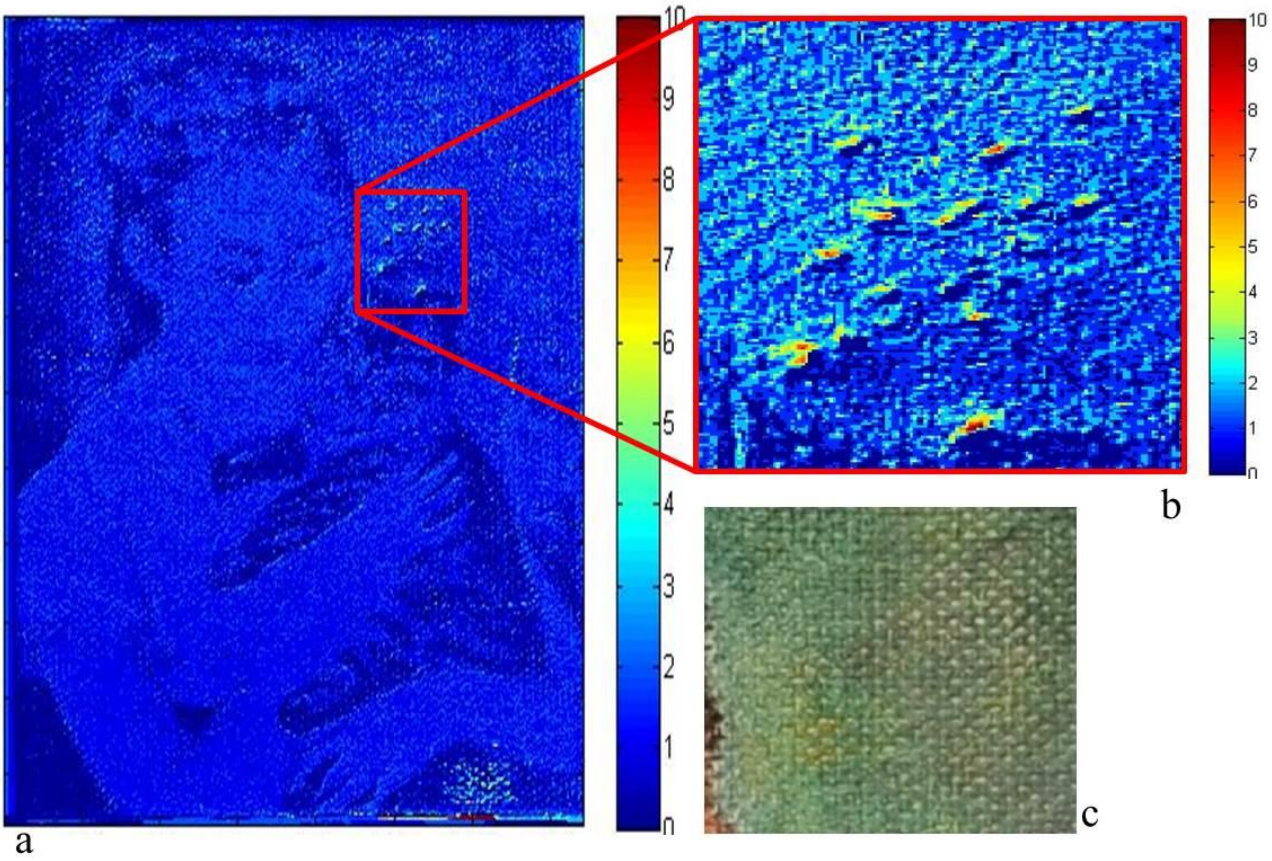

Fig. 44: intensity map of change of the damaged painting (a), macro of the intensity map of the area damaged with some holes (b) and color image of the respectively damaged area (c).

Figure 45a represents the bi-dimensional projection of the x values of the normal of an area damaged with an artificial crack: the damage is clearly recognizable and th intensity map of change in figure 45b easily points it out.

The resolution of the images is of 254 d.p.i. and the width of the crack is about 2-3 pixels: this means that the method is able to detect a physical change of less than 0.3 mm which is a very small morphological change.

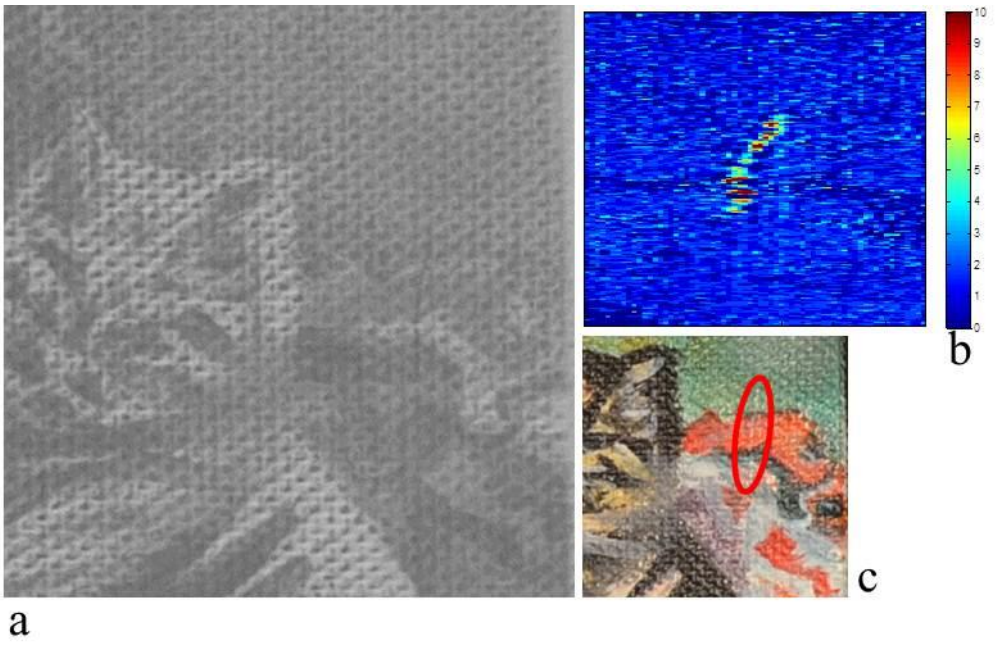

Fig. 45: bi-dimensional image of the x values of the normal of an area with an artificial crack (a), macro of the intensity map of the crack (b) and color image of the damaged area (c).

We further damaged the drawing by creating a small bend from the back in order to get a non-visible damage and without a change of colors: then we captured the RTI again and we built the map of changes.

In Figure 46 is represented the color image (a) of the damaged area (red rectangle), the respective bi-dimensional projection of the y values of the normal (b) with a macro of the damaged area (c): the damage is not recognizable looking at the color image but the intensity map of changes in figure 46d easily detect it.

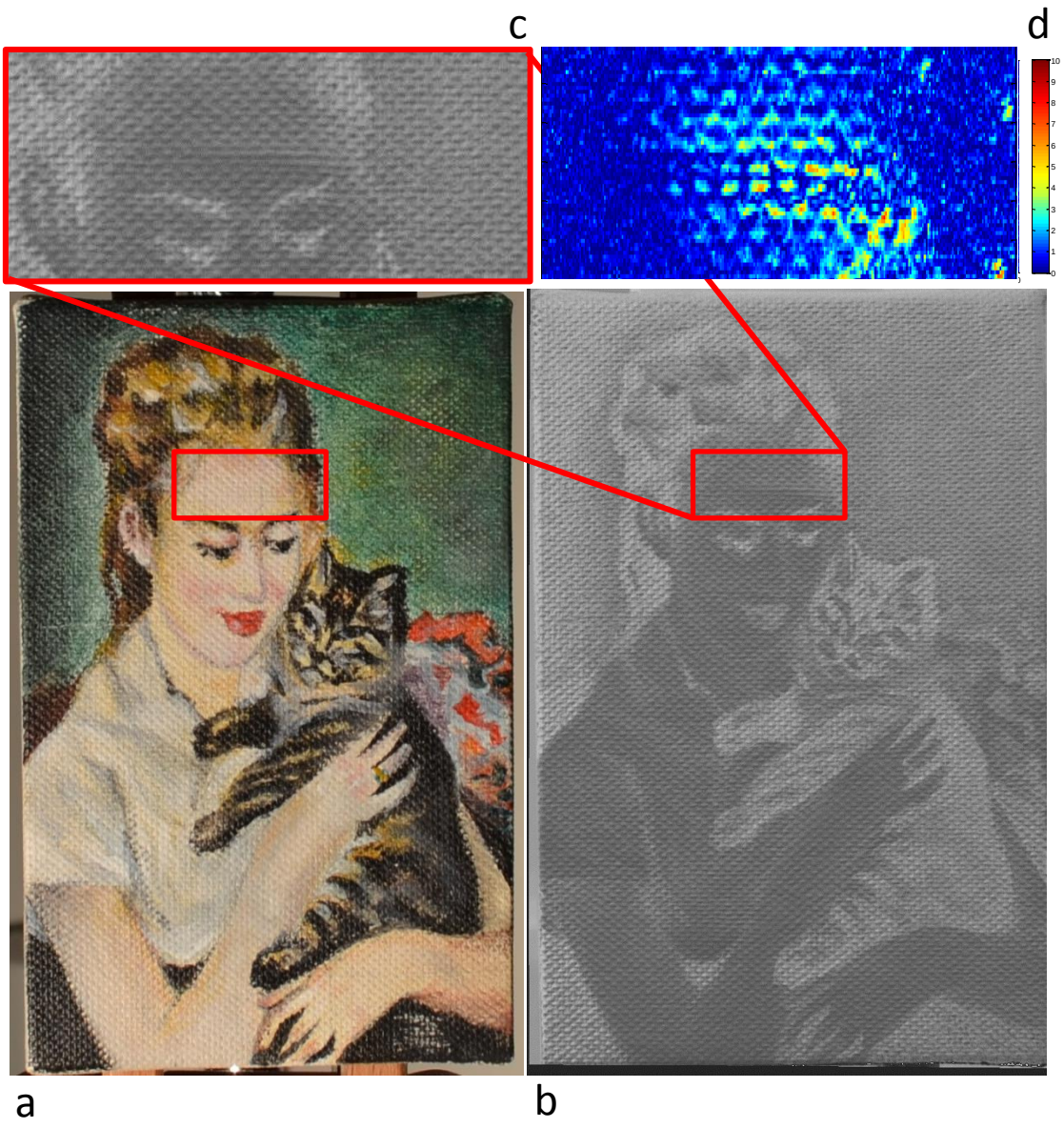

Figure 46: Color image of the painting after damaged creating a bend(a), bi-dimensional image of the y values of the normal of the damaged painting (b) with a macro of the area interested by the bend (c), the intensity map of the damaged area (d).

CONCLUSIONS

In this research we introduce a reliable RTI technique for the non-invasive detection of morphological and physical changes in painting. Using RTI we provided detailed information on the geometry and morphology of the painting surface. In order to have a reproducible and quantitative method that can be used

as practical technique for measuring change in objects we built a custom semi arch arm with LED lights to illuminate the surface of the painting. We developed a monitoring protocol which includes an imaging protocol, the extraction of the normals and comparison within statistical limits. After characterizing the natural variability of the method and of the painting, we damaged the drawing by creating different types of damages: some small holes, three cracks and one abrasion area. We then captured the RTI and compared the normals to the limits: the method was able to detect all the damages.

We can affirm that we are able to detect morphological changes and not only color changes because the abrasion of the canvas is clearly seen and represented by the normal vector images. Moreover, the method was clearly able to detect small holes and the intensity map of change succeed in pointing out and describing the physical changes caused by them. We calculated that the technique can detect a physical change of less than 0.3 mm, which is a very small morphological change, and in general non-visible damages.

Our method is a completely non-invasive monitoring technique: we obtained an accurate and quantitative measure of the deterioration and degradation present in the painting after artificial damages. This non-invasive tool may be very useful to examine paintings and artwork before they travel on loan or during a restoration.

3. NON-INVASIVE CHARACTERIZATION OF PARCHMENT TREATMENTS USING DART-MS AND STATISTICS

The long term conservation of these treasures is a challenge that could be overcome only with an interdisciplinary approach, creating new partnerships and collaborations, using new conservation technologies and promoting their diffusion.

The Dead Sea Scrolls (DSS) are a collection of over 900 manuscripts, few are relatively well preserved, the majority comprises of thousands of fragments. These fragile manuscripts, which include the oldest existing copies of the Hebrew Bible, were preserved for two thousand years by the hot, dry desert climate and the darkness of the Judean Desert caves where they were hidden. The scrolls provide an unprecedented picture of the diverse religious beliefs of ancient Judaism, and of daily life during the turbulent Second Temple period when Jesus lived and preached[83, 84].

Most of the scrolls were written on parchment, and were unintentionally mishandled for the first four decades after their discovery. In the first years after they were discovered there was no awareness of their conservation needs: irreversible damage was caused by using adhesive tape for joining fragments, castor oil was lavishly spread on the fragments to enhance their reading, glycerol, BMLD (British Museum Leather Dressing, which is anhydrous lanolin, beeswax and cedar wood oil mixed into hexane) and other unknown chemicals were used in order to preserve the scrolls. After the Six-Day War in 1967 the adhesive tape and some of the stains were removed with trichloroethylene and the fragments were reinforced with rice paper, polyvinyl acetate, i.e. of an

organic glass of polymethylmetacrylate (PMMA), was used as adhesive. Other scrolls were moistened and loosely flattened between plates of windows glass without framing the edges[85].

Over the years the adhesives penetrated the fragments and the ageing of the oils caused them further darkening so that today some of the texts are no longer legible and the edges in some cases have further gelatinized (Fig. 46).

The task of preserving and conserving the DSS is crucial for their survival for future generations thus in 1991 the Israel Antiquities Authorities (IAA), the state authority in charge of its archeological activities, established a conservation laboratory dedicated solely to the conservation and preservation of the DSS. At the end of 2007, on the occasion of the 60th anniversary of the discovery of the scrolls the IAA began a project with the aim of developing a monitoring system to regulate the conservation state of these precious manuscripts[86, 87]. The non-invasive investigation of the treatment to which they were subjected is a crucial step in order to undertake the best conservation and preservation strategies.

A wide variety of analytical techniques has been applied in order to contribute to parchment conservation and restoration[88-91]. However, practical and non-invasive methods to help curators and conservation experts are still needed. Non-invasive techniques and those requiring no sampling are always preferred.

A non-destructive analytical technique that will provide fast results and identification of relevant organic compounds with no sample preparation requirements and with high sensitivity and simplicity would be of great help in the conservation and characterization of cultural heritage.

Direct analysis in real time mass spectrometry (DART-MS) is a recent MS method that identifies organic compounds in a variety of matrices quickly and directly with no need of extractions, derivatizations and chromatographic separation.

This method has already been applied in the field of cultural heritage for the characterization of paper, organic dyes and ink[92-94]. DART is an atmospheric pressure ion source coupled with a mass spectrometer (MS) that instantaneously ionizes gases, liquids and solids in open air under ambient conditions. The sample can be heated from room temperature to 300°C: heating is often necessary to desorb organic compounds from the sample but is obviously dangerous for the sample.

Chemometric techniques like principal component analysis, classification methods, cluster analysis, etc. have already been applied to extract systematic information from complex dataset in the field of cultural heritage[95-98].

The aim of this work is to develop a non-invasive method for the identification of interventions/treatments of the Dead Sea Scrolls using DART-MS and multivariate statistical analysis.

DART-MS analysis with the ion source at room temperature was performed on castor oil and glycerol parchment treatments in order to characterize the two different classes of treatment processes.

A first principal component analysis was carried out on the DART-MS mass to charge ratio (*m/z*) from the treated and natural parchment (untreated) and on glycerol and castor oil standards. Then, a forward stepwise-linear discriminant analysis (FS-LDA) was performed on the principal components (PCs) calculated on the treated and untreated samples, allowing the discrimination of the classes of samples and sorting the *m/z* peaks according to their relevance. Linear discriminant analysis was applied to the relevant PCs for classification and identification purposes. In order to investigate the effect of the ion source temperature on the mass spectra, the DART-MS analysis was also carried out using the ion at 45°C and 90°C. Then, principal component analysis was carried

out on the DART-MS *m/z* peaks from the treated and natural parchment (untreated) at the different temperatures.

Figure 46: Color images of some Dead Sea Scrolls fragments with well conserved (left) and with darkening problems: the Ten Commandments in the 4Q Deuteronomy (left), Plate/290 (center), 11Q PaleoLeviticus (right) and Apocryphal Psalms (bottom).

THEORY

PCA and LDA

PCA is a multivariate pattern recognition method. PCA has already been applied to separate systematic information from experimental noise and to describe the conservation treatments in a compact and efficient way by using the more significant PCs[99].

LDA is a Bayesian classification method providing the classification of the objects considering the multivariate structure of the data[96, 100]. In Bayesian methods each class is usually described by a Gaussian multivariate probability distribution and each object is assigned to a particular class if a discriminant score, calculated by taking into consideration the class covariance matrix (that is approximated with the pooled covariance matrix between classes) and the

centroid of the class, is the minimum. The variables used in the LDA model discriminating the classes can be chosen by a stepwise algorithm that selects the most discriminating variables.

In this study, FS-LDA was applied to select the best principal components. The classification performance of the LDA models can be evaluated by the calculation of the non-error rate (NER %) that represents the percentage of overall correct assignments.

DART-MS

The number of applications of DART-MS is vast and the method has been recognized throughout the world.

The DART source in its entirety comprises an enclosed ionization source (or source of primary ionization) and a reaction zone extending from its exit through the open atmosphere to the sample(surface). In the ionization source, helium is guided through an axially segmented tube. In the first compartment, a corona discharge between a needle electrode and a first perforated disk electrode produces ions, electrons, and excited atoms (Fig. 47).

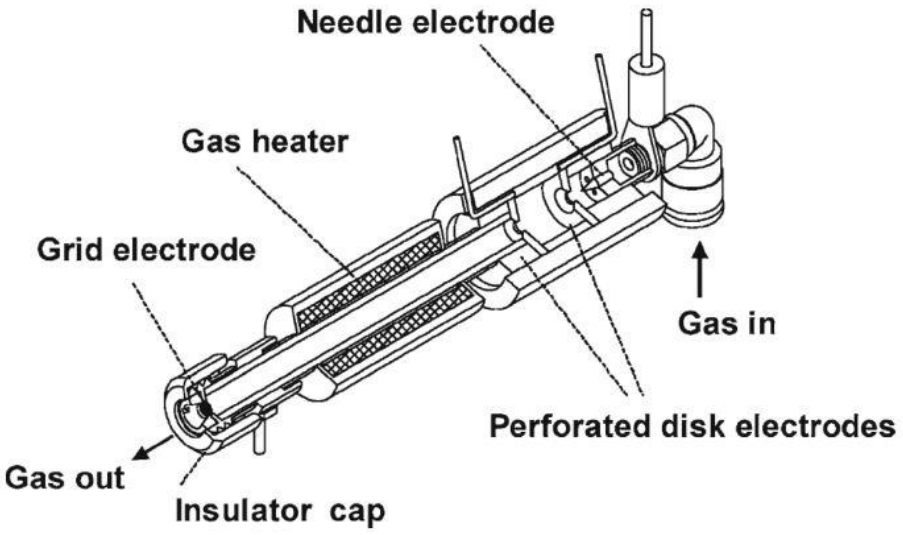

Fig. 47: Cutaway view of the DART ionization source. The exiting gas stream effects ionization of sample in the gap between exit and entrance into the mass spectrometer vacuum interface.

The cold plasma passes through a second chamber where cations are extracted from the gas stream by passing it through another perforated electrode. Next, the gas stream is variably heated by an ancillary heating element and guided through a third grid electrode to remove anions and electrons. Thus, the helium gas exiting the ionization source into the atmospheric reaction zone contains only electronically excited neutral species.

The potentials of the second perforated electrode and the exit grid electrode are set to positive potentials for positive-ion DART and to negative potentials in the order of a few hundred volts for negative-ion mode.

The ionization source delivers electronically excited helium atoms that, after emission from this unit, will immediately ionize surrounding gas (laboratory atmosphere), and eventually analyte material. Although the primary ionizing species are helium atoms, ionization of analyte molecules is mostly effected by secondary ions created from the surrounding air, i.e., by reagent ions. Ions of the analyte are thus formed by chemical ionization processes at atmospheric pressure and finally transferred into the mass analyzer[101].

EXPERIMENTAL

DART-MS. The analyses were conducted with a JEOL AccuTOF mass spectrometer (JEOL USA, Peabody, MA) equipped with a DART ion source (Ionsense, Saugus, MA) in positive ion mode, with helium as the ionization gas under the following conditions: flow rate of 2.5 L/min, gas temperature at 23°C, 45°C and 90°C, grid voltage of +350V. Orifice 1 was held at 120°C and 30V, orifice 2 was at 5 V and the ring lens voltage was set to 5 V. The peaks voltage

was held at 1500V and the instrument was calibrated with a solution of PEG 600 in methanol. The mass spectrum recording interval was 1.00 s and the *m/z* values from 50 to 800. The mass resolution was approximately 6000. The ceramic outlet of the ion source was positioned 15mm away from the pinhole orifice that leaks into the mass analyzer. All equipment in contact with the parchment samples was cleaned using rinses of purified water and acetone.

Parchment samples. Parchment is a semittaned skin used as a writing surface. Of all the components that constitute the living skin, only insoluble proteins and water remain when this is transformed into a parchment. The proteins are grouped together, forming fibers of considerable physical consistency and excellent hydration capacity. Water is the only binding agent: so its role and, more specifically, humidity, is of prime importance in the conservation of parchments[102-104]. High humidity can degrade parchment by hydrolysis of the collagen as well as by denaturation. Low humidity and high temperature can dry out the parchment with the skin that becomes rigid, promoting the possibility of cracks and exfoliation.

Water has often been used to flatten the parchments to make their information more accessible and to facilitate further repairs like mending with starch paste. Vegetable adhesives like flour paste, synthetic polymers (poly vinyl acetate solutions PVA), and acrylic resin solutions were widely used in the past in order to support the parchments.

Sometimes parchments were lubricated with organic materials like glycerol, petroleum jelly, lanolin, oils, or other very different substances in a misguided attempt to "condition" the parchments and to enhance their readability. The use of lubricants caused alteration of the surface texture, increase of transparency, attraction of surface dirt and darkening the skin. The use of unknown organic solvents caused damages to the collagen structure.

Glycerol, which is a simple polyol compound, and castor oil, a vegetable oil obtained from the castor bean, were often used in the past for the lubrication of horny parchments.

For this research/experiment/study we used a goat parchment made by an Orthodox Rabbi from Jerusalem in 2009. The parchment was prepared in compliance with rabbinical rules.

Castor oil and glycerol parchment treatments were investigated in order to evaluate two different intervention processes that are suspected to have been applied to the Dead Sea Scrolls in the past and to be the cause of some of their evident deteriorations. Two separate parchment samples were spread with commercial castor oil (CVS, Woonsocket, Rhode Island, USA) and glycerol. The samples were left for 48 hours at room temperature and were then analyzed by DART-MS.

Methodology. Parchment samples were cut into 5x20 mm strips using clean scissors: then, they were positioned at room temperature in helium atmosphere at a distance of 1 mm from the ceramic outlet of the DART ion source by using fine-point steel tweezers. No sample preparation was necessary.

RESULTS AND DISCUSSION

The aim of the research was the development of a non-destructive methodology for the analysis of unknown interventions of parchment by using DART-MS.

The temperature of helium significantly impact the information obtained by DART-MS: the substances detected by the instrument strongly depend on the temperature of the carrier gas in the ion source.

Parchment is an organic material mainly made of collagen and water: temperature is one of its worst enemies. We performed the analysis using the

flux of helium at room temperature in order to avoid causing any damage to the parchment surface.

We analyzed an untreated parchment sample, a parchment sample treated with castor oil, a parchment sample treated with glycerol, and castor oil and glycerol standards as shown by the total ion chromatogram (TIC) (Fig. 48).

Although the carrier gas in the ion source temperature was set at 23°C low-mass thermolysis products (≈ 80 to 400 u) from untreated and treated parchment and from castor oil and glycerol are clearly identifiable. Figure 49a, b, c, d and e show respectively the mass spectrum of untreated parchment, parchment treated with castor oil, parchment treated with glycerol, castor oil standard and glycerol standard. The *m/z* of fragments of untreated parchment, parchment treated with castor oil and castor oil are not assignable because of the complexity of the matrix and of the low working temperature. Moreover the three mass spectra are very similar to each other because both parchment and castor oil contains lipid groups.

The mass spectrum of parchment treated with glycerol and of standard glycerol (Fig. 49 c and e) show that *m/z* 93.04 ($M+H^+$) and 185.06 ($M+M+H^+$) are major fragments and correspond respectively to protonated glycerol and protonated glycerol clusters. The *m/z* 110 correspond to the glycerol water adduct ($M+H_20$).

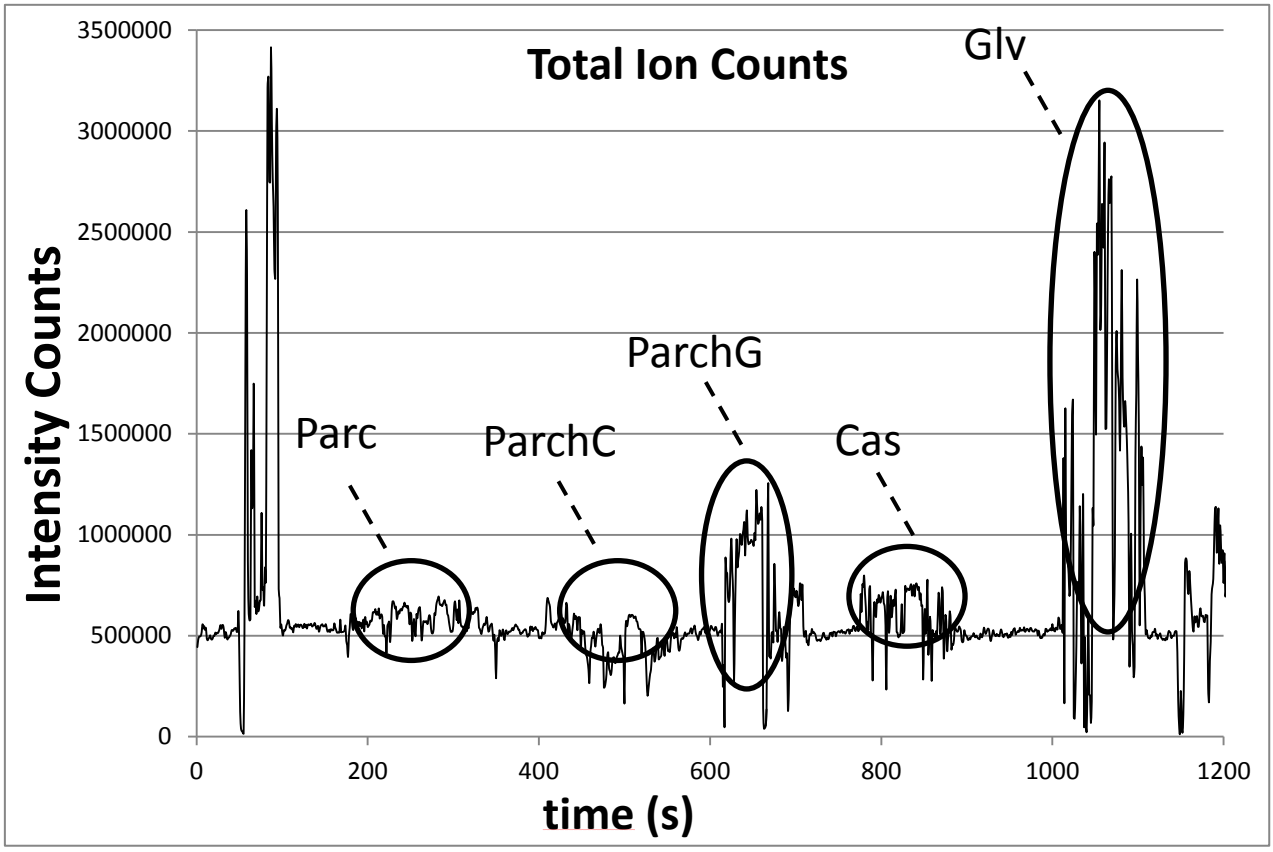

Figure 48: Total ion chromatogram of analyzed samples: from time 230 to 300 seconds an untreated parchment sample was positioned in the helium stream; from time 500 to 550 seconds a piece of parchment treated with castor oil was analyzed; from time 630 to 700 seconds a piece of parchment treated with glycerol was analyzed; from time 780 to 880 seconds a standard of castor oil was inserted in the gap and analyzed; form time 1020 to 1100 seconds a standard of glycerol was positioned in the helium flux and analyzed.

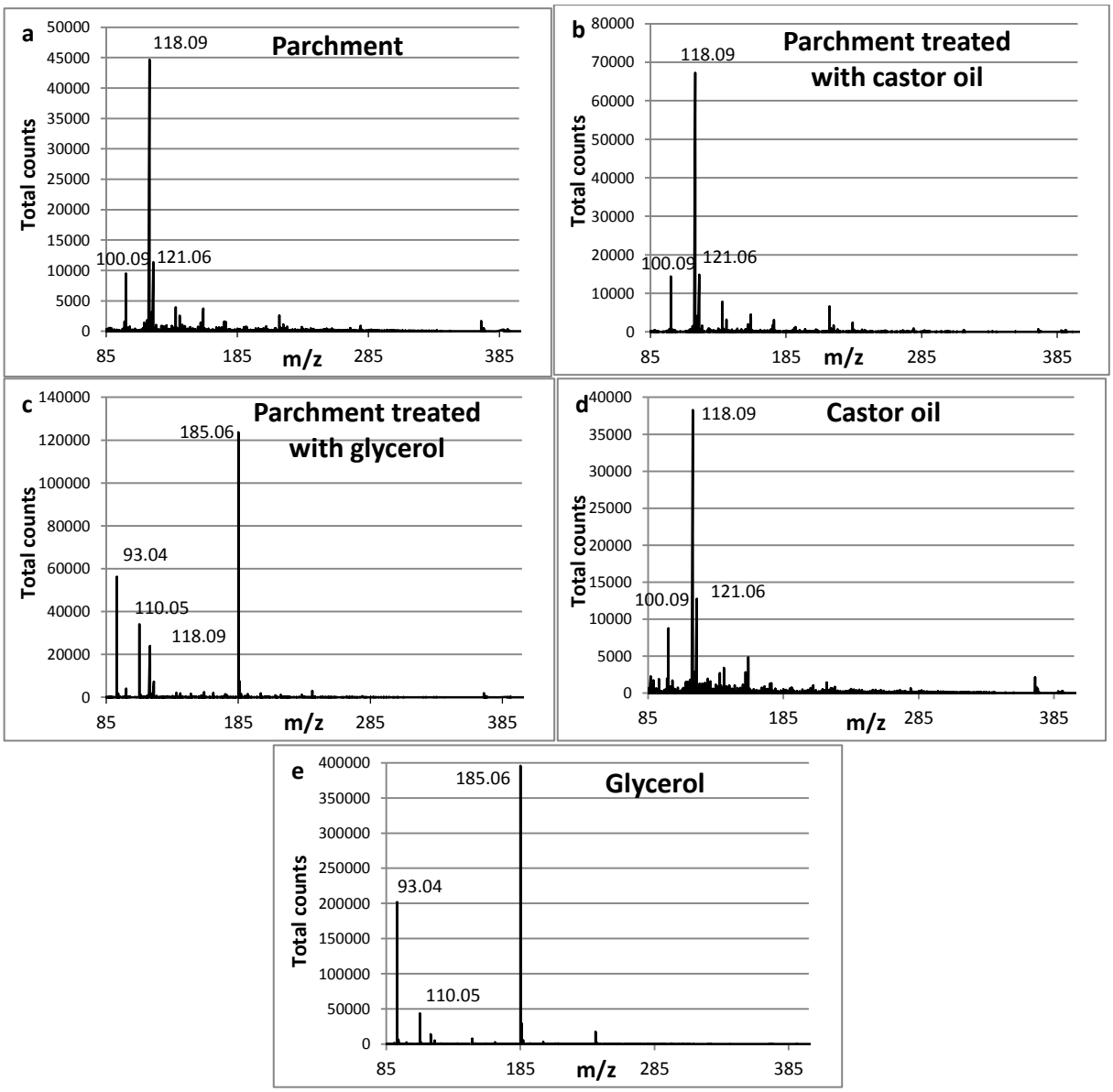

Figure 49: (a) mass spectrum of untreated parchment, (b) mass spectrum of parchment treated with castor oil, (c) mass spectrum of parchment treated with glycerol, (d) mass spectrum of castor oil standard and (e) mass spectrum of glycerol standard.

The glycerol treatment on parchment is recognizable by looking at the mass spectrum: the characteristic *m/z* 93, 110 and 185 of glycerol are clearly present. While, looking at the mass spectra of parchment treated with glycerol, it is not possible identify the treatment because parchment and castor oil have a similar mass spectrum profile. In order to identify unknown parchment treatment without interpreting mass spectrum, especially when the interpretation is not easy to perform because of the complexity of the spectra, we performed a multivariate statistical analysis on the data collected by DART-MS.

Statistical analysis and variable selection

Principal Component Analysis on overall dataset

The mass spectra of the different samples were matched one to each other and the results were arranged in a 106x6346 matrix: 106 being the number of samples (19 parchment samples, 28 parchment samples treated with castor oil, 21 parchment samples treated with glycerol, 16 samples of castor oil and 22 samples of glycerol) and 6346 being the *m/z* intensity count for each sample. PCA was carried out after range scaling between -1 and 1. The amount of explained variance is distributed along several PCs showing a relatively low correlated data structure (PC_1=6.9%, PC_2=5.9%, PC_3=3.5%, PC_4=2.4%, PC_5=1.7%). The low correlation is explained by a significant sample heterogeneity. In the score plot of PC_1 vs PC_2 vs PC_3 (Fig. 50a) the samples are well separated along the three PCs in five clusters that represent the untreated parchment sample (red), the parchment sample treated with castor oil (blue), the parchment sample treated with glycerol (green), the castor oil standard (yellow) and the glycerol standard (pink). The first component explains the differences between untreated parchment (red) and the treated samples(blue, green, yellow and pink), the second component explains the differences between the

parchment samples (red, blue and green) and the standard samples (yellow, pink) as is shown in figure 50b.

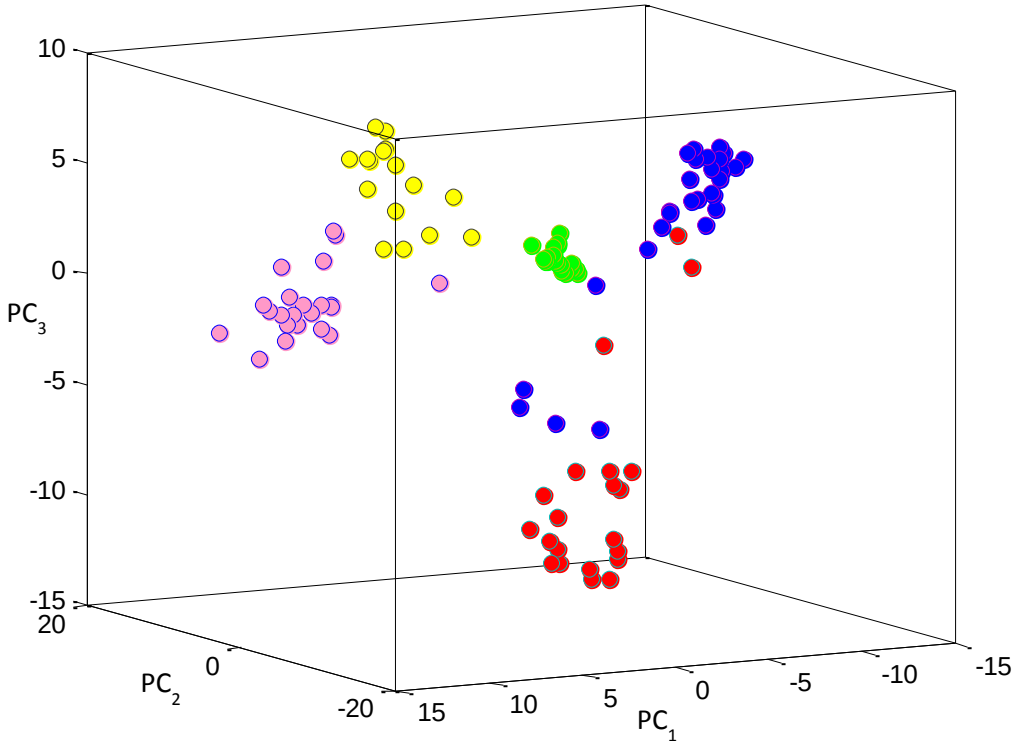

a

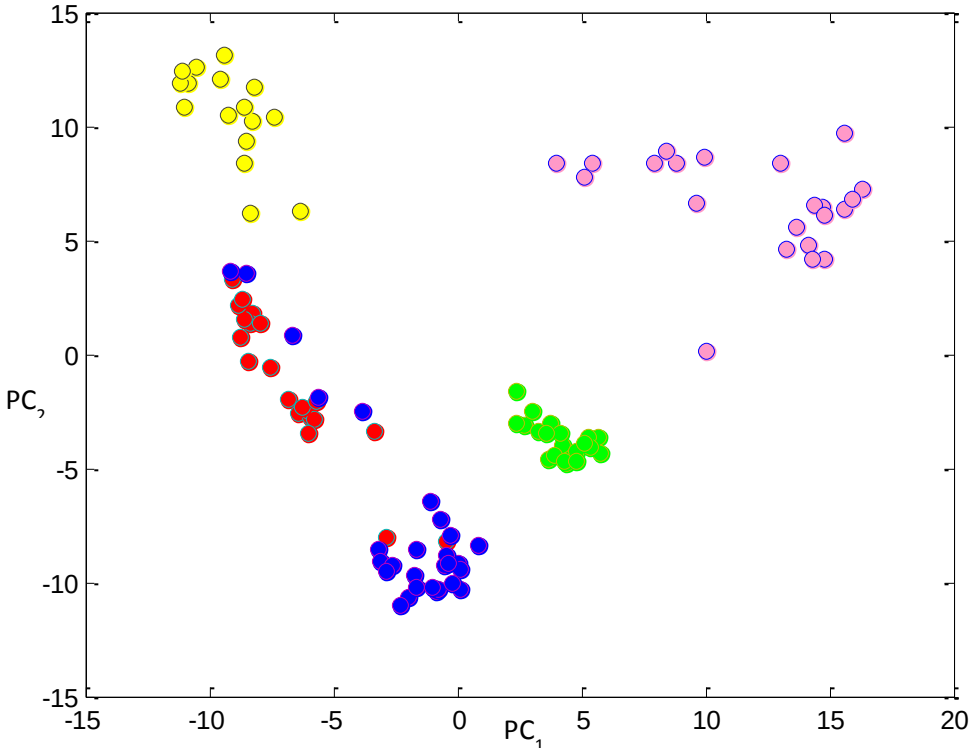

b

Figure 50: score plot of PC_1, PC_2 and PC_3(a). The samples are separated along the three PCs in five clusters: untreated parchment sample (red), the parchment sample treated with castor oil (blue), the parchment sample treated with glycerol (green), the castor oil standard (yellow) and the glycerol standard (pink). Figure 50b represents the score plot of PC_1 and PC_2.

Principal Component Analysis on parchment samples

Since the main target was the identification of unknown parchment treatments, the analysis was restricted to parchment samples in order to find the most significant PCs useful to discriminate the conservation treatments.

PCA was then applied to the restricted set of data: the spectra were arranged in a 68x5329 matrix: 68 being the number of samples (19 parchment samples, 28 parchment samples treated with castor oil and 21 parchment samples treated with glycerol) and 5329 being the *m/z* intensity count for each sample. PCA was carried out after range scaling between -1 and 1. The amount of explained variance is quite distributed along several PCs (PC_1=9.0%, PC_2=6.4%,

PC_3=3.1%, PC_4=2.8%, PC_5=2.7%). In the score plot of PC_1 vs PC_2 vs PC_3 (Fig. 51a) the samples are well separated along the three PCs in three clusters that represent the untreated parchment sample (red), the parchment sample treated with castor oil (blue) and the parchment sample treated with glycerol (green). The first component explains the differences between untreated parchment (red) and the conservation treatment (blue and green) and the second component explains the differences between the two different conservation treatment, castor oil (blue) and glycerol (green) as is shown in figure 51b.

PCA allows to reduce the variable dimensionality: the latest PC mainly accounting for noise and experimental error, are not considered further in this study

The score plot shows that the parchment samples treated with glycerol are characterized by a small dispersion; untreated parchment and parchment treated with castor oil are characterized by a quite large dispersion: this can be explained by the complexity of the analyzed matrix of the samples that is difficult to ionizing using the helium stream at room temperature.

Regarding the separation between classes, the score plot shows that the samples are quite well separated: this is particularly true for the samples treated with glycerol. Instead, some untreated parchment samples overlapped with the samples treated with castor oil and vice versa: this can be explained by the fact that parchment and castor oil are characterized by a quite similar chemical composition mainly due to lipid groups.

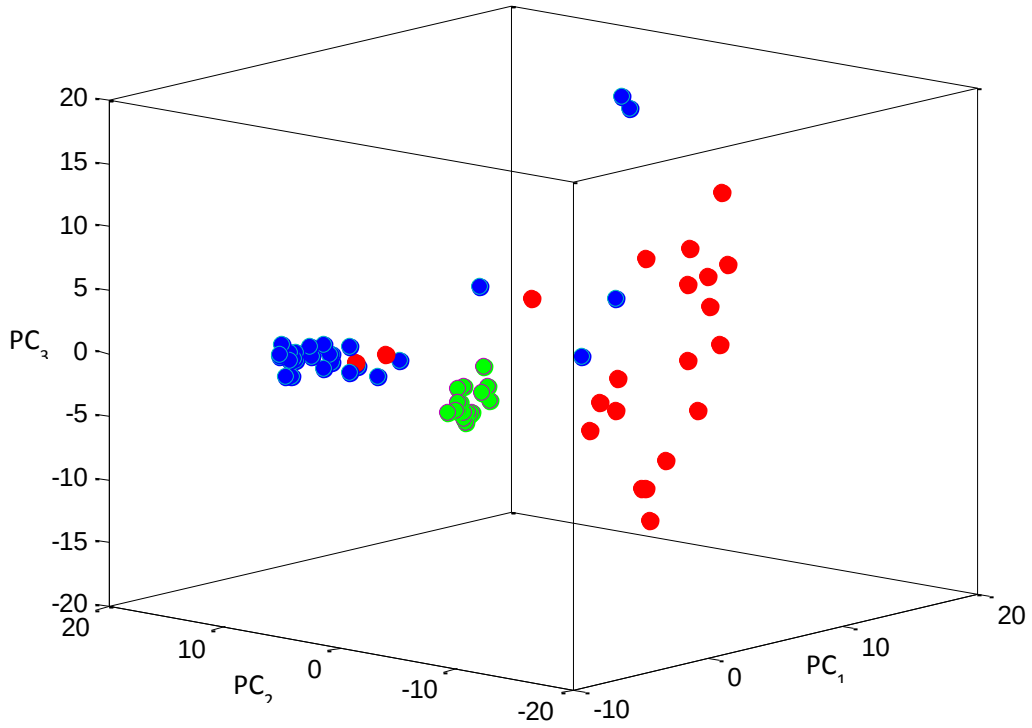
20
15
10
5
0
-5
-10
-15
-20
PC3
20
10
0
-10
-20
PC2
-10
0
10
20
PC1

a

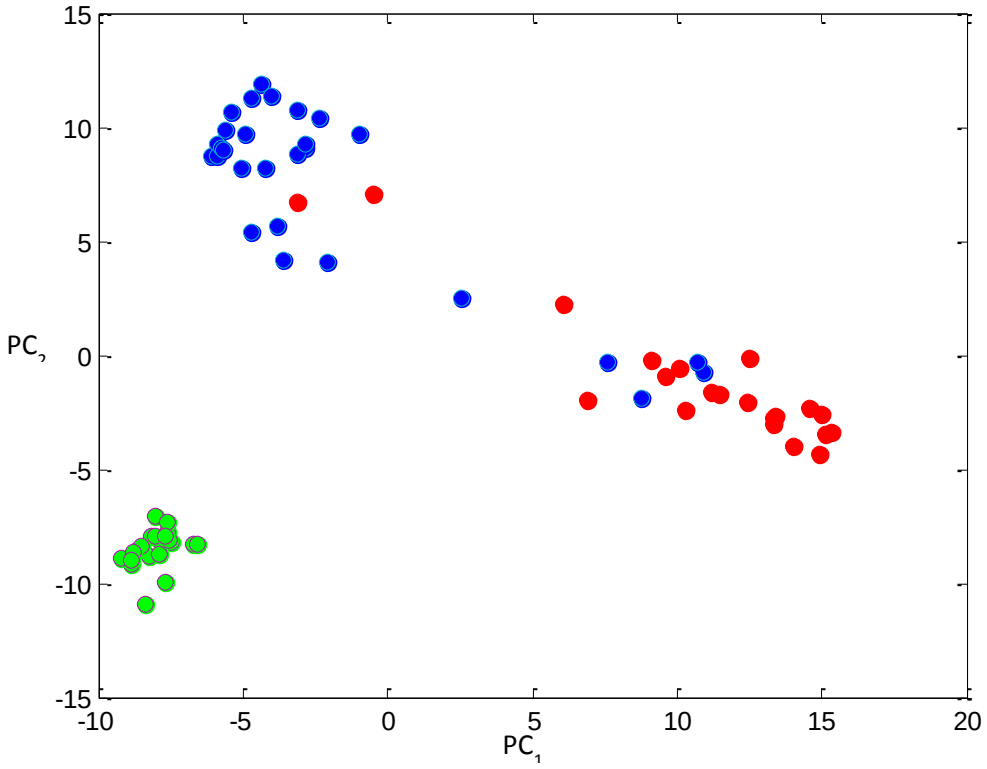
15
10
5
0
-5
-10
-15
PC2
-10
-5
0
5
10
15
20
PC1

b

Figure 51: score plot of PC1, PC2 and PC3(a). The samples are separated along the three PCs in three clusters: untreated parchment sample (red), the parchment sample treated with castor oil (blue) and the parchment sample treated with glycerol (green). Figure 51 b represents the score plot of PC_1 and PC_2.

Linear Discriminant Analysis

The identification of possible markers, which are able to discriminate the conservation treatment, was then achieved by linear discriminant analysis applied to the first 20 PCs calculated: the use of the PCs instead of the original variables allows the dimensionality reduction and the elimination of the experimental noise. Moreover, a variable selection procedure was applied exploiting a stepwise algorithm in forward search ($F_{to\text{-}enter}$=6) to select only PCs effective for classification purposes.

The final model contains PC_1, PC_2, PC_3, PC_4, PC_5, PC_6, PC_7, PC_8, PC_{11}, PC_{19} and PC_{20} (Table 7) at a significance level of 95% (p level<0.05); Table 1 reports the coefficients of each PC included in the LDA classification models built (untreated samples, treatment with castor oil and treated with glycerol) together . LDA provided very good results in calibration: all samples were correctly assigned (NER and specificity of 100% for all classes) and no overlap was detected (selectivity of 100% for all classes). The performance of the model in prediction was then evaluated in cross-validation by a leave-one-out procedure: again LDA provided very good results, all samples were correctly classified as shown in Table 8.

	F Fisher	p-level	untreated	Castor oil treatment	Glycerol treatment
PC_2	599.04	0.0000	1.92	2.49	-5.07
PC_1	724.08	0.0000	3.61	0.95	-4.52
PC_3	27.93	0.0000	-1.12	0.27	0.66

PC_4	20.11	0.0000	0.77	-0.44	-0.1309
PC_{12}	9.36	0.0003	0.75	-0.32	-0.25
intercept			-23.19	-9.90	-40.57

Table 7: Coefficients of the significant PCs included in the LDA model for untreated samples, treated with castor oil samples and treated with glycerol samples with the corresponding p-level and F Fisher values.

Treatment	Untreated	Castor oil	Glycerol	Corr. Percentages
Untretated	19	0	0	100%
Castor oil	0	28	0	100%
Glycerol	0	0	21	100%
Total	19	28	21	100%

Table 8: Classification matrix of parchment samples in crossvalidation: rows correspond to the observed classification and columns corresponds the expected observations for each group. The last column corresponds to the corrected percentages of classification.

Effect of the working temperature

The effect of the ion source temperature on the mass spectra has been investigated by analyzing the treated parchment samples and the natural parchment samples (untreated) using several source (carrier gas) temperatures: 23°C, 45°C and 90°C. The mass spectra of the different samples were matched one to each other and the results were arranged in a 232x5323 matrix: 232 being the number of samples (69 samples analyzed at 23°C, 78 samples analyzed at 45°C and 85 samples analyzed at 90°C) and 5323 being the *m/z* intensity count for each sample. PCA was carried out after range scaling between -1 and 1. The amount of explained variance is distributed along several PCs showing a relatively low correlated data structure (PC_1=10.1%, PC_2=7.4%, PC_3=6.5%, PC_4=3.5%, PC_5=1.7%).

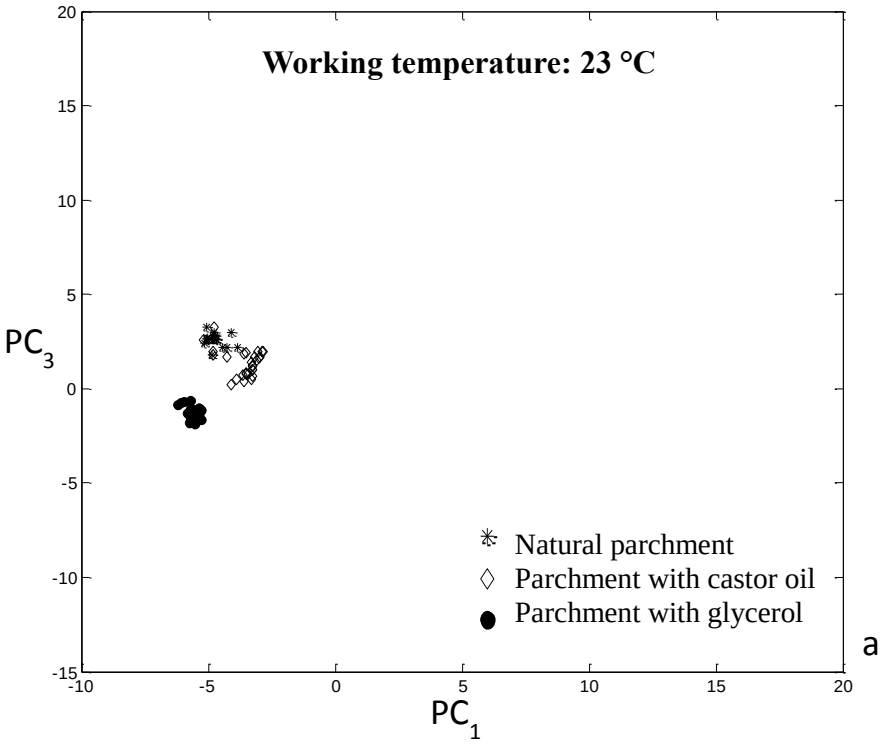
Working temperature: 23 °C
PC3
PC1
Natural parchment
Parchment with castor oil
Parchment with glycerol

a

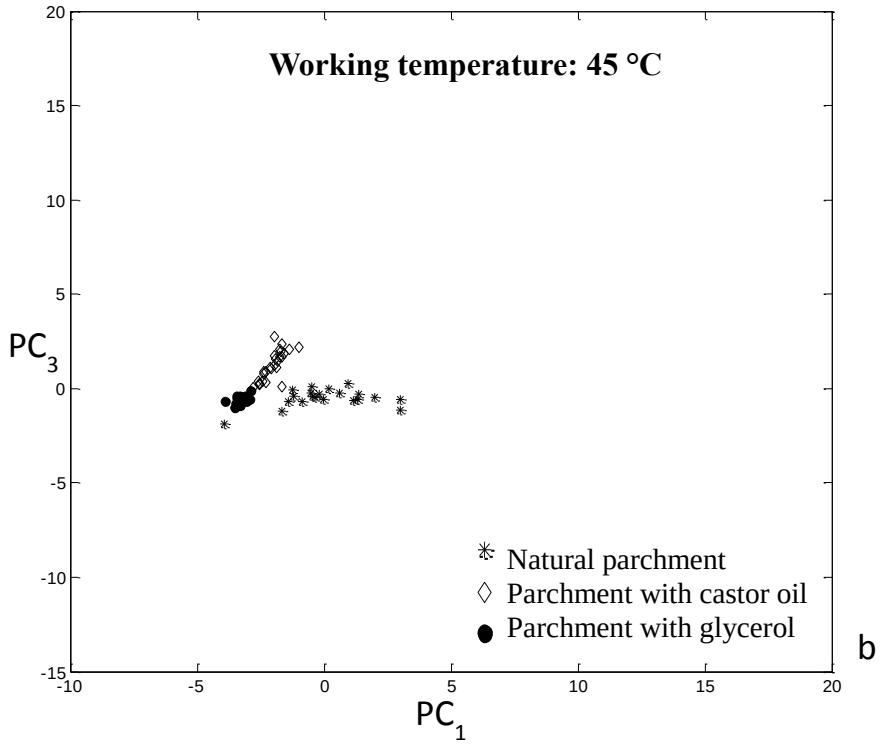
Working temperature: 45 °C
PC3
PC1
Natural parchment
Parchment with castor oil
Parchment with glycerol

b

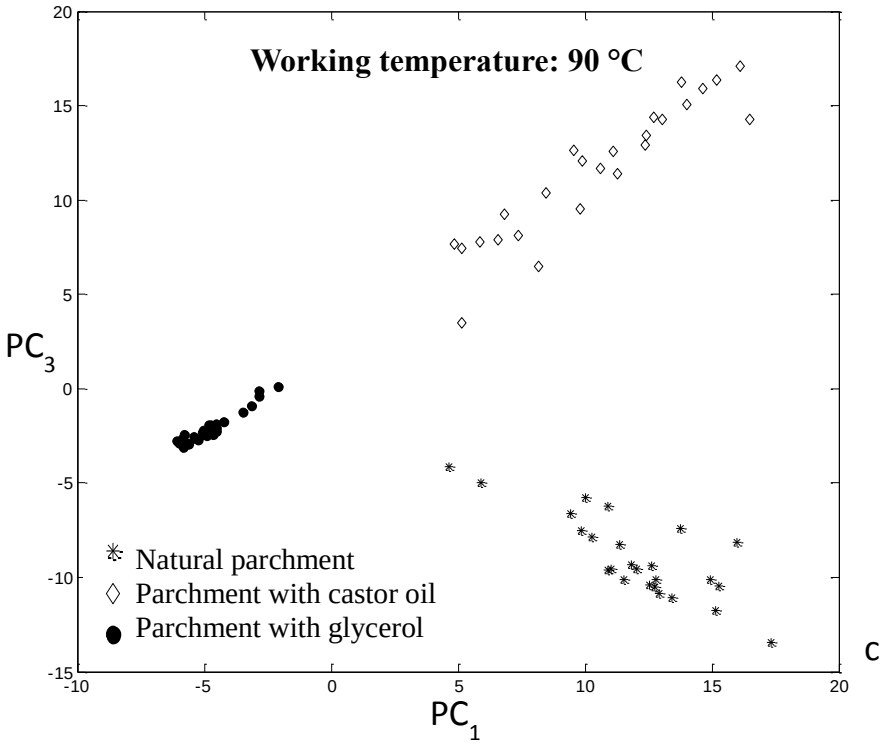

Figure 52: score plots of PC_1 and PC_3 for each working temperature and for the 3 different group of samples. PC_3 separates the samples in three clusters: untreated parchment samples (star), parchment samples treated with castor oil (diamond) and parchment samples treated with glycerol (circle) all analyzed at 90°C (Fig. 52-c); all the parchment samples treated with glycerol (circle) analyzed at 23°C (Fig. 52-a), 45°C (Fig. 52-b) and 90°C (Fig. 6-c) are grouped together and have a low dispersion Natural parchment samples (star) and parchment samples treated with castor oil (diamond) at 23°C (Fig. 52-a) and at 45°C (Fig. 52-b) have a similar pattern and are not well separated: increasing the temperature causes an increase of the distance between the 3 groups of samples in the PC reference system.

For each working temperature it is possible to identify groups corresponding to the different types of treatment: natural parchment (star), parchment treated with glycerol (circle) and parchment treated with castor oil (diamond). The position of the clusters changes with temperature, with the exception of the samples treated with glycerol that remains approximately in the same position at all temperatures.

At lower working temperature (Fig.52a-b) the groups of samples are separated, but closer one to each other and more homogeneous within the same group: increasing the temperature causes an increase of the distance between the 3 groups of samples in the PC reference system and a spread of the samples within each group. In particular the scores of natural parchment samples (star) and parchment samples treated with castor oil (diamond) move towards larger values.

In the score plot of PC_1 vs PC_3 (Fig. 52c) the first principal component explains mainly the effect of the temperature at 90°C: at high scores there are the natural parchment samples (52c-star) and the parchment samples treated with castor oil (52c-diamond) analyzed at 90°C. Parchment samples treated with glycerol (circle) at 23°C, 45°C and 90°C are characterized by a smaller dispersion: the mass spectra of these samples do not significantly change working at different temperature, probably since glycerol is volatile enough at room temperature to obtain good mass spectra also in the least extreme conditions.

The third principal component mainly explains the differences between the natural parchment samples (52c-star) and parchment samples treated with castor oil (52c-diamond) at 90°C.

Increasing the carrier temperature the identification of different parchment treatment is easier because the gas ionizes also the less volatile molecules. Unfortunately this condition is not feasible for the analysis of the original dead sea scrolls, as using high temperature make the analysis to become destructive.

CONCLUSIONS

In this study we developed a new non-invasive method for the identification of unknown conservation treatments of parchment by using DART-MS and statistics.

Many traditional interventions can result in irreversible alteration of an artifact, because of its animal origin, parchment might respond to treatments in unpredictable ways. The conservator's approach to the treatment of parchment must be extremely cautious and due to the simplicity and no sample preparation requirement, the proposed analytical tool could help in the challenging analysis of unknown treatments in cultural heritage.

Castor oil and glycerol parchment treatments were investigated using the DART carrier gas in the ion source at room temperature in order not to cause any damage to parchment samples: this is very important while working with any cultural heritage and even more with the Dead Sea Scrolls which are extremely fragile and precious.

The method was able to identify both treatments: FS-LDA performed on principal components revealed to be a robust tool that could be employed for the classification of unknown treatments, over all in presence of samples with similar mass spectrum profiles.

A DART-MS library of treatments may be created and extended including also the degradation products that may appear after the ageing of the object. The technique may also be applied other cultural heritage objects, such as paintings and other artifacts. Moreover, the investigation of the working temperature of the ion source could help in the identification of unknown substances because at higher temperature the ionization of molecules is easier, even if the analysis could become destructive.

In conclusion, using chemometrics we are able to identify unknown parchment treatment without using high temperature, preserving the integrity and the state of conservation of the sample.

4. NON-INVASIVE CHARACTERIZATION OF ARTWORKS USING PORTABLE DRIFT

4.1 Non-invasive identification of canvas ground: IR spectra reference collection

Paintings are made by different layers of material, which roughly are support, primer, different layers of paint and varnish. Other layers such as glue, a preparatory drawing, an imprimatur and additional layers of paint can complement the painting composition. Moreover, the material composition of paintings is often dominated by composite materials of different chemical substances.

Canvas ground is the layer or group of layers that are between the canvas support and the paint layer. For both technical and aesthetical reasons ground is made by a thin layer of inert material mixed with binder and often colored with pigments. Applied on a canvas support is used to reduce the color absorption and to protect the fibers from the degradation.

Since the antiquity, artists used grounds to keep the canvas surface more uniform, flat and to reduce weave irregularities. There are several kinds of grounds. Knowing the type of ground that was used is very important for conservative purposes: the binders used can affect the degradation of the paint film. In particular, if the composition of ground binder and color binder is not the same, the degradation may accelerate and the restoration may results challenging. Moreover, grounds, like pictorial techniques, are often the digital printing of artists and historical period and so can be used to validate authenticity.

In recent years, several analytical methods have been employed for the investigation and characterization of cultural heritage objects. Analytical

methodologies that require micro sampling or no sampling have always been preferred.

FTIR spectroscopy has long been used for the analysis and characterization of objects of art in support of efforts to preserve and restore them. The stratigraphic information, useful to art historians and restorers, can be obtained by studying cross sections with optical and electronic microscopy, micro-FTIR and Raman spectroscopy. Typical applications include analysis of paint pigments and binders, lacquers and finishes. FTIR has been used also to measure and monitoring the deterioration of artworks and in support to conservator.

A series of paint cross sections from an oil painting were studied by attenuated total reflection in conjunction with Fourier transform infrared spectroscopy (ATR-FTIR)[105, 108-111] .This study demonstrates the possibilities offered by macro-ATR-FT-IR imaging for a simple identification of the different compounds present in paint cross-sections[107].

A statistic approach using principal component analysis for the interpretation of the hyperspectral data arrays obtained by μATR-FTIR of paint cross-sections using was proposed[106].

But most of FTIR spectrometers are located in labs, therefore the measurement often requires a small sample from the artwork. Moreover, a micro sampling may not be representative of the area that must be analyzed and the monitoring of the restoration is not possible because it would require many samples of the artifact. On particularly precious paintings sampling is usually forbidden: this suggests the need of an in situ non-invasive techniques for the analysis.

We present here a portable diffuse reflectance infrared Fourier transform (DRIFT) method for the non-invasive characterization of grounds in painting: with this method there is no need to touch the sample and the analysis can be done directly on site.

No sample needs to be removed to analyze the object, and in fact, a number of areas on the object can be analyzed quickly in a non-destructive manner.
We prepared 16 canvas grounds: all of them were used by the most important artist from XIV to XX century such as Vasari, Mantegna, Veronese, Caravaggio and De Chirico. We analyzed them using DRIFT and we built a reference library of spectra.
We measured the DRIFT spectra of ground on a Moncalvo's painting, who can be considered the most important artist of Piedmont in the XVI century, in order to identify the type of ground that was used.

EXPERIMENTAL

DRIFT analysis. Diffuse Reflectance Infrared Fourier Transform Spectroscopy (DRIFT) has been performed with an Agilent 4100 Exoscan FTIR portable spectrometer.
Sample spectra were obtained in absorption mode using a diffuse reflectance device over a wavelength of 650 cm^{-1} to 4000 cm^{-1} at 32 scans per sample and a resolution of 4 cm^{-1}. Background readings of air were established prior to data collection. The background was subsequently subtracted from each spectrum before data output.

Canvas ground preparation. Canvas ground is the layer or group of layers that are between the canvas support and the paint layer. Since medieval, canvas has been used for painting: from the XV century, with the spreading of tempera paint, canvases were prepared using rabbit skin glue. Successively, artists introduced the use of fine gypsum. In the XVI century, the use of oil paints brought painters to mix pigments and colors in ground mixture. Then, the addition of flour, oil and white lead was introduced in the preparation receipts. During the XVII and the XVIII centuries painters used clays, while in the XIX

century they employed white zinc. In the last century new receipts were experimented introducing titanium white and synthetic resins.

In table 9 are described the 16 grounds prepared and analyzed by DRIFT spectroscopy.

Samples	Receipts
Ground 1 [112] (XV century)	rabbit skin glue
Ground 2 [112] (Bellini, Mantegna, Tiziano)	gypsum, rabbit skin glue and honey
Ground 3 [113] (Vasari)	lower layer: flour, linseed oil, white lead, rabbit skin glue; upper layer: yellow lead (PbO), black vine, stand oil, white lead ($(PbCO_3)_2 \cdot Pb(OH)_2$)
Ground 4 [113] (Vasari)	lower layer: flour, linseed oil, white lead($(PbCO_3)_2 \cdot Pb(OH)_2$), rabbit skin glue; upper layer: red lead (Pb_3O_4), black vine, stand oil
Ground 5 [114] (Armenini – XVI)	flour, walnut oil and white lead ($(PbCO_3)_2 \cdot Pb(OH)_2$)
Ground 6 [112] (Caliari-Veronese)	gypsum and rabbit skin glue (lower layer); linseed oil, white lead, red ochre (Fe_2O_3) and yellow earth (Fe_2O_3) (upper layer).
Ground 7 [115] (Caravaggio)	red bole (FeO and silicate), yellow earth (Fe_2O_3), stand oil, white lead ($(PbCO_3)_2 \cdot Pb(OH)_2$), black vine, sand and cinnabar (HgS)
Ground 8 [116] (Van Baburen, caravaggesco)	red bole (FeO and silicate), stand oil, Venetian turpentine (pine resin), egg and sand
Ground 9 [117] (Volpato)	red bole (FeO and silicate), stand oil, Siena earth ($Fe(OH)_3$) and raw umber ($Fe(OH)_3$)
Ground 10 [118] (De Mayerne)	litargirium oil (stand oil + yellow lead), red lead (Pb_3O_4), yellow earth (Fe_2O_3) and black vine
Ground 11 [118] (De Mayerne)	litargirium oil (stand oil + yellow lead) and yellow earth (Fe_2O_3)
Ground 12 [112] (Jan Vermeer)	kaolin, white lead, yellow earth (Fe_2O_3), rabbit skin glue, stand oil
Ground 13 [119] (Max Doerner)	gypsum, zinc white, rabbit skin and stand oil

Ground 14 [120] (Pierre A. Renoir)	white lead, kaolin, stand oil
Ground 15 [121] (De Chirico)	Meudon white, egg yolk, poppy oil, Venetian turpentine, white vinegar, glycerin, water
Ground 16 [112] (synthetic binders)	titanium white, chalk,0 acrylic resin and kaolin

Table 9: composition of the 16 grounds prepared and analyzed by DRIFT.

RESULTS AND DISCUSSIONS

The 16 grounds prepared following the ancient receipts of the most relevant painter of world from XV to XX centuries were analyzed by using a portable DRIFT spectrometer. The analysis was carried out just pointing the infrared beam on the ground surface without touching the sample.

Ground 1 (XV century): rabbit skin glue.

The sample G1 was prepared spreading rabbit skin glue on the canvas. Figure 53a shows the IR spectra of the sample: the strong and broad band centered near 3500 cm^{-1} is assigned to the stretching of NH groups, near 2900 cm^{-1} there are the C-H stretching bands. The peak at 1690 cm^{-1} is of the C=O stretching band and at 1574 cm^{-1} there is the bending band of the C-N-H. Peak at 1464 cm^{-1} represents the bending band of C-H.

Ground 2 (Bellini, Mantegna, Tiziano): Gypsum, rabbit skin glue and honey.

Figure 53b shows the IR spectra of the sample G2: the strong an broad band between 3700 and 3200 cm^{-1} is assigned at the anti-symmetric and symmetric O-H stretching bands of gypsum; the band at 1140 cm^{-1} is the asymmetric SO_4^{2-} stretching band. The peaks at 1679 and 1632 cm^{-1} are the deformation vibrations of the O-H link of water. Near 2900 cm^{-1} there are the C-H stretching bands of the rabbit skin glue.

Ground 3 (Vasari): lower layer: flour, linseed oil, white lead, rabbit skin glue; upper layer: yellow lead (PbO), black vine, stand oil, white lead ($(PbCO_3)_2 \cdot Pb(OH)_2$) .

In figure 53c is represented the IR spectra of the sample G3: the peak at 3539 cm^{-1} is from the O-H stretching and the two bands at 2945 and 2865 cm^{-1} are the stretching bands of the stand oil. At 1750 cm^{-1} there is the stretching band of the C=O, the C-H bending at 1481 cm^{-1} and at 1177 cm^{-1} the C-O stretching band. The band at about 1392 cm^{-1} correspond to the vibration of the CO_3^{-2} mode of the white lead.

Ground 4 (Vasari): lower layer: flour, linseed oil, white lead($(PbCO_3)_2 \cdot Pb(OH)_2$), rabbit skin glue; upper layer: red lead (Pb_3O_4), black vine, stand oil.

Figure 53d shows the IR spectra of the sample G4. The infrared spectra is the same of the sample G3 except for a new peak at 1560 cm^{-1} of the red lead and the disappearance of the band of the white led at 1392 cm^{-1}.

Ground 5 (Armenini – XVI): flour, walnut oil and white lead ($(PbCO_3)_2 \cdot Pb(OH)_2$).

In figure 53e is presented the IR spectra of the sample G5: the peak at 2945 and 2868 cm^{-1} are the C-H stretching bands of the walnut oil. At 1750 cm^{-1} there is the stretching band of the C=O, the C-H bending at 1497 cm^{-1}. The band at 1392 cm^{-1} correspond to the vibration of the CO_3^{-2} mode of the white lead.

Ground 6 (Caliari-Veronese): gypsum and rabbit skin glue (lower layer); linseed oil, white lead, red ochre (Fe_2O_3) and yellow earth (Fe_2O_3) (upper layer).

In figure 53f is presented the IR spectra of the sample G6: the peak at 2925 and 2857 cm^{-1} are the C-H stretching bands, 1742 cm^{-1} there is the stretching band of the C=O and the C-H bending at 1497 cm^{-1} of the linseed oil. The band at 1399 cm^{-1} correspond to the vibration of the CO_3^{-2} mode of the white lead. At 3541 cm^{-1} there is the O-H stretching band of the red ochre and yellow earth.

Ground 7 (Caravaggio): red bole (FeO and silicate), yellow earth (Fe_2O_3), stand oil, white lead ($(PbCO_3)_2 \cdot Pb(OH)_2$), black vine, sand and cinnabar (HgS).

In figure 53g is represented the IR spectra of the sample G7: the band at 3539 cm^{-1} is from the O-H stretching, the two bands at 2946 and 2868 cm^{-1} are the stretching bands, at 1740 cm^{-1} there is the stretching band of the C=O, the C-H bending at 1463 cm^{-1} of the stand oil. The band at about 1392 cm^{-1} correspond to the vibration of the CO_3^{-2} mode of the white lead. The primary inorganic material in the red bole is a clay: there are silicate bands near 3600 cm^{-1}. The strong band at 1070 cm^{-1} represents

the C-O stretching of cinnabar.

Ground 8 (Van Baburen, caravaggesco): red bole (FeO and silicate), stand oil, Venetian turpentine (pine resin), egg and sand.

In figure 53h is represented the IR spectra of the sample G8: the broad band at 3539 cm^{-1} is from the O-H stretching, the two bands at 2958 and 2877 cm^{-1} are stretching bands and the peak at 1756 cm^{-1} of the stretching band of the C=O are all signals of the stand oil. There are silicate bands near 3600 cm^{-1} of the red bole. Peak at 1452, 1467,1270 and 1125 are from Venetian turpentine.

Ground 9 (Volpato): red bole (FeO and silicate), stand oil, Siena earth ($Fe(OH)_3$) and raw umber ($Fe(OH)_3$).

Figure 53i shows the IR spectra of the sample G9: the two bands at 2950 and 2872 cm^{-1} are stretching bands and the peak at 1752 cm^{-1} of the stretching band of the C=O are all signals of the stand oil. There are silicate bands near 3600 cm^{-1} of the red bole.

Ground 10 (De Mayerne): litargirium oil (stand oil + yellow lead), red lead (Pb_3O_4), yellow earth (Fe_2O_3) and black vine.

Figure 53l shows the IR spectra of the sample G10: the two bands at 2944 and 2865 cm^{-1} are stretching bands and the peak at 1733 cm^{-1} of the stretching band of the C=O are all signals of the stand oil. The peaks at 1563 and 1433 cm^{-1} are

of the red lead, the band at 1160 cm^{-1} and the broad band near 2200 cm^{-1} are of the yellow earth

Ground 11 (De Mayerne): litargirium oil (stand oil + yellow lead) and yellow earth (Fe_2O_3).

Figure 54a shows the IR spectra of the sample G11: the two bands at 2947 and 2870 cm^{-1} are stretching bands and the peak at 1739 cm^{-1} of the stretching band of the C=O are all signals of the stand oil. The band at 1160 cm^{-1} and the broad band near 2200 cm^{-1} are of the yellow earth.

Ground 12 (Jan Vermeer): Kaolin, white lead, yellow earth (Fe_2O_3), rabbit skin glue, stand oil.

Figure 54b shows the IR spectra of the sample G12: the two bands at 2938 and 2862 cm^{-1} are stretching bands and the peak at 1749 cm^{-1} of the stretching band of the C=O are all signals of the stand oil. The broad band near 2200 cm^{-1} is of the yellow earth.

The Kaolin peak is at 1410 cm^{-1}.

Ground 13 (Max Doerner): Gypsum, zinc white, rabbit skin and stand oil.

Figure 54c shows the IR spectra of the sample G13: the strong an broad band between 3700 and 3200 cm^{-1} is assigned at the anti-symmetric and symmetric O-H stretching bands of gypsum; the band at 1140 cm^{-1} is the asymmetric SO_4^{2-} stretching band. The two bands at 2932 and 2859 cm^{-1} are stretching bands and the peak at 1744 cm^{-1} of the stretching band of the C=O are all signals of the stand oil.

Ground 14 (Pierre Auguste Renoir): white lead, kaolin, stand oil.

Figure 54d shows the IR spectra of the sample G14: the two bands at 2942 and 2865 cm^{-1} are stretching bands and the peak at 1751 cm^{-1} of the stretching band of the C=O are all signals of the stand oil. The Kaolin peak is at 1410 cm^{-1}.

Ground 15 (De Chirico): Meudon white, egg yolk, poppy oil, Venetian turpentine, white vinegar, glycerin, water.

Figure 54e shows the IR spectra of the sample G16: the two bands at 2944 and 2867 cm^{-1} are stretching bands and the peak at 1745 cm^{-1} of the stretching band of the C=O are all signals of the poppy oil. The chalk peak is at 1793 cm^{-1}. At 3400 – 3200 cm^{-1} there are the N-H stretching band of the egg yolk, the C-N-H bending band is confirmed at 1562 cm^{-1}. The peak of turpentine is at 1460 cm^{-1}.

Ground 16 (for synthetic binders): Titanium white, chalk, acrylic resin and kaolin. Figure 54f shows the IR spectra of the sample G16: at 3100 and 2800 cm^{-1} there are the stretching bands of the C-H, at 1750 cm^{-1} there is the stretching band of C=O of the acrylic resin. Around 760 cm^{-1} there is the broad band of the titanium white. The Kaolin peak is at 1396 cm^{-1}.

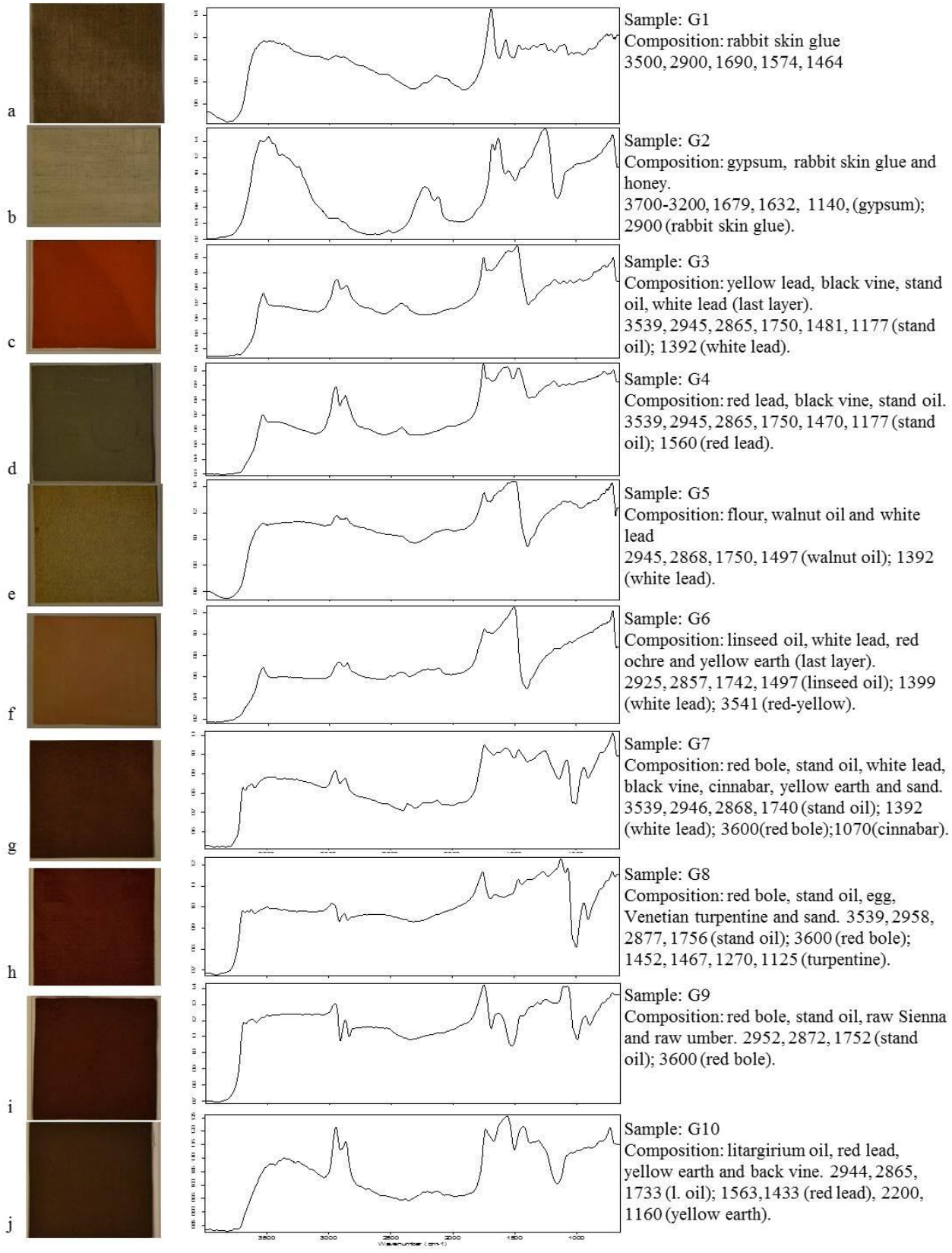

Figure 53: images, infrared spectra with the main peaks and composition of each ground analyzed by DRIFT. The reference collection can be used to identify unknown canvas grounds.

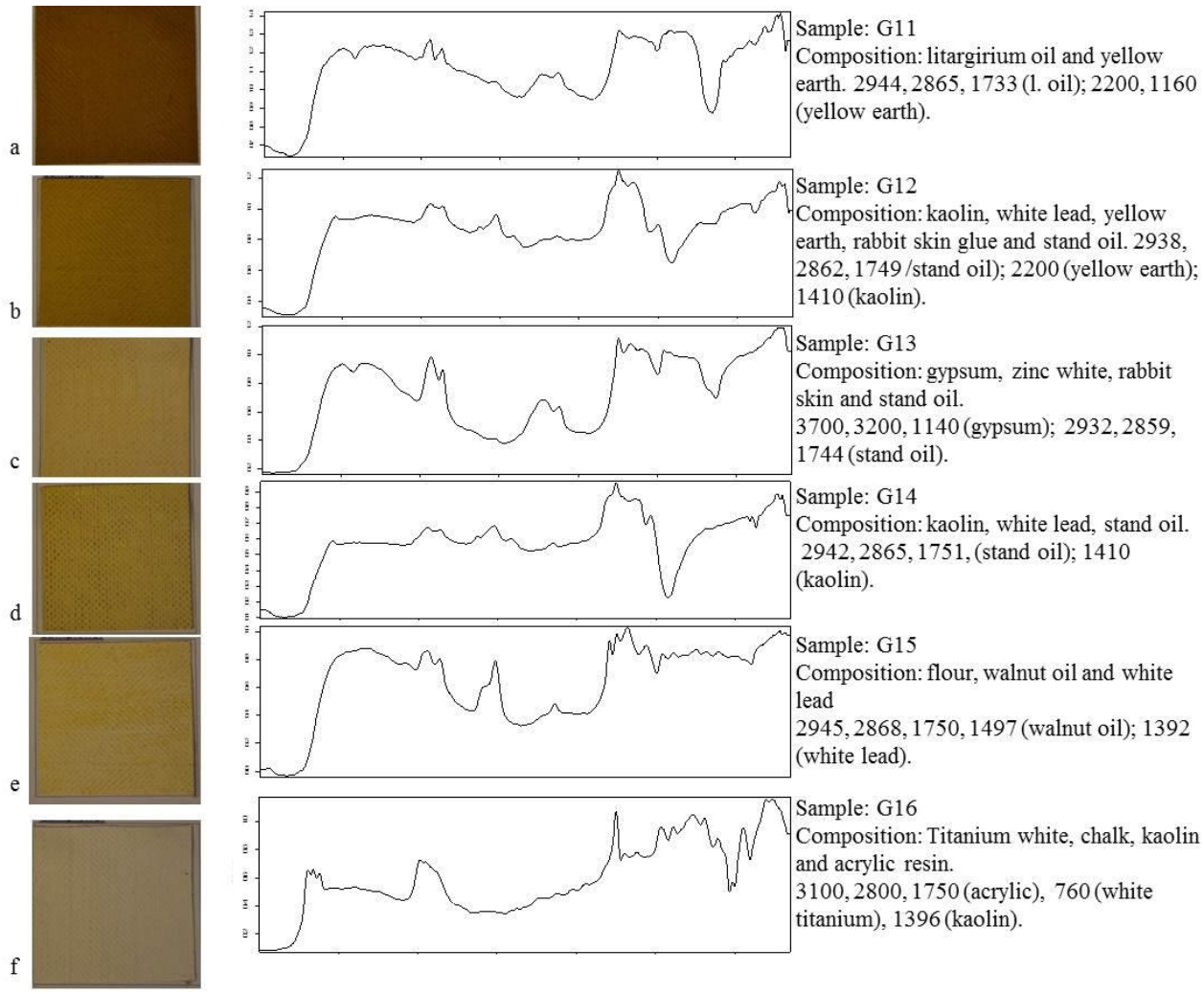

Figure 54: images, infrared spectra with the main peaks and composition of each ground analyzed by DRIFT. The reference collection can be used to identify unknown canvas grounds.

REAL APPLICATION:

The method for the non-invasive identification of ground in canvas has been used to characterize the preparation employed by the painter Guglielmo Caccia called “Il Moncalvo” on his painting “Madonna con Bambino tra San Rocco e San Michele” represented in figure 55.

Fig. 55: canvas image of the “Madonna con bambino tra San Rocco e San Michele” from Guglielmo Caccia called “Il Moncalvo”.

The analysis was carried out pointing the infrared beam on the ground surface to the side of the frame as shown in figure 56a. Often, ground measurements can be performed on the back of the painting: ground tends to pass through the canvas and if the back was not cleaned or brushed a characterization can be done (figure 56b).

Fig 56: portable DRIFT at work on two different canvas: on the side (a) and on the back (b) of the canvas.

Figure 57 shows the infrared spectra of the measured ground of the Moncalvo's painting: comparing the spectra with the reference collection of grounds developed previously we were able to easily identify the composition of the ground used by the artist. The painter used the preparation identified as G2 made by gypsum and animal glue. The strong an broad band between 3700 and 3200 cm^{-1}, the band at 1140 cm^{-1} and the peaks at 1679 and 1632 cm^{-1} were assigned to gypsum and the bands near 2900 cm^{-1} to the animal glue.

The results are confirmed by conservator: in fact the painter is from the XVI century when the most used ground was made by gypsum and animal glue.

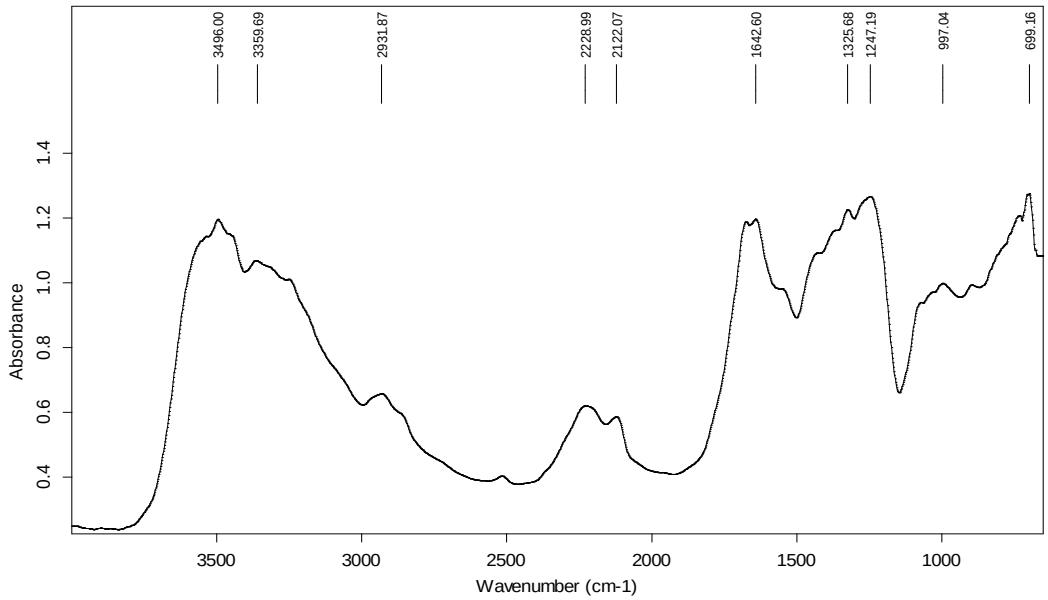

Fig. 57: DRIFT spectra of the Moncalvo's painting: the analysis revealed that the painter used gypsum and rabbit skin glue as ground.

CONCLUSIONS

We present here a portable diffuse reflectance infrared Fourier transform (DRIFT) method for the non-invasive characterization of grounds in painting: with this method there is no need to touch the sample and the analysis can be done directly on site.

We prepared 16 canvas grounds: all of them were used by the most important artist from XIV to XX century such as Vasari, Mantegna, Veronese, Caravaggio and De Chirico. We analyzed grounds using DRIFT and we built a reference library of spectra. We measured the DRIFT spectra of ground on a Moncalvo's painting, who can be considered the most important artist of Piedmont in the XVI century, in order to identify the type of ground that was used. Comparing the spectra with the reference collection we were able to easily identify the composition of the ground used by the artist made by gypsum and animal glue. Moreover the results were confirmed by conservator: in fact the painter is from the XVI century when the most used ground was made by gypsum and animal glue.

4.2 Non-invasive characterization of parchment: a comparison between portable and bench IR

We present here a portable diffuse reflectance infrared Fourier transform (DRIFT) method for the non-invasive characterization of parchment: with this method there is no need to touch the sample and the analysis can be done directly on site. We compared the IR spectra of the portable instrument with bench ATR FTIR results.

EXPERIMENTAL

ATR-FT-IR

Fourier transform infrared spectral analysis of parchment was conducted using ATR-FT-IR. All spectra were obtained using a Thermo Nicolet 670 FT-IR Spectrometer. Sample spectra were obtained in absorption mode over a wavelength of 400 cm^{-1} to 4000 cm^{-1} at 64 scans per sample and a resolution of 4 cm^{-1}. Background readings of air were established prior to data collection. The background was subsequently subtracted from each spectrum before data output. All data was recorded using OMNIC software.

DRIFT ANALYSIS. Diffuse Reflectance Infrared Fourier Transform Spectroscopy (DRIFT) has been performed with an Agilent 4100 Exoscan FTIR portable spectrometer.

Sample spectra were obtained in absorption mode using a diffuse reflectance device over a wavelength of 650 cm^{-1} to 4000 cm^{-1} at 32 scans per sample and a resolution of 4 cm^{-1}. Background readings of air were established prior to data collection. The background was subsequently subtracted from each spectrum before data output.

RESULTS AND DISCUSSION

Diffuse Reflectance Infrared Fourier Transform Spectroscopy (DRIFT) has been used to analyze a parchment sample as shown in figure 58: there is no need to touch the sample.

Fig. 58: Portable DRIFT spectrometer working on parchment sample.

The diffuse reflection (blue) and ATR (red) data are presented as absorbance in figure 59. The results showed that DRIFT spectra are identical to the ATR: the

method can be used as non-invasive tool for the characterization of parchment materials.

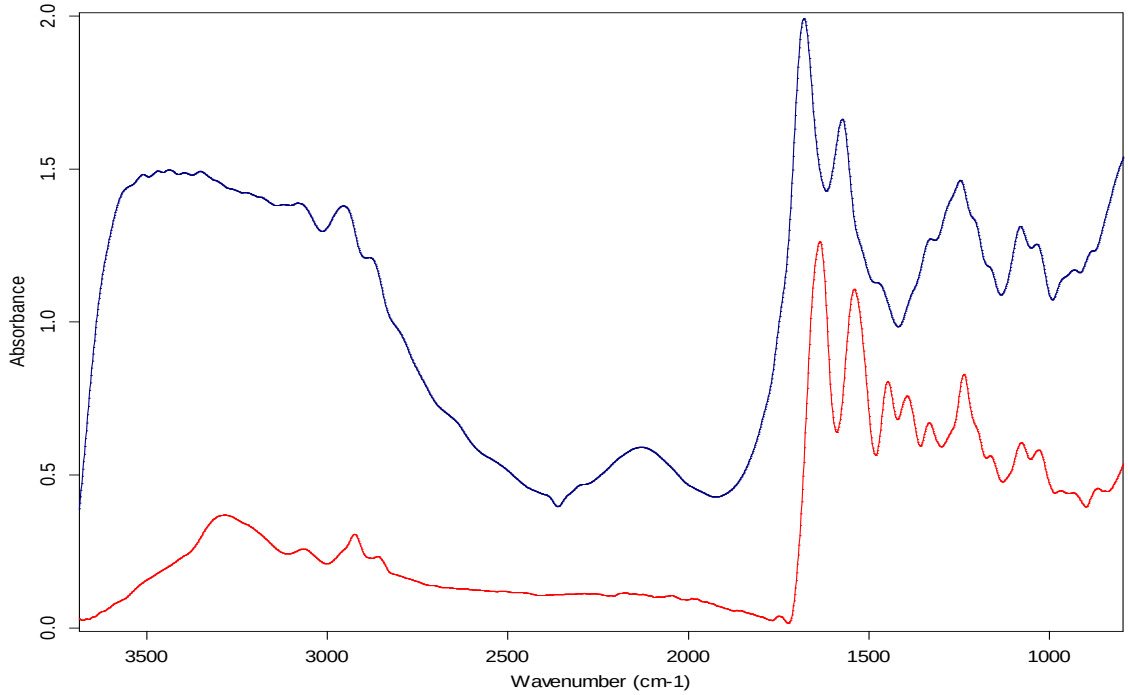

Fig. 59: DRIFT (blue) and ATR (red) spectra of goat parchment.

The use this non-destructive method of analysis for parchment characterization open the opens new horizons about conservation strategies and characterization of this organic material: in fact even if ATR is considered a non-invasive technique, the pressure of the point that is used to measure the spectra usually marks and damages the surface of the object. The non-invasive characterization of the most fragile and important manuscripts of the world, such as the Dead Sea Scrolls, can be performed with the aim to identify the type of parchment used. Again, the non-invasive identification of conservation treatments to which parchment was subjected to with the aim to help conservators to define the best conservation strategies. Moreover, the identification of the state of conservation/grade of ageing of parchment materials can be performed. In fact, is well known that the intensity of amide band of parchment is correlated with the degradation state of the material.

5. CONCLUSIONS

The aim of this doctoral dissertation was the development and application of analytical and statistical techniques for the non-invasive monitoring and analysis of cultural heritage.

Firstly, my research focused on the development of a non-invasive technique based on LED multispectral imaging coupled to statistics for monitoring the conservation state of cultural heritage objects, specifically of the Dead Sea Scrolls. The method developed follows a new approach in the context of cultural heritage aimed at the automatic and fast detection of a developing deterioration process, and its localization and identification. The technique requires the direct measurement of the reflectance spectrum of the artifact through a LED multispectral imaging, leaving the object unchanged for successive examinations.

We performed some simulations on multispectral images of parchment that were virtually degraded: the simulation showed that the control charts built on the relevant PCs are able to accurately detect the degradation process.

We tested the technique by monitoring the degradation of modern parchment artificially aged using sun light exposure, T° and RH%. In all cases the method was able to detect the degradation before it was visible to human eyes and before was detected by other common analytical techniques usually used to determine the ageing of parchment.

We developed a custom software for the automatic elaboration of the data which is actually in use to the IAA conservation laboratory in Jerusalem. In fact, they are employing the method for monitoring the conservation state of the Dead Sea Scrolls, which are manuscripts of inestimable archaeological cultural and religious value. A number of fragments have been selected for periodic imaging and analysis. These are representative of the state of the scrolls as identified by

the conservators. Issues include delamination, gelatinization, organic residues and cockling.

The same methodology has been used for monitoring the conservation state of S. Maria di Castello frescoes in Valle Lomellina (PV) for which a new portable LED multispectral imager was built. Wall paintings were monitored for three and six months and we found that the frescoes were in good state of conservation.

We can affirm that the proposed approach may yield rapid and accurate measurements of the preservation state of cultural heritage objects: the advantages of been non-invasive, fast and a surface-analysis instrument makes this quantitative imaging approach the future of conservation monitoring strategies.

My research has dealt with the development of a 3D imaging method for the evaluation and quantification of changes and defects of cultural heritage.

We developed a reliable RTI imaging method for the non-invasive detection of morphological and physical changes in paintings and drawings. We showed that RTI can be reproducible and quantified to the level where it can be used as practical method for measuring change in objects. We developed a monitoring protocol which includes an imaging protocol, the extraction of the normals and comparison within statistical limits. After characterizing the natural variability of the method and of the monitored object, we damaged the sample by creating different types of damages, then captured the RTI and compared the normals to the limits. The method was able to detect all the damages.

Our method is a completely non-invasive monitoring technique: we obtained an accurate and quantitative measure of the deterioration and degradation present in the painting and drawing after artificial damages. This non-invasive tool may be

very useful to examine paintings and artwork before they travel on loan or during a restoration.

During my research I developed a quick and direct method for the non-destructive identification of the various conservation treatments of parchment by means of direct analysis in real time ionization and high resolution time-of-flight mass spectrometry (DART-MS) and chemometrics. Many traditional interventions can result in irreversible alteration of an artifact and, because of its animal origin, parchment might respond to treatments in unpredictable ways. The conservator's approach to the treatment of parchment must be extremely cautious and due to the simplicity and no sample preparation requirement, the proposed analytical tool could help in the challenging analysis of unknown treatments in cultural heritage. Castor oil and glycerol parchment treatments were investigated using the DART carrier gas in the ion source at room temperature in order not to cause any damage to parchment samples: this is very important while working with any cultural heritage and even more with the Dead Sea Scrolls which are extremely fragile and precious. The method was able to identify both treatments: FS-LDA performed on principal components revealed to be a robust tool that could be employed for the classification of unknown treatments, over all in presence of samples with similar mass spectrum profiles. A DART-MS library of treatments may be created and extended including also the degradation products that may appear after the ageing of the object.

A portable diffuse reflectance infrared Fourier transform (DRIFT) method for the non-invasive characterization of grounds in painting was developed: with this method there is no need to touch the sample and the analysis can be done directly on site. No sample needs to be removed to analyze the object and, in

fact, a number of areas on the object can be analyzed quickly in a non-destructive manner. We prepared 16 canvas grounds: all of them were used by the most important artist from XIV to XX century such as Vasari, Mantegna, Veronese, Caravaggio, De Chirico and we performed the analysis using DRIFT, building a reference library of spectra.

We measured the DRIFT spectra of ground on a Moncalvo's painting, who can be considered one of the most important artist of Piedmont in the XVI century, in order to identify the type of ground that was used. Comparing the spectra with the reference collection we were able to easily identify the composition of the ground used by the artist made by gypsum and animal glue.

The technique was also applied for the non-invasive characterization of parchment and the results were compared with the bench IR instrument results.

We can state that the non-invasive characterization of the most fragile and important manuscripts of the world, such as the Dead Sea Scrolls, can be performed using DRIFT method with the aim: to identify the type of parchment used; to determine the conservation treatments to which parchment was subjected to; to identify the state of conservation and grade of ageing of parchment materials.

As a general conclusion, it could be affirmed that non-invasive quantitative imaging techniques such as multispectral and reflectance transformation imaging coupled with a statistical approach present potentialities that make them very suitable to deal with conservation and preservation of cultural heritage objects. Moreover, the analytical methods DART-MS and DRIFT spectroscopy may be a very useful tools for the non-invasive characterization of artworks.

REFERENCES

1. Shewhart, Walter Andrew. 1931. Economic Control of Quality of Manufactured Product. Princeton NJ: Van Nostramd.
2. Montgomery, Douglas C. 2007. Introduction to Statistical Quality Control, 4Th Ed. New York: John Wiley & Sons.
3. E. Marengo, E. Robotti, M.C. Liparota, et al., Anal. Chem. 2003, Vol. 75 Issue: 20, 5567-5574.
4. E. Marengo, et al., Talanta 2004,63 987-1002.
5. K.C.S. Pillai, in: S. Kotz, N.I. Johnson (Eds.), Encyclopedia of Statistical Science. Vol. 3, Wiley, New York, 1983, pp. 668-673.
6. H. Hotelling, in: Hastay, Wallis (Eds.), Multivariate Quality Control-Techniques of Statistical Analysis, McGraw-Hill, New York, 1947.
7. B.G.M Vandeginste, D.L. Massart, L.M.C. Buydens, S.DE Jong, P.J. Lewi and J. Smeyers-Verbeke, Handbook of Chemometrics and Qualimetrics: Part B, Elsevier, Amsterdam, 1998.
8. D.L. Massart, B.G.M Vanderginste, S.N. Deming, Y. Michotte, L. Kaufman, Chemometrics: A Textbook, Elsevier, Amsterdam, 1988.
9. Hayter, A. J.; Tsui, K. L. J. Qual. Technol. 1994 26 197-208.
10. Wold, S.; Esbensen, K.; Geladi, P. Chemom. Intell. Lab. Syst. 1987 2 37-52.
11. Johannes Schindelin, Ignacio Arganda-Carreras, Erwin Frise, Verena Kaynig, Mark Longair, Tobias Pietzsch, Stephan Preibisch, Curtis Rueden, Stephan Saalfeld, Benjamin Schmid, Jean-Yves Tinevez, Daniel James White, Volker Hartenstein, Kevin Eliceiri, Pavel Tomancak and Albert Cardona (2012) Fiji: an open-source platform for biological-image analysis, Nature Methods 9(7): 676-682
12. Thévenaz, U.E. Ruttimann, M. Unser, "A Pyramid Approach to Subpixel Registration Based on Intensity," IEEE Transactions on Image Processing, vol. 7, no. 1, pp. 27-41, January 1998. Other relevant on-line publications are available at http://bigwww.epfl.ch/publications/.
13. Ignacio Arganda-Carreras, Carlos O. S. Sorzano, Roberto Marabini, Jose M. Carazo, Carlos Ortiz de Solorzano, and Jan Kybic, "Consistent and Elastic Registration of Histological Sections using Vector-Spline Regularization", Lecture Notes in

Computer Science, Springer Berlin / Heidelberg, volume 4241/2006, CVAMIA: Computer Vision Approaches to Medical Image Analysis, pages 85-95, 2006.

14. Knox, K. Proc. SPIE 2008, 6810, 681004-1-11.
15. Carlotto, M. J.; Lazaroff, M. B.; Brennan, M. W. 124/SPIE 1992 Vol. 1819.
16. Colarusso, P.; Kidder, L. H.; Levin, I. W.; Fraser, J. C.; Arens, J. F.; Lewis, E. N. Appl. Spectrosc.1992, 52: 106A-120A.
17. Paquit, V. C.; Tobin, K. W.; Price, J. R.; Mèriaudeau, F. Opt. Express 2009, 17(14), 11360–11365.
18. Bearman, G. H.; Spiro, S. Biblical Archaeol. 1996, 59: 56–66.
19. Easton, R.; Noel, W. Gazette du Livre Médiéval 2004, 45, 39-49.
20. Delaney, J. K.; Zeibel, J. G.; Thoury, M.; Littleton, R.; Palmer, M. R.; Morales, K. M.; René de la Rie, R.; Hoenigswald, A. Appl. Spectrosc. 2010, 64: 584–594.
21. France, F.; Christens-Barry, W.; Toth, M.; Boydston, K. Proc. SPIE 2010 Vol. 7531, edited by David Stork.
22. Elena Paz Rebollo San Miguel, "Applications of imaging spectroscopy to the chemistry of cultural heritage field", PhD Thesis, University of Padova, 2011.
23. J. R. Mansfield, M. G. Sowa, C. Majzels, C. Collins, E. Cloutis, H. H. Mantsch, "Near infrared spectroscopic reflectance imaging: supervised analysis using an art conservation application", Vibrational Spectroscopy, Vol. 19, No. 1, FEB 1999, pp. 33-45.
24. J. R. Mansfield, M. Attas, C. Majzels, E. Cloutis, Collins C, H.H. Mantsch, "Near infrared spectroscopic reflectance imaging: a new tool in art conservation", Vibrational Spectroscopy, Vol. 28, No 1, FEB 2002, pp 59-66.
25. M. Attas, E. Cloutis, C. Collins, D. Goltz, C. Majzels, J.R. Mansfield, H.H. Mantsch, "Near-infrared spectroscopic imaging in art conservation: investigation of drawing constituents", Journal of Culturla Heritage, Vol. 4, No. 2, APR-JUN 2003, pp. 127-136.
26. A. Casini, F. Lotti, M. Picollo, L. Stefani, E. Buzzegoli, Image spectroscopy mapping technique for non-invasive analysis of paintings", Studies in conservation, Vol. 44, No. 1, 1999, pp. 39-48.
27. S. Baronti, A. Casini, F. Lotti, S, Porcinai, "Principal component analysis of visible and near-infrared multispectral images of works of art", Chemometrics and intelligent laboratory systems, Vol. 39, No. 1, NOV 1997, pp. 103-114.

28. S. Baronti, A. Casini, F. Lotti, S, Porcinai, “Multispectral imaging system for the mapping of pigments in works of art by use of principal component analysis”, Applied Optics, Vol. 37, No. 8, MAR 1998, pp 1299-1309.
29. M. Bacci, A. Casini, C. Cucci, A. Muzzi, S. Porcinai, “A study on a set of drawing by Parmigianino: integration of art historical analysis with imaging spectroscopy”, Journal of Cultural Heritage, Vol. 6, No. 4, DEC 2005, pp. 329-336.
30. M. Picollo, M. Bacci, L. Boselli, C. Cucci, A. Casini, F. Lotti, M. Poggesi, B. Radicati, L. Stefani “ Non-invasive spectroscopic techniques for the diagnosis and conservation of historic surfaces and wall paintings”, Proceedings of the International Workshop SMW08. In Situ Monitoting Of Monumental Surfaces. “7-29 October 2008, Florence, Edited by P. Tiano and C. Pardini, Florence, Edifir, pp. 31-36.
31. P. Carcagni, A. Della Patria, R. Fontana, M. Greco, M. Mastroianni, M. Materazzi, E. Pampaloni, L. Pezzati, “Multispectral imaging of painitngs by optical scanning”, Optics and lasers engineering, Vol. 45, No. 3, MAR 2007, pp. 329-336.
32. C. Balas, V. Papadakis, N. Papadakis, A. Papadakis, E. Vazgiouraki, G. Themelis “ A novel hyper-spectral imaging apparatus for the non-destructive analysis of objects of artistic and historic value”, Journal of Cultural Heritage, Vol. 4, Supplement 1, JAN 2003, pp. 330s-337s.
33. K. Rapantzikos, C. Balas, “Hyperspectral imaging: potential in non-destructive analysis of palimpsest”, IEEE International Conference on Image Processing, Genova, Italy, September 2005.
34. J.K. Delaney, E. Walmsley, B. H. Berrie, C. F. Fletcher, “Multispectral imaging of painting in the infrared to detect and to map blue pigments”, Sackler NAS Colloquium, Scientific Examination of art: Modern Techniques in Conservation and Analysis, Proceedings of the national Academy of Sciences, Washington, 2003, The National press, Washington, D.C., 2005, pp. 120-136.
35. J.K. Delaney, J.G. Zeibel, M. Thoury, R. Littleton, M. Palmer, K. M. Morales, E. R. de la Rie, A. Hoenigswald, “Visible and Infrared Imaging Spectroscopy of Picasso’s Harlequin Musician: Mapping and Identifican of Artist Materials in situ” Applied Spectroscopy, Vol. 64, No. 6, JUN 2010, pp. 584-594.
36. P. Ricciardi, J. K. Delaney, M. Thoury, M. Facini, “New trends in the in situ analysis of medieval illuminated manuscripts: the use of imaging spectroscopy techniques for improved pigment identification and mapping”, 3 rd Course Non-innavsive analysis of

painting materials, International School Hubert Curien Structural and Molecular Archaelogy, Erice-Sicily (Italy) 14-21 June 2010.

37. D.M. Chabries, S.W. Booras, G.H. Bearman, Antiquity 2003, Vol. 77, Number 296.
38. G. Bearman, W. A. Christens-Barry, Palarch's J. Arch. of Egypt/Egyptology 2009, 6(7) 1-20.
39. Y. Yadin, The Message of the Scrolls, Simon and Schuster, New York, 1957, p 161-162.
40. G. Bearman, W. A. Christens-Barry, Palarch's J. Arch. of Egypt/Egyptology 2009, 6(7) 1-20.
41. Christens-Barry, W. A.; Boydston, K.; Easton, R. L. Proc. of Eikonopoiia 2010, Helsinki, Finland, pp. 27-38.
42. France, F. G. Proc. of Eikonopoiia 2010, Helsinki, Finland, pp. 51-64.
43. Reed, R. The Nature and Making of Parchment, Elmete Press: Leeds, 1975.
44. Bykova, G. Z. Restaurator 1993, 14(3), 188-197.
45. Hansen, E. F.; Lee, S.; Sobel, H. J. Am. Inst. Conserv. 1992 31, 3 : 325-342.
46. http://www.unesco.org/webworld/ramp/html/r8817e/r8817e00.htm#Contents
47. Kathpalia, Y. P. Conservation and Restoration of Archive Materials, Paris, Unesco, 1973.
48. Bearman, G.; Christens-Barry, W.; Boydston, K. Proc. of Eikonopoiia 2010, Helsinki, Finland, pp. 108-114 (2010).
49. B. Dolgin, V. Bulatov, I. Schechter, Rev. Anal. Chem. 28 (2009) 15-307.
50. E. Mannucci, R. Pastorelli, G. Zerbi, C. E. Bottani and A. Facchini, J. Raman Spectrosc. 31, 1089–1097 (2000).
51. E. Badea, L Miu, P. Budrugeac, Maria Giurginca¸ N. Badea and G. Della Gatta, Journal of Thermal Analysis and Calorimetry, Vol. 91 (2008) 1, 17–27.
52. Budrugeac P., Miu L., Journal of cultural heritage 9 (2008) 146-153.
53. Fessas D., Signorelli M., Schiraldi A., Kennedy C., Wess T., Hassel B., Nielsen K., Thermochimica Acta 447 (2006)30-35.
54. Budrugeac P., Badea E., Della Gatta G., Miu L., Comanescu A., Thermochimica Acta 500 (2010) 51-62.
55. Chahine, C., Thermochimica Acta 365 (2000) 101-110.
56. Wang Y., Guo J., Chen H.,Shan Z., J Therm Anal Calorim (2010) 99:295-300.

57. B. Roduit and M. Odlyha, Journal of Thermal Analysis and Calorimetry, Vol. 85 (2006) 1, 157–164.
58. Stirlic M., Kralj Cigic I., Rabin I., Kolar J., Pihlar B., Cassar M., Polymer Degradation and Stabilty 94 (2009) 886-890.
59. A. Možir, M. Strliˇc, T. Trafela, I. Kralj Cigi´c, J. Kolar, V. Deselnicu, G. de Bruin, Appl Phys A (2011) 104:211–217.
60. Wess, T., Orgel, J., Thermochimica Acta 365 (2000)119-128.
61. C. Kennedy, J. Hiller, D. Lammie, M. Drakopoulos, M. Vest, M. Cooper,| W Adderley, T. Wess, Nano Lett., Vol. 4, No. 8, 2004.
62. B. Dolgin, V. Bulatov, I. Schechter, Anal Bioanal Chem (2007) 388:1885–1896.
63. E. Robotti, M. Bobba, A. Panepinto, E. Marengo, Anal Bioanal Chem (2007) 388:1249–1263.
64. A. Nevin, I. Osticioli, D. Anglos, A. Burnstock, S. Cather, E. Castellucci, J. Raman Spectrosc. 2008; 39: 993–1000.
65. A. Kamiriska, A. Sionkowska, Polymer Degradation and Stability 51 (1996) 15-19.
66. Marengo E.; Manfredi, M.; Zerbinati, O.; Robotti,E.; Mazzucco, E.; Gosetti, F.; Bearman, G.; France, F.; Shor, P.; Anal. Chem. 2011, 83, 6609–6618.
67. Marengo E.; Manfredi, M.; Zerbinati, O.; Robotti,E.; Mazzucco, E.; Gosetti, F.; Bearman, G.; France, F.; Shor, P.; Analytica Chimica Acta 2011, 706, 229– 237.
68. Chabries, D M, S.W. Booras and G.H. Bearman. 2003. "Imaging the Past." Antiquities 77: 359–372.
69. "Appunti per una storia di Valle Lomellina", ed. Comune di Valle Lomellina, seconda ristampa anno 1997, ed. Società Storica Vigevanese anno 2000.
70. Anal. Chem. 2011, 83, 5101–5106 Linda Cefalvayov, Matija Strlic and Harri Karjalainen, Quantitative NIR Chemical Imaging in Heritage Science.
71. Fresco restoration: digital image processing approach, Jan Blazek1, Barbara Zitová, Miroslav Bene, and Janka Hradilová, 17th European Signal Processing Conference (EUSIPCO 2009) Glasgow, Scotland, August 24-28, 2009.
72. Luís Granero-Montagud et all, Optics for Arts, Architecture, and Archaelogy IV, Proc. Of SPIE Vol. 8790, 879008-1.
73. State-of-The-Art and Applications of 3D Imaging Sensors in Industry, Cultural Heritage, Medicine, and Criminal Investigation, Giovanna Sansoni, Marco Trebeschi and Franco Docchio Sensors 2009, 9, 568-601;

74. Malzbender, T., Gelb, D., Wolters, H. and Zuckerman, B. (2000) Enhancement of Shape Perception by Surface Reflectance Transformation. Tech. Rep. HPL- 2000-38R1, Hewlett-Packard Laboratories, Palo Alto, California.
75. Malzbender, T., Gelb, D. and Wolters, H. (2001) Polynomial Texture Maps. In SIGGRAPH ‟01: Proceedings of the 28th annual conference on Computer graphics and interactive techniques (New York, NY, USA), ACM Press, pp. 519–528.
76. Mudge, M., Malzbender, T., Chalmers, A., Scopigno, R., Davis, J., Wang, O., Gunawardane, P., Ashley, M., Doerr, M., Proenca, A. and Barbosa, J. (2008) Image-Based Empirical Information Acquisition, Scientific Reliability, and Long-Term Digital Preservation for the Natural Sciences and Cultural Heritage. Eurographics.
77. Sarah M. Duffy, Multi-light Imaging for Heritage Applications, English Heritage 2013.
78. L. Macdonald and S. Robson (2010), Polynomial Texture Mapping and 3D Representations, International Archives of Photogrammetry, Remote Sensing and Spatial Information Sciences, Vol. XXXVIII, part 5 Commission V Symposium, Newcastle Upon Tyne, UK.
79. P. Gautron, J. Krivanek, S. Pattanaik, K. Bouatouch (2004), A Novel Hemispherical Basis for Accurate and Efficient Rendering, Eurographics Symposium on Rendering, H. W. Jensen, A. Keller (Editors).
80. Luís Granero-Montagud et all, Optics for Arts, Architecture, and Archaelogy IV, Proc. Of SPIE Vol. 8790, 879008-1.
81. M. Morawitz, N. Hein , I. Alexeenko, M. Wilke, G. Pedrini, C. Krekel, W. Osten, Optics for Arts, Architecture, and Archaelogy IV, Proc. Of SPIE Vol. 8790, 879004-1.
82. Burmester, A. and Müller, M., “The registration of transportation damage using digital image processing.,” Zeitschrift für Kunsttechnologie und Konservierung 6(2), 335345 (1992).
83. http://www.deadseascrolls.org.il/featured-scrolls.
84. Yadin, Y. The Message of the Scrolls; Simon and Schuster: New York, 1957; pp 161_162.
85. Boyd-Alkalay, E., Libman, L. Restaurator, 1997, 92-101.
86. Marengo E.; Manfredi, M.; Zerbinati, O.; Robotti,E.; Mazzucco, E.; Gosetti, F.; Bearman, G.; France, F.; Shor, P.; Anal. Chem. 2011, 82, 6609–6618.

87. Marengo E.; Manfredi, M.; Zerbinati, O.; Robotti,E.; Mazzucco, E.; Gosetti, F.; Bearman, G.; France, F.; Shor, P.; Analytica Chimica Acta 2011, 707, 229– 237.
88. Simileanu, M.; Giurginca, M.; Miu, L.; Radvan, R. J of Optoelec. and Adv. Materials, 2008, Vol: 10, Issue: 8, 2168-2173.
89. Facchini, A. Malara, C. Bazzani, G. Cavallotti, P. J. of Coll. and Interf. Sc., 2000, Vol. 231, Issue: 2, 213-220.
90. Dolgin, B.; Bulatov, V.; Schechter, I. Chemistry Central Journal, 2012, Vol. 6, -24.
91. Mozir, A.; Strlic, M.; Trafela, T.; Cigic, I.; Kolar, J.; Deselnicu, V.; de Bruin, G. Appl Phys A 2011, 104:211–217.
92. Adams, J. International Journal of Mass Spectrometry, 2011; 301, 109–126.
93. Geiger, J., Armitage, R., DeRoo, C.; ACS Symposium Series, 2012, Vol. 1103, 123-129.
94. Jones, R.W., Cody R.B., McClelland, J.F.; J. Forensic. Sci. 2006, Vol. 51, 915–918.
95. Bentley, J.; Schneider, T. J. Comput. Statist. Data Anal. 2000, 32, 465–483.
96. Baronti, S.; Casini, A.; Lotti, F.; Porcinai, S. Chem. Intell. Lab. Syst. 1997, 39, 103–114.
97. Marengo, E.; Robotti, E.; Liparota, M. C.; Gennaro, M. C. Anal. Chem. 2003, 75 (20), 5567–5574.
98. Marengo, E.; Robotti, E.; Liparota, M. C.; Gennaro, M. C. Talanta 2004, 63, 987–1002.
99. Eisenbeis, 1972, Health Publisher.
100. Klecka 1980, Sage Publications, Inc, Newbury Park, CA, USA.
101. Jürgen H. Gross, Anal Bioanal Chem (2014) 406:63–80.
102. Reed, R. 1975, The Nature and Making of Parchment; Elmete Press: Leeds.
103. Bykova, G. Z., 1993, Restaurator, 14 (3), 188–197.
104. Hansen, E. F.; Lee, S.; Sobel, H. J. Am. Inst. Conserv. 1992, 31 (3), 325.
105. Kaszowska, Z., Malek, K., Pańczyk, M., Mikołajska, A., Vibrational Spectroscopy Volume 65, 2013, Pages 1-11.
106. G. Sciutto et al. Anal Bioanal Chem (2013) 405:625–633.
107. Joseph, E., Ricci, C., Kazarian, S.G., Mazzeo, R., Prati, S., Ioele, M., Vibrational Spectroscopy Volume 53, Issue 2, 20 July 2010, Pages 274-278.
108. A. Bonizzoni, S. Caglio, A. Galli, G. Poldi, Appl. Phys.A 92, 203–210(2008).

109. Infrared Spectroscopy in Conservation Science, Michele R. Derrick, Dusan Stulik, James M. Landry, Getty, Los Angeles, 1999.
110. Casadio F, Toniolo LJ (2001) J Cult Herit 2:71–78.
111. Low MJD, Baer NS (1977) Stud Conserv 22:116–128.
112. C. Maltese, Preparazione e finitura delle opere pittoriche, Mursia Editore, Milano, 1993.
113. Bettarini (a cura di), Vasari, introduzione alle tre arti del disegno cap. XXIII, "Della pittura", Edizione Barocchi, 1966, pp. 136, 137.
114. Gorreri (a cura di), Armenini (1586), "De'veri precetti della pittura", cap. IX, 1988, p. 143.
115. D. Pagano (a cura di), Caravaggio a Napoli, dalle opere di Misericordia alla Orsola trafitta, Electa Editore, Napoli, 1999.
116. T. De Mayerne, Pittura e scultura delle arti minori, 1620-1640, p. 220.
117. Volpato, Modo da tener nel dipinger, XVII secolo, p. 729.
118. T. De Mayerne, Pittura e scultura delle arti minori, 1620-1640, p. 120-121.
119. M. Doerner, The material of the artist: old masters, 1977, pp. 23-27.
120. D. Bernar, I capolavori di Pierre Auguste Renoir, Fabbri Editore, Milano, 1988.
121. G. De Chirico, Piccolo trattato di tecnica pittorica, Vanni Scheiviller Editore, Milano, 1928.